PALEOSEISMOLOGY OF UTAH, VOLUME 28

HOLOCENE SURFACE-FAULTING EARTHQUAKES AT THE SPRING LAKE AND NORTH CREEK SITES ON THE WASATCH FAULT ZONE: EVIDENCE FOR COMPLEX RUPTURE OF THE NEPHI SEGMENT

by Christopher B. DuRoss, Michael D. Hylland, Adam I. Hiscock, Stephen F. Personius, Richard W. Briggs, Ryan D. Gold, Gregg S. Beukelman, Greg N. McDonald, Ben A. Erickson, Adam P. McKean, Stephen J. Angster, Roselyn King, Anthony J. Crone, and Shannon A. Mahan

SPECIAL STUDY 159
UTAH GEOLOGICAL SURVEY
a division of
UTAH DEPARTMENT OF NATURAL RESOURCES
2017

Blank pages are intentional for printing purposes

PALEOSEISMOLOGY OF UTAH, VOLUME 28

HOLOCENE SURFACE-FAULTING EARTHQUAKES AT THE SPRING LAKE AND NORTH CREEK SITES ON THE WASATCH FAULT ZONE: EVIDENCE FOR COMPLEX RUPTURE OF THE NEPHI SEGMENT

by Christopher B. DuRoss[1], Michael D. Hylland[2], Adam I. Hiscock[2], Stephen F. Personius[3], Richard W. Briggs[3], Ryan D. Gold[3], Gregg S. Beukelman[2], Greg N. McDonald[2], Ben A. Erickson[2], Adam P. McKean[2], Stephen J. Angster[4], Roselyn King[5], Anthony J. Crone[6], and Shannon A. Mahan[7]

[1]Utah Geological Survey; currently U.S. Geological Survey, Golden, Colorado
[2]Utah Geological Survey, Salt Lake City, Utah
[3]U.S. Geological Survey, Golden, Colorado
[4]U.S. Geological Survey; currently University of Nevada, Reno
[5]U.S. Geological Survey; currently Colorado School of Mines
[6]U.S. Geological Survey––Emeritus
[7]U.S. Geological Survey, Denver, Colorado

Cover photo: The Spring Lake trench site on the northern strand of the Nephi segment of the Wasatch fault zone. View is to the east, toward an 8-m-high fault scarp (the base of which is marked by a yellow tripod) formed during surface-faulting earthquakes on the Wasatch fault zone.

ISBN: 978-1-55791-936-6

SPECIAL STUDY 159
UTAH GEOLOGICAL SURVEY
a division of
UTAH DEPARTMENT OF NATURAL RESOURCES
2017

STATE OF UTAH
Gary R. Herbert, Governor

DEPARTMENT OF NATURAL RESOURCES
Michael Styler, Executive Director

UTAH GEOLOGICAL SURVEY
Richard G. Allis, Director

PUBLICATIONS
contact
Natural Resources Map & Bookstore
1594 W. North Temple
Salt Lake City, UT 84116
telephone: 801-537-3320
toll-free: 1-888-UTAH MAP
website: mapstore.utah.gov
email: geostore@utah.gov

UTAH GEOLOGICAL SURVEY
contact
1594 W. North Temple, Suite 3110
Salt Lake City, UT 84116
telephone: 801-537-3300
website: geology.utah.gov

Research supported by the U.S. Geological Survey (USGS), Department of the Interior, under USGS award number G12AP200076. Although this product represents the work of professional scientists, the Utah Department of Natural Resources, Utah Geological Survey, makes no warranty, expressed or implied, regarding its suitability for a particular use. The Utah Department of Natural Resources, Utah Geological Survey, shall not be liable under any circumstances for any direct, indirect, special, incidental, or consequential damages with respect to claims by users of this product.

FOREWORD

The Paleoseismology of Utah series makes the results of paleoseismic investigations in Utah available to geoscientists, engineers, planners, public officials, and the general public. These studies provide critical information regarding paleoearthquake parameters such as earthquake timing, recurrence, displacement, slip rate, fault geometry, and segmentation, which can be used to characterize potential seismic sources and evaluate the long-term seismic hazard of Utah's Quaternary faults.

This Special Study, number 28 in the Paleoseismology of Utah series, presents the results of paleoseismic trench investigations conducted at the Spring Lake and North Creek sites, on the northern and southern strands, respectively, of the Nephi segment of the Wasatch fault zone. At least five to seven earthquakes ruptured the Spring Lake site since ~13.1 ka, yielding a mean recurrence of ~1.2–1.5 kyr and vertical slip rate of ~0.5–0.8 mm/yr. At least five earthquakes ruptured the North Creek site since ~4.7 ka, yielding a mean recurrence of 1.1–1.3 kyr and vertical slip rate of ~1.9–2.0 mm/yr. These new paleoseismic data help refine the Holocene surface-faulting earthquake history of the Nephi segment, suggest that complex ruptures of the northern and southern strands have occurred, and contribute to an improved understanding of the complexities of surface rupture and moment release on the Wasatch fault zone. Ultimately, these data will contribute to more accurate probabilistic earthquake forecasts for the Wasatch Front region.

William Lund, Editor
Paleoseismology of Utah Series

PALEOSEISMOLOGY OF UTAH SERIES PUBLICATIONS

UGS publications produced as part of the Paleoseismology of Utah series may be found online at http://geology.utah.gov/ghp/consultants/paleoseismic_series.htm and at http://geology.utah.gov/map-pub/publications/.

1. Fault behavior and earthquake recurrence on the Provo segment of the Wasatch fault zone at Mapleton, Utah County, Utah—Paleoseismology of Utah, Volume 1, 1991, by Lund, W.R., Schwartz, D.P., Mulvey, W.E., Budding, K.E., and Black, B.D.: Utah Geological Survey Special Study 75, 41 p.

2. Paleoseismic analysis of the Wasatch fault zone at the Brigham City trench site, Brigham City, Utah, and the Pole Patch trench site, Pleasant View, Utah—Paleoseismology of Utah, Volume 2, 1991, by Personius, S.F.: Utah Geological Survey Special Study 76, 39 p.

3. The number and timing of paleoseismic events on the Nephi and Levan segments, Wasatch fault zone, Utah—Paleoseismology of Utah, Volume 3, 1991, by Jackson, M.: Utah Geological Survey Special Study 78, 23 p., 3 plates.

4. Seismotectonics of north-central Utah and southwestern Wyoming—Paleoseismology of Utah, Volume 4, 1994, by West, M.W.: Utah Geological Survey Special Study 82, 93 p., 5 plates, scale 1:100,000.

5. Neotectonic deformation along the East Cache fault zone, Cache County, Utah—Paleoseismology of Utah, Volume 5, 1994, by McCalpin, J.P.: Utah Geological Survey Special Study 83, 37 p.

6. The Oquirrh fault zone, Tooele County, Utah—surficial geology and paleoseismicity—Paleoseismology of Utah, Volume 6, 1996, by Lund, W.R., editor: Utah Geological Survey Special Study 88, 64 p., 2 plates, scale 1:24,000.

7. Paleoseismic investigation on the Salt Lake City segment of the Wasatch fault zone at the South Fork Dry Creek and Dry Gulch sites, Salt Lake County, Utah—Paleoseismology of Utah, Volume 7, 1996, by Black, B.D., Lund, W.R., Schwartz, D.P., Gill, H.E., and Mayes, B.H.: Utah Geological Survey Special Study 92, 22 p., 1 plate.

8. Paleoseismic investigation at Rock Canyon, Provo segment, Wasatch fault zone, Utah County, Utah—Paleoseismology of Utah, Volume 8, 1998, by Lund, W.R., and Black, B.D.: Utah Geological Survey Special Study 93, 21 p., 2 plates.

9. Paleoseismic investigation of the Clarkston, Junction Hills, and Wellsville faults, West Cache fault zone, Cache County, Utah—Paleoseismology of Utah, Volume 9, 2000, by Black, B.D., Giraud, R.E., and Mayes, B.H.: Utah Geological Survey Special Study 98, 23 p., 1 plate.

10. Post-Bonneville paleoearthquake chronology of the Salt Lake City segment, Wasatch fault zone, from the 1999 "mega-trench" site—Paleoseismology of Utah, Volume 10, 2002, by McCalpin, J.P.: Utah Geological Survey Miscellaneous Publication 02-7, 38 p.

11. Post-Provo paleoearthquake chronology of the Brigham City segment, Wasatch fault zone, Utah—Paleoseismology of Utah, Volume 11, 2002, by McCalpin, J.P., and Forman, S.L.: Utah Geological Survey Miscellaneous Publication 02-9, 46 p.

12. Neotectonics of Bear Lake Valley, Utah and Idaho; a preliminary assessment—Paleoseismology of Utah, Volume 12, 2003, by McCalpin, J.P.: Utah Geological Survey Miscellaneous Publication 03-4, 43 p.

13. Holocene earthquake history of the northern Weber segment of the Wasatch fault zone, Utah—Paleoseismology of Utah, Volume 13, 2006, by Nelson, A.R., Lowe, M., Personius, S., Bradley, L., Forman, S.L., Klauk, R., and Garr, J.: Utah Geological Survey Miscellaneous Publication 05-8, 39 p., 2 plates.

14. Paleoseismic investigation and long-term slip history of the Hurricane fault in southwestern Utah—Paleoseismology of Utah, Volume 14, 2007, by Lund, W.R., Hozik, M.J., and Hatfield, S.C.: Utah Geological Survey Special Study 119, 81 p.

15. Surficial-geologic reconnaissance and scarp profiling on the Collinston and Clarkston Mountain segments of the Wasatch fault zone, Box Elder County, Utah—paleoseismic inferences, implications for adjacent segments and issues for diffusion-

equation scarp-age modeling—Paleoseismology of Utah, Volume 15, 2007, by Hylland, M.D.: Utah Geological Survey Special Study 121, 18 p.

16. Paleoseismic reconnaissance of the Sevier fault, Kane and Garfield Counties, Utah—Paleoseismology of Utah, Volume 16, 2008, by Lund, W.R, Knudsen, T.R., and Vice, G.S.: Utah Geological Survey Special Study 122, 31 p.

17. Paleoseismic investigation of the northern strand of the Nephi segment of the Wasatch fault zone at Santaquin, Utah—Paleoseismology of Utah, Volume 17, 2008, by DuRoss, C.B., McDonald, G.N., and Lund, W.R.: Utah Geological Survey Special Study 124, 33 p., 1 plate.

18. Paleoseismic investigation of the northern Weber segment of the Wasatch fault zone at Rice Creek trench site, North Ogden, Utah—Paleoseismology of Utah, Volume 18, 2009, by DuRoss, C.B., Personius, S.F., Crone, A.J., McDonald, G.N., and Lidke, D.J.: Utah Geological Survey Special Study 130, 37 p., 2 plates.

19. Late Quaternary faulting in East Canyon Valley, Northern Utah—Paleoseismology of Utah, Volume 19, 2010, by Piety, L.A., Anderson, L.W., and Ostenaa, D.A.: Utah Geological Survey Miscellaneous Publication 10-5, 40 p.

20. Compilation of U.S. Bureau of Reclamation Seismotectonic Studies in Utah, 1982–1999—Paleoseismology of Utah, Volume 20, 2011, compiled by Lund, W.R., Bowman, S.D., and Piety, L.A.: Utah Geological Survey Miscellaneous Publication 11-2, variously paginated.

21. Compilation of 1982–83 seismic safety investigation reports of eight SCS dams in southwestern Utah (Hurricane and Washington fault zones) and low-sun-angle aerial photography, Washington and Iron Counties, Utah, and Mohave County, Arizona—Paleoseismology of Utah, Volume 21, 2011, by Bowman, S.D., Young, B.W., and Unger, C.D.: Utah Geological Survey Open-File Report 583, 4 p., 2 plates, 6 DVD set.

22. Late Holocene earthquake history of the Brigham City segment of the Wasatch fault zone at the Hansen Canyon, Kotter Canyon, and Pearsons Canyon trench sites, Box Elder County, Utah—Paleoseismology of Utah, Volume 22, 2012, by DuRoss, C.B., Personius, S.F., Crone, A.J., McDonald, G.N., and Briggs, R.: Utah Geological Survey Special Study 142, 28 p., 3 plates, 5 appendices.

23. Compilation of U.S. Geological Survey National Earthquake Hazards Reduction Program Final Technical Reports for Utah—Paleoseismology of Utah, Volume 23, 2013, by Bowman, S.D., and Lund, W.R.: Utah Geological Survey Miscellaneous Publication 13-3, 9 p. + 56 reports.

24. Evaluating surface fault chronologies of graben-bounding faults in Salt Lake Valley, Utah—new paleoseismic data from the Salt Lake City segment of the Wasatch fault zone and the West Valley fault zone—Paleoseismology of Utah, Volume 24, 2014, by DuRoss, C.B., and Hylland, M.D.: Utah Geological Survey Special Study 149, 76 p., 2 plates, 14 appendices.

25. History of late Holocene earthquakes at the Willow Creek site on the Nephi segment, Wasatch fault zone, Utah—Paleoseismology of Utah, Volume 25, 2014, by Crone, A.J., Personius, S.F., DuRoss, C.B., Machette, M.N., and Mahan, S.A.: Utah Geological Survey Special Study 151, 43 p., 3 appendices.

26. Compilation of 1970s Woodward-Lundgren & Associates Wasatch fault investigation reports and low-sun-angle aerial photography, Wasatch Front and Cache Valley, Utah and Idaho—Paleoseismology of Utah, Volume 26, 2015, compiled by Bowman, S.D., Hiscock, A.I., and Unger, C.D., Utah Geological Survey Open-File Report 632, (8 p., 6 pl., 9 DVD set.

27. Geologic mapping and paleoseismic investigations of the Washington fault zone, Washington County, Utah, and Mohave County, Arizona—Paleoseismology of Utah, Volume 27, edited by William R. Lund, Utah Geological Survey Miscellaneous Publication 15-6, 175p.

CONTENTS

FIGURES

TABLES

PLATES

HOLOCENE SURFACE-FAULTING EARTHQUAKES AT THE SPRING LAKE AND NORTH CREEK SITES ON THE WASATCH FAULT ZONE: EVIDENCE FOR COMPLEX RUPTURE OF THE NEPHI SEGMENT

by Christopher B. DuRoss, Michael D. Hylland, Adam I. Hiscock, Stephen F. Personius, Richard W. Briggs, Ryan D. Gold, Gregg S. Beukelman, Greg N. McDonald, Ben A. Erickson, Adam P. McKean, Stephen J. Angster, Roselyn King, Anthony J. Crone, and Shannon A. Mahan

ABSTRACT

The Nephi segment of the Wasatch fault zone (WFZ) comprises two fault strands, the northern and southern strands, which have evidence of recurrent late Holocene surface-faulting earthquakes. We excavated paleoseismic trenches across these strands to refine and expand their Holocene earthquake chronologies; improve estimates of earthquake recurrence, displacement, and fault slip rate; and assess whether the strands rupture separately or synchronously in large earthquakes. Paleoseismic data from the Spring Lake site expand the Holocene record of earthquakes on the northern strand: at least five to seven earthquakes ruptured the Spring Lake site at 0.9 ± 0.2 ka (2σ), 2.9 ± 0.7 ka, 4.0 ± 0.5 ka, 4.8 ± 0.8 ka, 5.7 ± 0.8 ka, 6.6 ± 0.7 ka, and 13.1 ± 4.0 ka, yielding a Holocene mean recurrence of ~1.2–1.5 kyr and vertical slip rate of ~0.5–0.8 mm/yr. Paleoseismic data from the North Creek site help refine the Holocene earthquake chronology for the southern strand: at least five earthquakes ruptured the North Creek site at 0.2 ± 0.1 ka (2σ), 1.2 ± 0.1 ka, 2.6 ± 0.9 ka, 4.0 ± 0.1 ka, and 4.7 ± 0.7 ka, yielding a mean recurrence of 1.1–1.3 kyr and vertical slip rate of ~1.9–2.0 mm/yr. We compare these Spring Lake and North Creek data with previous paleoseismic data for the Nephi segment and report late Holocene mean recurrence intervals of ~1.0–1.2 kyr for the northern strand and ~1.1–1.3 kyr for the southern strand. The northern and southern strands have similar late Holocene earthquake histories, which allow for models of both independent and synchronous rupture. However, considering the earthquake timing probabilities and per-event vertical displacements, we have the greatest confidence in the simultaneous rupture of the strands, including rupture of one strand with spillover rupture to the other. Ultimately, our results improve the surface-faulting earthquake history of the Nephi segment and enhance our understanding of how structural barriers influence normal-fault rupture.

INTRODUCTION

Purpose and Scope

The five central segments of the Wasatch fault zone (WFZ) (figure 1) trend through the most densely populated part of Utah's Wasatch Front and have the potential to generate large-magnitude (M ~6.5–7.5) surface-faulting earthquakes. These segments have been the subject of numerous paleoseismic trench investigations, which have revealed evidence of repeated middle to late Holocene earthquakes, and helped resolve the per-segment earthquake chronologies, recurrence intervals, and slip rates (see summaries in Machette and others [1992], Lund [2005], and DuRoss and others [2016a]). Here, we present new paleoseismic data for the Nephi segment, which includes two separate fault strands (the northern and southern strands) that bound the southern Wasatch Front between Payson and Nephi (figure 1).

The Nephi segment is one of the most active segments of the WFZ, having paleoseismic evidence in support of three surface-faulting earthquakes since about 2.5 ka, including a barely prehistoric most recent earthquake (~210 cal yr B.P., or ~A.D. 1740) and a short (<1.0 kyr) mean earthquake recurrence interval (Crone and others, 2014). At the time of our investigation, uncertainty in the segment's Holocene earthquake history stemmed from (1) conflicting paleoseismic data for the southern strand of the segment, (2) limited paleoseismic data for the northern strand, (3) uncertainty in the rupture extent of Holocene earthquakes on the segment, and (4) the poorly understood potential for synchronous rupture of the Nephi and Provo segments (DuRoss and others, 2008; Crone and others, 2014). For example, investigations of the southern strand identified earthquakes older than 2.5 ka, but geologic evidence in support of the earthquakes is weak and the events

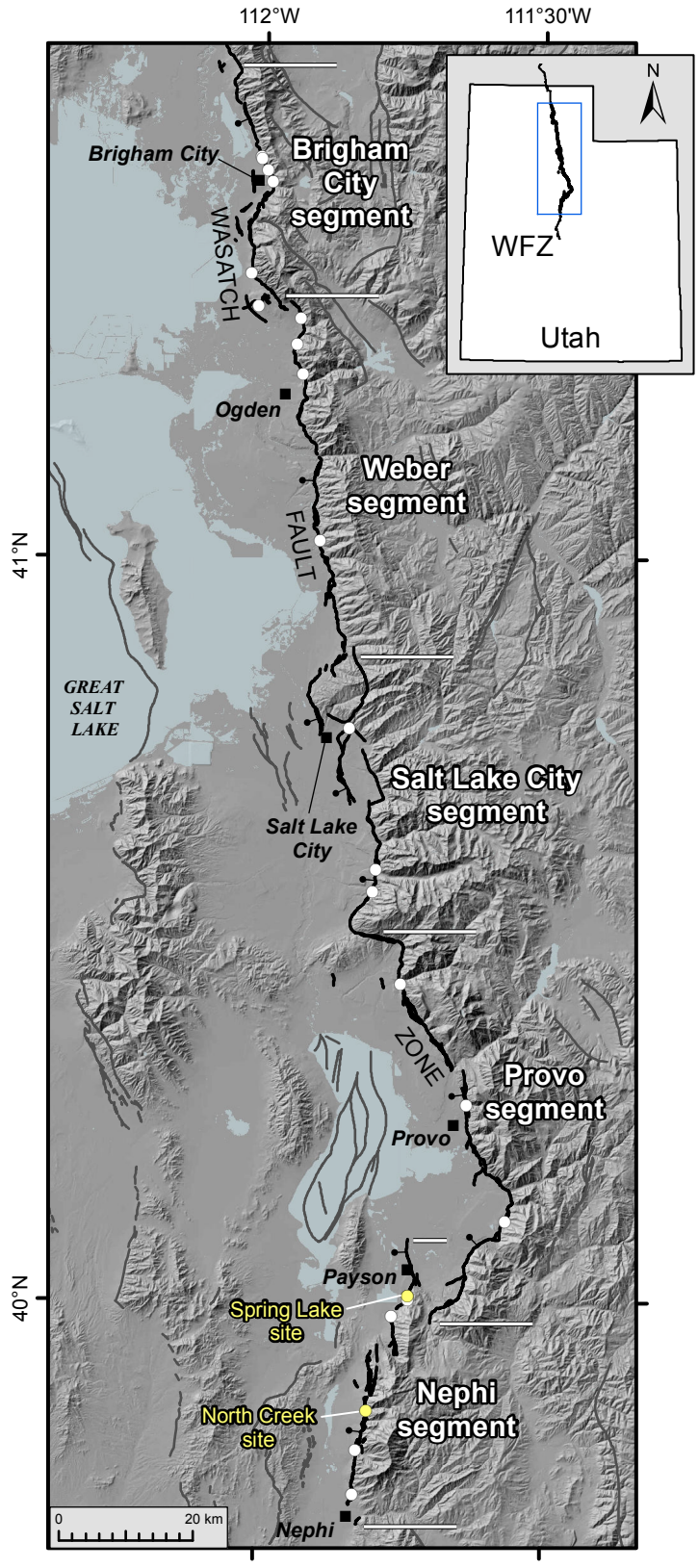

Figure 1. *Central segments of the Wasatch fault zone (WFZ) in northern Utah, which have evidence of repeated Holocene surface-faulting earthquakes. Horizontal bars show segment boundaries; circles indicate paleoseismic trench sites. Ball and bar indicates downthrown side of fault. Other Quaternary faults are shown in dark gray. Fault traces from Black and others (2003); base map is a 10-m DEM with hillshade (Utah AGRC, 2017).*

have large (~2–3 kyr) timing uncertainties. Paleoseismic data for the northern strand constrained only one or two late Holocene earthquakes. The need to resolve the history and complexity of moment release on the Nephi segment and southern WFZ, and to improve earthquake-probability forecasts and seismic-hazard assessments for the Wasatch Front region, formed the impetus for our paleoseismic study.

To refine and expand earthquake timing and displacement data for the Nephi segment, we excavated trenches at two sites—one on the northern strand at the Spring Lake site and one on the southern strand at the North Creek site (figure 2). At each site, we (1) constructed detailed topographic and geologic maps of the trench site, (2) measured scarp profiles, (3) excavated a single trench and mapped the trench-wall exposures in detail, (4) sampled organic soils for radiocarbon (^{14}C) dating and fine-grained detrital sediment for luminescence dating, (5) developed probabilistic models of earthquake timing using OxCal software (Bronk Ramsey, 1995, 2001), and (6) estimated per-event vertical displacements. Using these data, we calculated inter-event and mean earthquake recurrence intervals and vertical slip rates. We evaluate these data in the context of previous paleoseismic data and investigate the rupture history of the segment, calculate more robust mean recurrence intervals for the fault strands, and improve our understanding of independent versus synchronous rupture of the northern and southern strands. Ultimately, these results, together with a synthesis and comparison of paleoseismic data for the adjacent Provo and Levan segments, will help quantify the extent of ruptures on the Nephi segment and the segmentation of the southern WFZ.

Geologic Setting

The 350-km-long WFZ is a complex normal fault system that forms a prominent structural and topographic boundary between the actively extending Basin and Range Province to the west and the relatively more stable Middle Rocky Mountains and Colorado Plateau provinces to the east. The WFZ consists of three distinct subgroups defined using surface-faulting earthquake timing and slip rate: (1) the northern segments, composed of three segments that last ruptured prior to the highstand of Lake Bonneville (~18 ka; Oviatt and others, 1992; Oviatt, 1997) and have slow, less than ~0.1 mm/yr slip rates (Machette and others, 1992; Hylland, 2007a); (2) the central segments, comprising five segments that have evidence of recurrent Holocene surface-faulting earthquakes and ~1–2-mm/yr slip rates (Machette and others, 1992; Lund, 2005; DuRoss, 2008); and (3) the southern segments, which include two possibly Holocene-active segments that have slow, less than ~0.3 mm/yr slip rates (Machette and others, 1992; Hylland, 2007b). The central segments follow the base of the Wasatch Front between Brigham City and Nephi and include the Brigham City, Weber, Salt Lake City, Provo, and Nephi segments (figure 1).

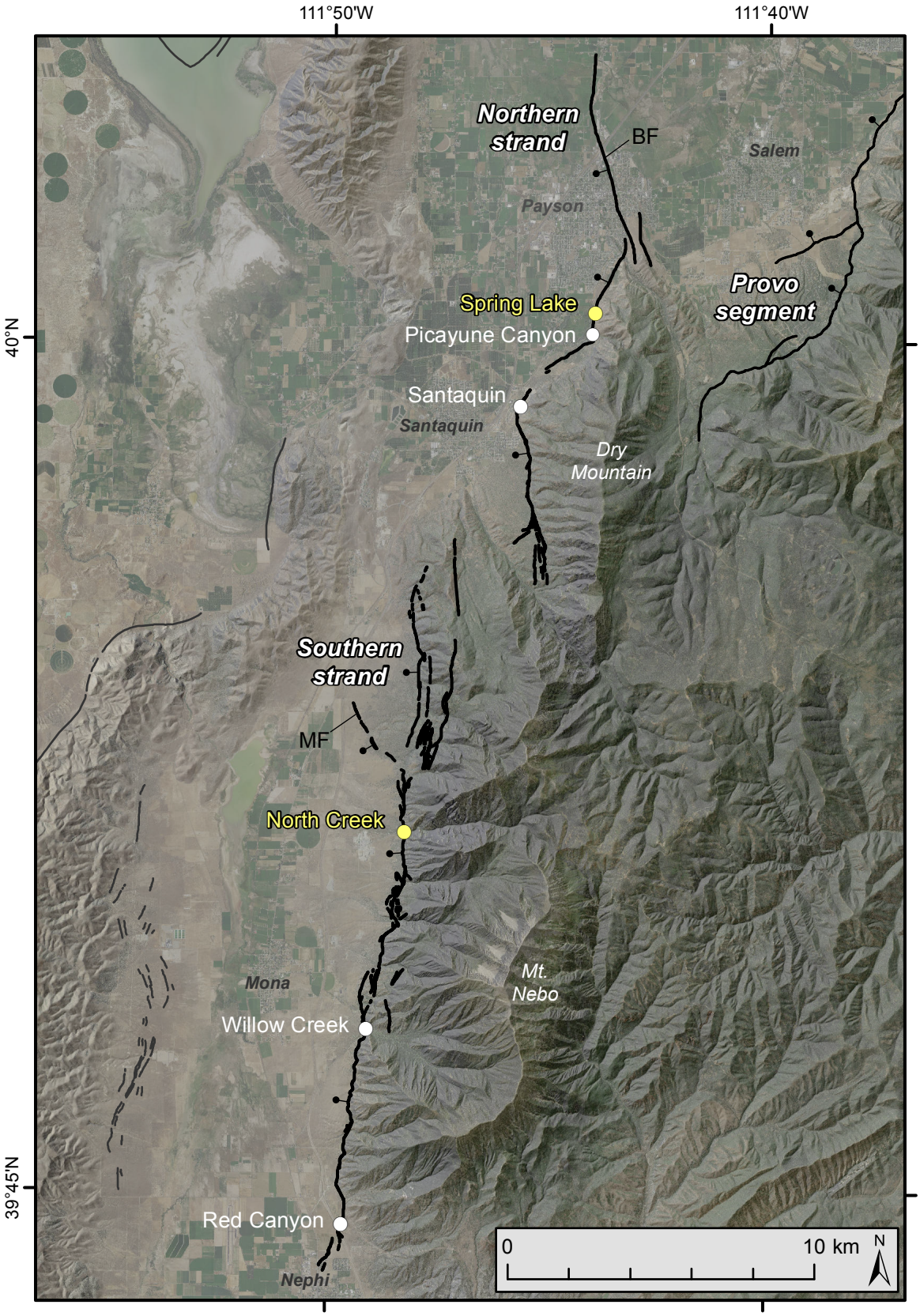

Figure 2. *Nephi segment of the WFZ, showing the northern and southern fault strands and the southern extent of the Provo segment. Ball and bar indicates downthrown side of fault. Gray faults are other Quaternary faults in the area (all fault traces from Black and others, 2003). Circles indicate paleoseismic trench sites: white – previous investigations; yellow – this study. BF – Benjamin fault, MF – Mendenhall fault. Base map is 2014 NAIP aerial photography (USDA, 2017) overlain on a 10-m DEM with hillshade (Utah AGRC, 2017).*

The Nephi segment has a complex, north-trending fault trace that bounds the west side of the Wasatch Range and, together with the southernmost Provo segment, forms a prominent right-stepping relay ramp in the trace of the WFZ (figure 1). The Nephi segment comprises two separate fault strands—the northern and southern strands, which have Holocene surface traces separated by a 4-km-wide right step (figure 2). The southern strand terminates 6 km north of surface faulting on the Levan segment to the south (Machette and others, 1992; Hylland and Machette, 2008; Hiscock and Hylland, 2015), whereas the northern 12 km of the northern strand overlaps with the southern 13 km of the Provo segment to the east, forming a 5–9-km right step in the trace of the WFZ (Machette, 1992; Machette and others, 1992). From the northern terminus of the northern strand to the southern terminus of the southern strand, the Nephi segment is 43 km long (all length measurements in this section are linear, end-to-end).

The northern strand is 17 km long and bounds the west side of Dry Mountain (3006 m [9865 ft] elevation), which has about 1.2 km of vertical relief (figure 2). The 7-km-long, west-dipping Benjamin fault (Hintze, 1973; Machette, 1992; Solomon and others, 2007) makes up the northern part of the northern strand. Based on small, 1–2-m-high scarps in Lake Bonneville lacustrine deposits and the lack of uplifted bedrock in its footwall (Machette, 1992), the Benjamin fault presumably has a slow slip rate or young (Holocene?) time of initial faulting. In addition, Machette (1992) and Solomon and others (2007) only mapped scarps along the northern 1.0–2.5 km and southern 1.0–1.5 km of the Benjamin fault; the 3–5-km-long center of the fault is concealed by Holocene stream and alluvial-fan sediments near Payson. South of the Benjamin fault, north- to northeast-oriented fault scarps, some of which form a complex zone of several overlapping and right-stepping scarps, follow a 2-km-wide right step in the range front. The southern part of the northern strand bounds Dry Mountain and consists of north-south-oriented scarps across Holocene alluvial-fan surfaces having 4–7 m of vertical offset (DuRoss and Bruhn, 2005). The majority of fault scarps on the northern strand are below the Lake Bonneville highstand shoreline (~1550 m [5100 ft]; Solomon and others, 2007) and near or above the Provo-phase shoreline (~1440–1450 m [4740–4760 ft]; Solomon and others, 2007). These shorelines provide a latest Pleistocene datum: regression from the highstand shoreline to the Provo-phase shoreline (~110 m drop during the Bonneville Flood) occurred at ~18 ka (Oviatt and others, 1992; Reheis and others, 2014; Oviatt, 2015), and the lake occupied the Provo-phase level until about 15 ka (Godsey and others, 2005, 2011). Scarps on the southernmost part of the northern strand are above the highstand shoreline.

The 25-km-long southern strand bounds the west side of the Wasatch Range (figure 2) near Mount Nebo, which, at 3635 m (11,928 ft) elevation, has 1.8 km of vertical relief and is the highest peak in the Wasatch Range. The southern strand has a mostly linear, north-south-oriented fault trace that is locally complex, including multiple parallel and anastomosing scarps. The southern strand includes a 4-km-long southwest-dipping fault (the Mendenhall fault of DuRoss, 2004) that branches to the northwest and continues 2 km west of the range front. Similar to the Benjamin fault, the Mendenhall fault lacks uplifted bedrock exposures in its footwall and may have either a slow slip rate or relatively young (latest Pleistocene to Holocene?) time of initial faulting. At the southern end of the southern strand, short (<1 km) and disconnected scarps both north and southeast of the city of Nephi mark the southern terminus of the Nephi segment. Scarps along the southern strand are above the elevation of the Bonneville highstand shoreline.

Machette and others (1992) postulated that a northeast-trending and northwest-dipping normal fault within the bedrock of the Wasatch Range (Davis, 1983; Witkind and Weiss, 1985; Harty and others, 1997) provides a connection between the northern and southern strands. However, DuRoss (2004) and DuRoss and Bruhn (2005) used fault geometry coupled with the geomorphology and estimated initiation ages of fault scarps to conclude that the step-over between the strands is a structural boundary that may have impeded some Holocene surface ruptures. More recently, DuRoss and others (2008) and Crone and others (2014) analyzed differences in paleoseismic earthquake chronologies for the northern and southern strands and raised questions as to whether the fault strands rupture together or are separate sources of large earthquakes. An additional possibility is that the northern strand could rupture synchronously with the Provo segment. At the time of this study, existing paleoseismic data were insufficient to resolve the rupture extent of surface-faulting earthquakes on the Nephi segment.

Previous Paleoseismic Investigations

Previous paleoseismic data for the Nephi segment fall into three categories: (1) early trench investigations (North Creek and Red Canyon sites; table 1; figure 2) that revealed evidence of multiple surface-faulting earthquakes, but resulted in poorly constrained event times because of large dating uncertainties (e.g., bulk-soil ages and conflicting ^{14}C and luminescence ages); (2) more recent investigations that used modern dating methods (e.g., accelerator mass spectrometry [AMS] dating of charcoal) and OxCal modeling, but were only able to constrain the timing of earthquakes younger than about 2.5 ka (Willow Creek and Santaquin sites; table 1; figure 2); and (3) trenches excavated for educational purposes (geology field courses) (the Picayune Canyon site; table 1; figure 2) that have limited documentation. These previous data are summarized here. For additional discussions see DuRoss and others (2008) and Crone and others (2014). OxCal models of the North Creek, Red Canyon, Willow Creek, and Santaquin sites are included in Crone and others (2014) and DuRoss and others (2016a, 2016b).

Surface-faulting earthquakes identified at sites along the Nephi segment are referred to using their site abbreviation and an earthquake number (e.g., 1 being the youngest event). For example, the youngest earthquake at the North Creek site is NC1.

Table 1. *Summary of previous earthquake timing data for the Nephi segment.*

Northern strand		Southern strand			Segment-wide
Picayune Canyon[1]	Santaquin[2]	North Creek[3]	Willow Creek[4]	Red Canyon[5]	Segment chronology[6]
~2.5 ka	0.5 ± 0.1 ka	0.4 ± 0.5 ka	0.2 ± 0.1 ka	0.5 ± 0.5 ka	0.2 ± 0.1 ka
~3.5 ka	*NE*	1.4 ± 0.3 ka	1.2 ± 0.1 ka	1.2 ± 0.3 ka	1.2 ± 0.1 ka
NE	-	1.9 ± 0.5 ka	1.9 ± 0.6 ka	*NE*	2.0 ± 0.4 ka
-	-	*NE*	4.7 ± 1.8 ka	4.7 ± 2.7 ka	4.7 ± 1.8 ka

[1] Based on preliminary data from Horns and others (2009); referred to as the Picayune Canyon site to avoid confusion with the Spring Lake site (this study).

[2] Based on the OxCal model reported in DuRoss and others (2008). DuRoss and others (2016a) include an alternative model with an earthquake time of 0.3 ± 0.2 ka.

[3] Based on the OxCal model reported in Crone and others (2014), using numerical data from Hanson and others (1981, 1982).

[4] Based on numerical data and the OxCal model of Crone and others (2014).

[5] Based on the OxCal model reported in Crone and others (2014) using numerical data from Jackson (1991).

[6] Segment-wide chronology developed for the Nephi segment (using southern-strand data) for the Working Group on Utah Earthquake Probabilities and reported in Crone and others (2014).

NE – not exposed.

North Creek Site

Hanson and others (1981, 1982; included in Bowman and Lund, 2013) excavated trenches at the North Creek (NC) site on the southern strand (figure 2), but limited and conflicting numerical ages raised concerns regarding the Holocene earthquake chronology (Lund, 2005). Hanson and others (1981, 1982) found colluvial-wedge evidence of the most recent earthquake (NC1), but were only able to date organics from a soil within the faulted late Holocene fan deposits that predate this colluvial wedge, thus loosely constraining NC1 to <0.8–1.2 ka. An older earthquake (NC2) also ruptured the site; however, seven ^{14}C ages for a soil A horizon developed on the NC2 colluvial wedge yielded conflicting ages clustering at ~1.3–1.4 ka and ~3.7–4.1 ka. Hanson and others (1981, 1982) preferred the older age estimates for the timing of NC2; however, DuRoss and others (2008) and Crone and others (2014) noted that the more recent earthquake time (~1.4 ka) is also possible and more consistent with the ages for overlying alluvial-fan deposits. Hanson and others (1981, 1982) did not find stratigraphic evidence for older earthquakes in their trenches, but used a footwall terrace riser and a ^{14}C age for a charcoal sample from a natural exposure of footwall fan sediments (Bucknam, 1978; included in Bowman and Lund, 2013) to constrain the time of an earthquake (NC3) to less than ~5.3 ka. Using additional soil ages (~2.2 ka) from the hanging wall (Hanson and others, 1981, 1982), Crone and others (2014) reported an NC3 time of ~1.9 ka. Per-event vertical displacements are 2.0–2.5 m for NC2 and 2.0–2.2 m for NC1 (Hanson and others, 1981; DuRoss, 2008).

Red Canyon Site

Jackson (1991) excavated a trench at the Red Canyon (RC) site near the southern terminus of the southern strand (figure 2). Jackson (1991) found evidence of three surface-faulting earthquakes; however, conflicting ^{14}C and thermoluminescence (TL) ages complicate the earthquake-timing interpretation. The most recent earthquake (RC1) occurred after 1.3–1.5 ka, but the event is not limited by a minimum constraint. Jackson (1991) reported conflicting ^{14}C and TL ages that constrain the second earthquake (RC2) to either ~1.1–1.7 ka or ~3.8 ka. Jackson (1991) considered the 1.1–1.7-ka ages too young and interpreted an RC2 time of ~3.0–3.5 ka; however, similar to North Creek, the ~1.1–1.7-ka earthquake time is possible. Jackson (1991) found colluvial-wedge evidence for the oldest earthquake at the Red Canyon site (RC3). A ^{14}C age on soil organics from the scarp colluvium provided a minimum time of ~3.6 ka; however, RC3 is not constrained by a maximum age. Per-event vertical displacements for RC3, RC2, and RC1 are 1.4–2.0 m, 1.3–1.7 m, and 1.1–1.7 m, respectively (Jackson, 1991).

Willow Creek Site

A more recent trench investigation on the southern strand at the Willow Creek (WC) site (Machette and others, 2007; Crone and others, 2014) (figure 2) improved the post-2.5 ka earthquake chronology of the southern strand. Crone and others (2014) reported three surface-faulting earthquakes constrained

by optically stimulated luminescence (OSL) and ^{14}C ages: WC1 at ~0.3 ka, WC2 at ~1.2 ka, and WC3 at ~2.0 ka. These data yield a relatively short mean earthquake recurrence interval of ~0.9 kyr (WC3–WC1), which is considerably shorter than ~1.3–1.5-kyr mean estimates for other WFZ segments (Lund, 2005, 2013). Crone and others (2014) also reported scarp-offset evidence of at least one older earthquake (WC4); however, stratigraphic (e.g., colluvial-wedge) evidence of the earthquake(s) was not exposed in the trenches. Using the WC3 time range and OSL ages for sediments exposed in the footwall of the fault, WC4 is broadly constrained to about 2.9–6.5 ka (Crone and others, 2014). Using the total displacement of 7.1 ± 0.2 m across the Willow Creek site, the average per-event vertical displacement for WC3–WC1 is 2.4 m (Crone and others, 2014).

Santaquin Site

DuRoss and others (2008) excavated trenches across a scarp on the northern strand at the Santaquin (SQ) site (figure 2) and constrained the timing of a single surface-faulting earthquake. SQ1 occurred at 0.5 ± 0.1 ka (DuRoss and others, 2008), or 0.3 ± 0.2 ka if a minimum limiting age (of 0.4 ka that is very close in age to the faulted soil) is excluded. DuRoss and others (2008) did not find geologic evidence for older events at this site, but ^{14}C ages suggest the next older event occurred before ~1.5 ka (based on a soil-A-horizon age from within alluvial-fan sediments) and possibly prior to ~5–6 ka (using detrital-charcoal ages from alluvial-fan sediments). SQ1 had 3.0 ± 0.2 m of vertical displacement (DuRoss and others, 2008).

Picayune Canyon Site

Horns and others (2009) excavated a trench across a prominent scarp at the mouth of Picayune Canyon (PC; figure 2), ~3 km northeast of the SQ site, and 0.7 km south of the Spring Lake site (this study). Crone and others (2014) refer to this site as the Spring Lake site; however, to avoid confusion we herein refer to it as the Picayune Canyon site. Horns and others (2009) reported earthquake times of ~2.5 ka (PC1) and ~3.5 ka (PC2) based on ^{14}C ages for soils faulted and buried by scarp-derived colluvium. Although the soil ages may reflect the approximate earthquake times, it is important to note that these earthquakes do not have minimum age constraints. Horns and others (2009) reported a vertical displacement of 3 m for PC1, but did not report a displacement for PC2. However, both events postdate the faulted late Holocene alluvial-fan surface, which has 3 m of vertical offset (Machette, 1992). Thus, attributing the 3-m displacement to both events, PC1 and PC2 may have had ~1.5 m of vertical displacement each.

OVERVIEW AND METHODS

Trench Investigations

We identified trench sites on the Nephi segment using (1) fault-trace and surficial-geologic mapping by Machette (1992) and Harty and others (1997); (2) our interpretation of 1970s (low-sun-angle) aerial photographs (Cluff and others, 1973; included in Bowman and others, 2015) and 2006–11 orthophotography from the National Agricultural Imagery Program (NAIP) (U.S. Department of Agriculture [USDA], 2017; hosted by the Utah Automated Geographic Reference Center [Utah AGRC], 2017); (3) 2008 (EarthScope) and (State of Utah) lidar data for the Nephi segment (hosted by Open Topography, 2016); and (4) field reconnaissance. We also considered the discussions and analyses of Nephi-segment paleoseismic data by the Utah Quaternary Fault Parameters Working Group (UQFPWG; e.g., Lund, 2005) and Working Group on Utah Earthquake Probabilities (e.g., Lund, 2010) prior to selecting preferred sites. We selected two sites—the Spring Lake site on the northern strand and the North Creek site on the southern strand—for their moderately large (~8 m high) scarps that were relatively unmodified by human activity and crossed approximately mid-Holocene or older alluvial-fan deposits.

Spring Lake Site

At the Spring Lake (SL) site, on the central part of the northern strand, a prominent, ~6–8-m-high, west-facing scarp crosses a post-Bonneville alluvial-fan surface (Machette, 1992). The fan surface and fault scarp are below the Bonneville highstand shoreline, but above the Provo shoreline. We chose the site because of the simple fault trace geometry and moderately large height of the fault scarp, and minimal evidence of cultural disturbance based on the 1970s and 2006–11 aerial photographs.

We excavated a 36-m-long and less than 4-m-deep trench at the Spring Lake site in May 2012. To map the exposures, we constructed a 1-m-square grid using an electronic distance meter (Trimble TTS 500) (projecting points to an average, vertical plane parallel to the trench wall). We photographed the trench, and then color-balanced, cropped, and rectified the photos. To create photomosaics, we tiled the photos for both the northern and southern walls of the trench. Using the photomosaics as a base map, we mapped key stratigraphic contacts and faults observed in both trench walls at 1:20 scale on clear film. Plate 1 (Spring Lake north wall) and plate 2 (Spring Lake south wall) include map and photomosaic digital overlays of the exposures with a single, local coordinate system, referenced herein using horizontal (h-) and vertical (v-) meter marks. For example, the fault zone is exposed in the north wall at h-25 m, v-7 m (plate 1). Stratigraphic units are described in appendix A.

North Creek Site

The North Creek (NC) site is on the north-central part of the southern strand, where a prominent, ~9-m-high, west-facing scarp crosses a Holocene alluvial-fan surface (Harty and others, 1997). The North Creek site is above the Bonneville highstand shoreline. We chose the site because of the simple fault trace geometry and moderately large height of the fault scarp, and because the site had minimal evidence of cultural distur-

bance based on the 1970s and 2006–11 aerial photographs. In addition, North Creek is the site of the original (1978) paleoseismic investigation by Hanson and others (1981, 1982), and thus, the site represented an opportunity to apply more modern trench-excavation and dating techniques and possibly resolve conflicting numerical ages for the earliest Nephi-segment earthquakes.

We excavated a 40-m-long and less than 4-m-deep trench at the North Creek site in May 2012. Similar to the Spring Lake site, we photographed, created photomosaics, and photomapped the North Creek trench exposures. However, because of difficulty accessing the upper part of the south wall, we limited our photomosaics and mapping to the entire north wall and lowermost part (from the fault zone to the west) of the south wall. Plate 3 (North Creek north wall) and plate 4 (North Creek south wall) include map and photomosaic digital overlays of the exposures with a single, local coordinate system, referenced herein using horizontal (h-) and vertical (v-) meter marks. For example, the fault zone exposed in the south wall is at h-21.5 m, v-2.0 m (plate 4). Stratigraphic units are described in appendix B.

Numerical Dating

Radiocarbon Dating

We sampled bulk soil A-horizon sediment (appendix C) and radiocarbon (^{14}C) dated discrete fragments of soil charcoal (appendices D and E) to estimate the ages of buried soil A horizons and constrain the timing of paleoearthquakes. For discussions of common sources of uncertainty in radiocarbon dating and paleoseismic studies, see Nelson and others (2006) and DuRoss and others (2011). To increase the likelihood of dating locally derived charcoal (e.g., sagebrush) rather than non-local (detrital) charcoal (e.g., a conifer fragment transported long distance from higher elevations), PaleoResearch Institute (Golden, Colorado) separated and identified (if possible) charcoal fragments from the bulk A-horizon sediment samples. Locally derived charcoal fragments are more likely burned in place or very close by, and thus their ^{14}C ages are likely a close representation of the sampled deposit. Detrital charcoal fragments (e.g., conifer from above the elevation of the site) are more likely to have experienced an unknown duration of downhill transport, and thus their ^{14}C ages could overestimate the age of the sampled deposit (e.g., Puseman and Cummings, 2005). For each sample, small, unidentified fragments were recombined into samples of at least ~0.5 mg, which then yielded composite charcoal ages.

We had partial success in identifying charcoal fragments (appendix C). At the Spring Lake site, only 2 of 23 individual charcoal samples could be identified, including *Artemisia* (flowering plants such as sagebrush) and *Asteraceae* (sunflower family) charcoal. At the North Creek site, 11 of 22 charcoal samples were identified and included *Asteraceae*, *Quercus* (oak), *Juniperus*, and *Pseudotsuga menziesii* (Douglas fir) charcoal. We preferentially dated the *Asteraceae* and *Quercus* charcoal samples over the longer-lived *Juniperus* and *Pseudotsuga menziesii* samples. The remaining Spring Lake and North Creek samples only produced collections of small, unidentified charcoal fragments.

We submitted the charcoal samples to the National Ocean Sciences Accelerator Mass Spectrometry (NOSAMS) Facility of the Woods Hole Oceanographic Institution (Woods Hole, Massachusetts) for AMS ^{14}C dating. We report the radiocarbon ages as the mean and two-sigma (2σ) uncertainty rounded to the nearest century in thousands of calendar years before present (ka) (where present is A.D. 1950) using the Reimer and others (2013) terrestrial calibration curve applied in OxCal (Bronk Ramsey, 1995, 2001).

Luminescence Dating

We used optically stimulated luminescence (OSL) dating to estimate burial ages of lacustrine and colluvial-wedge sediments at both sites (appendices F and G). OSL dating relies on the cumulative dose of in situ natural radiation in sediment (e.g., quartz grains) to estimate the time when the sediment was last exposed to sunlight prior to deposition and burial (Huntley and others, 1985). Ideally, the sunlight exposure was sufficiently long (at least several seconds to minutes; Gray and others, 2015) during erosion and transport to fully reset or "zero" any preexisting luminescence signal in the grains, and thus the luminescence age should represent the time when the sediment was deposited (Aitken, 1994). If the sediment's exposure to sunlight was not long enough to fully zero the sediment (e.g., because of rapid deposition, a short travel path, or filtered light in turbid water), then it may retain an inherited luminescence signal (Duller, 2008), which results in an overestimated (maximum) age for the deposit. In contrast, underestimated (minimum) ages result if the luminescence signal becomes saturated, where the signal does not increase despite continued exposure of the sediment to radiation (Duller, 2008). Saturation results in a maximum age limit for OSL dating of ~75–300 ka, depending on the radiation dose rate and mineral dated (Duller, 2008; Rhodes, 2011).

Our luminescence samples were processed at the U.S. Geological Survey Luminescence Dating Laboratory (Denver, Colorado). Background radiation from potassium, uranium, and thorium was measured in the field using a portable gamma-ray spectrometer. Samples for field moisture were sealed in the field and measured in the laboratory. We report OSL ages as the mean and one-sigma (1σ) uncertainty rounded to the nearest decade (appendices F and G). However, where discussed in the text, the error is doubled (2σ rounded to the nearest century) for continuity with the calendar-calibrated radiocarbon ages and the modeling of earthquake times in OxCal. In discussing the OSL ages, we report the ages in thousands of years before the sample processing date (2012) (ka) and do not account for the 62-year difference in the OSL sample date (2012) versus the reference standard for

^{14}C (1950). This difference is minor compared to the large OSL age uncertainties (between 0.3 and 1.9 kyr at 2σ). Importantly, this 62-year difference is taken into account in our modeling of earthquake times in OxCal.

OxCal Modeling Methods

To evaluate earthquake timing, we used OxCal radiocarbon calibration and analysis software (version 4.2; Bronk Ramsey, 1995, 2001; using the IntCal09 calibration curve of Reimer and others, 2013). OxCal probabilistically models the timing of undated events (e.g., earthquakes) by weighting the time distributions of chronological constraints (e.g., radiocarbon and OSL ages and historical constraints) included in a stratigraphic model (Bronk Ramsey, 2008, 2009). The program uses a Markov Chain Monte Carlo sampling method (Bronk Ramsey, 1995, 2001) to generate a probability density function (PDF) for each undated event in the model (i.e., the likelihood that an earthquake occurred at a particular time) using the chronologic and stratigraphic constraints. For more detailed discussions of the application of OxCal modeling to paleoseismic data, see Lienkaemper and Bronk Ramsey (2009) and DuRoss and others (2011).

OxCal depositional models for the Spring Lake and North Creek sites (appendix H) use stratigraphic ordering information, radiocarbon and OSL ages, and a historical constraint that no large surface-faulting earthquakes (M ~6.5+) have occurred since pioneer settlement of the region (1847) to define the time distributions of earthquakes identified at the site. Where necessary, we removed numerical-age outliers using geologic judgment (knowledge of sediments, soils, and sample contexts), the degree of inconsistency with other ages in the model for comparable deposits (e.g., stratigraphically inverted ages), and agreement indices for the original (unmodeled) and modeled numerical ages and the OxCal model as a whole (Bronk Ramsey, 1995, 2008). We report earthquake times for each site as the mean and ~2σ uncertainty in thousands of calendar years before present (ka) rounded to the nearest century. For earthquakes having skewed (highly asymmetric) time distributions, we also report the mode (peak of the probability distribution) and 95% confidence interval. For skewed distributions, the mode better characterizes the earthquake time than the mean or median values, which are influenced by the tail of the time distribution.

SPRING LAKE TRENCH SITE

Surface Faulting and Geology

The Spring Lake site is located on the north-central part of the northern strand, where a moderately large, north-trending scarp offsets a small (~0.02 km^2) post-Bonneville alluvial-fan surface that is inset below Lake Bonneville transgressive and highstand sediments (Machette, 1992) (figures 3 and 4). The Spring Lake scarp, discontinuous scarps north and south of the site, and the Benjamin fault together make up the northern part of the northern strand that forms an en echelon right step with the Provo segment (figure 2). The Spring Lake site is between ~1470 and 1510 m (~4800–5000 ft) elevation, below the Bonneville highstand shoreline (locally ~1500 m; ~5100 ft) and above the Provo shoreline (locally ~1440–1450 m; 4740–4760 ft) (based on mapping by Solomon and others, 2007).

Surficial geology near the Spring Lake site is dominated by Lake Bonneville lacustrine sediments and related geomorphic features, and post-Bonneville alluvial-fan deposits. Deposits associated with the Lake Bonneville highstand include sand to coarse gravel that form wave-built terraces. The post-Bonneville alluvial fan surface slopes gently west and is underlain by stream and debris-flow sediments derived from a ~0.8 km^2 drainage basin cut in the Mississippian limestone bedrock of the Wasatch Range to the east and deposited into a small canyon incised into the Lake Bonneville sediments (Solomon and others, 2007).

The Nephi segment is expressed at the Spring Lake site as a single, prominent, ~100-m-long by 8-m-high, west-facing scarp (figures 5 and 6). Locally, both the fault scarp and the uplifted fan surface have been incised by recent (late Holocene?) stream and debris flows. We estimate 5.0 m of vertical surface offset across the scarp based on a 130-m-long profile (figure 6); however, based on the trench stratigraphy (discussed below), it is unlikely that the fan surfaces above and below the scarp are contemporaneous.

Trench Stratigraphy and Structure

The Spring Lake trench exposed the WFZ and three distinct sedimentary packages: Lake Bonneville lacustrine sediments, post-Bonneville alluvial-fan deposits, and scarp-derived colluvium (colluvial wedges). In the footwall of the fault, Lake Bonneville transgressive and highstand lacustrine sediments are overlain by post-Bonneville stream and debris-flow deposits. In the hanging wall, presumably younger, post-Bonneville alluvial-fan sediments are interfingered with scarp-derived colluvial wedges deposited adjacent to the WFZ (figure 7; plates 1 and 2). Although we found similar stratigraphic units in the north and south walls of the trench, we discuss sedimentary units (with the exception of colluvial wedges) as either those on the north wall (e.g., N1c), south wall (e.g., S1c), or for the trench as a whole (e.g., N1c/S1c). Colluvial wedges have a single unit designation for both walls (e.g., C1).

Lake Bonneville Sediments

The oldest units exposed at the Spring Lake site are in the footwall of the Wasatch fault and consist of lacustrine sediments deposited during the transgression and highstand of Lake Bonneville. The lacustrine package comprises a distinct fining-upward sequence of interbedded gravel and sand (units

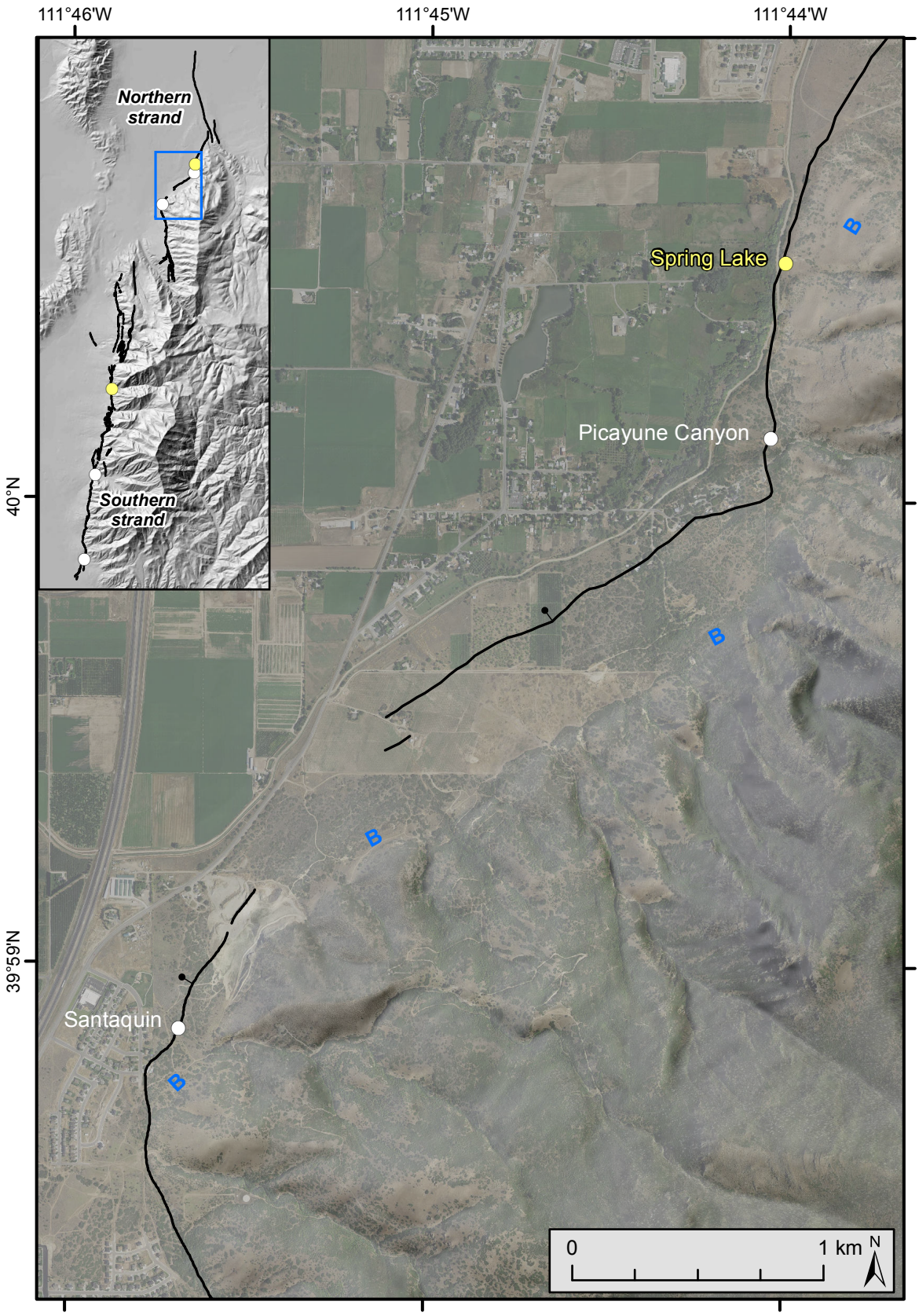

Figure 3. *Northern strand of the Nephi segment showing the Spring Lake and adjacent trench sites. Ball and bar indicates downthrown side of fault. Fault traces from Black and others (2003) show the approximate location of the WFZ. B indicates highstand shoreline of Lake Bonneville. Base map is 2014 NAIP aerial photography (USDA, 2017) overlain on a 10-m DEM with hillshade (Utah AGRC, 2017).*

Figure 4. *Spring Lake site on the northern strand of the Nephi fault segment. (A) View to the east of the alluvial fan (white dashed lines) inset into Lake Bonneville highstand sediments on the footwall of the WFZ (red line). The Spring Lake site is below the Lake Bonneville highstand shoreline and above the elevation of the Provo shoreline (not shown). (B) Excavation of the Spring Lake site. The scarp shown is approximately 8 m high. View to the southeast.*

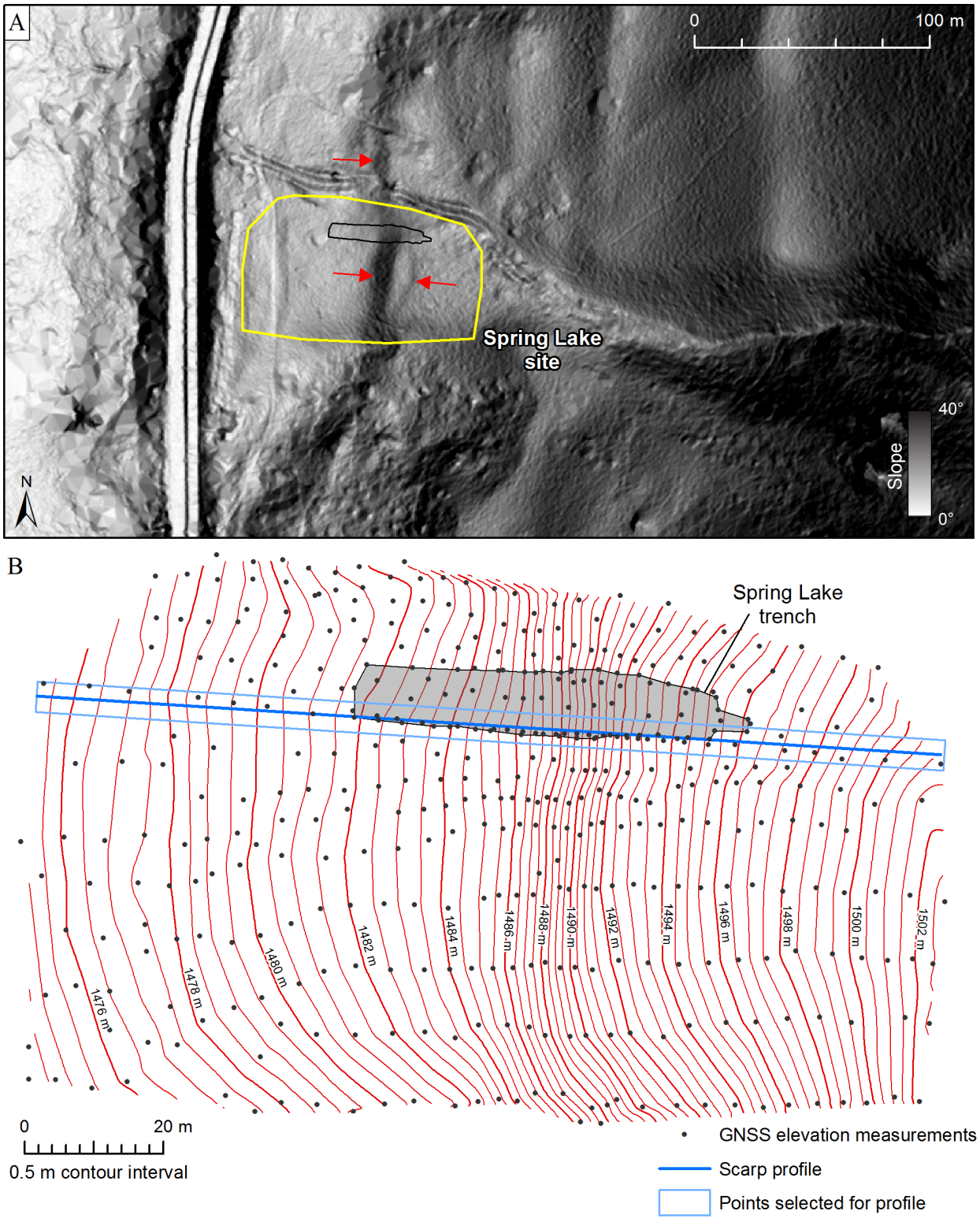

Figure 5. *Spring Lake site shown on (A) 2013–2014 lidar slopeshade map, and (B) topographic map based on high-precision GNSS data measured prior to trench excavation. Red arrows indicate Wasatch fault scarps. Gray filled polygon indicates extent of the Spring Lake trench; blue line indicates scarp profile (figure 6). Contours interpolated from a triangulated irregular network (TIN) generated using the point elevation data.*

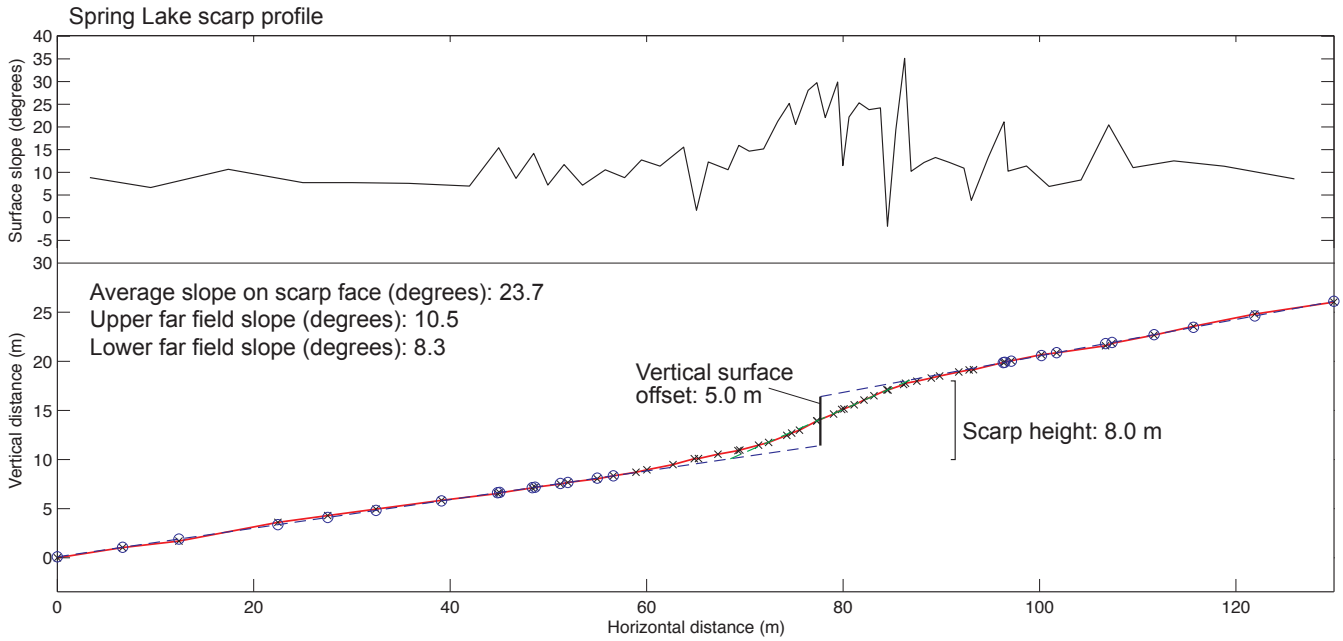

Figure 6. *Scarp profile measured across the Spring Lake site. Profile points (blue X's) measured using high-precision GNSS; vertical distance is relative to the minimum surface elevation at the site (1475 m above mean sea level). Upper panel shows surface slope measured at midpoint distances between profile points. On lower panel, blue circles indicate profile points selected for footwall and hanging wall surface-slope measurements. Vertical surface offset is the vertical separation of these projected surfaces, measured at the horizontal midpoint of the maximum scarp slope (green dashed line). Scarp height is the vertical distance between the intersections of the maximum scarp slope (dashed green line) with the footwall and hanging wall surface-slope projections (dashed blue lines).*

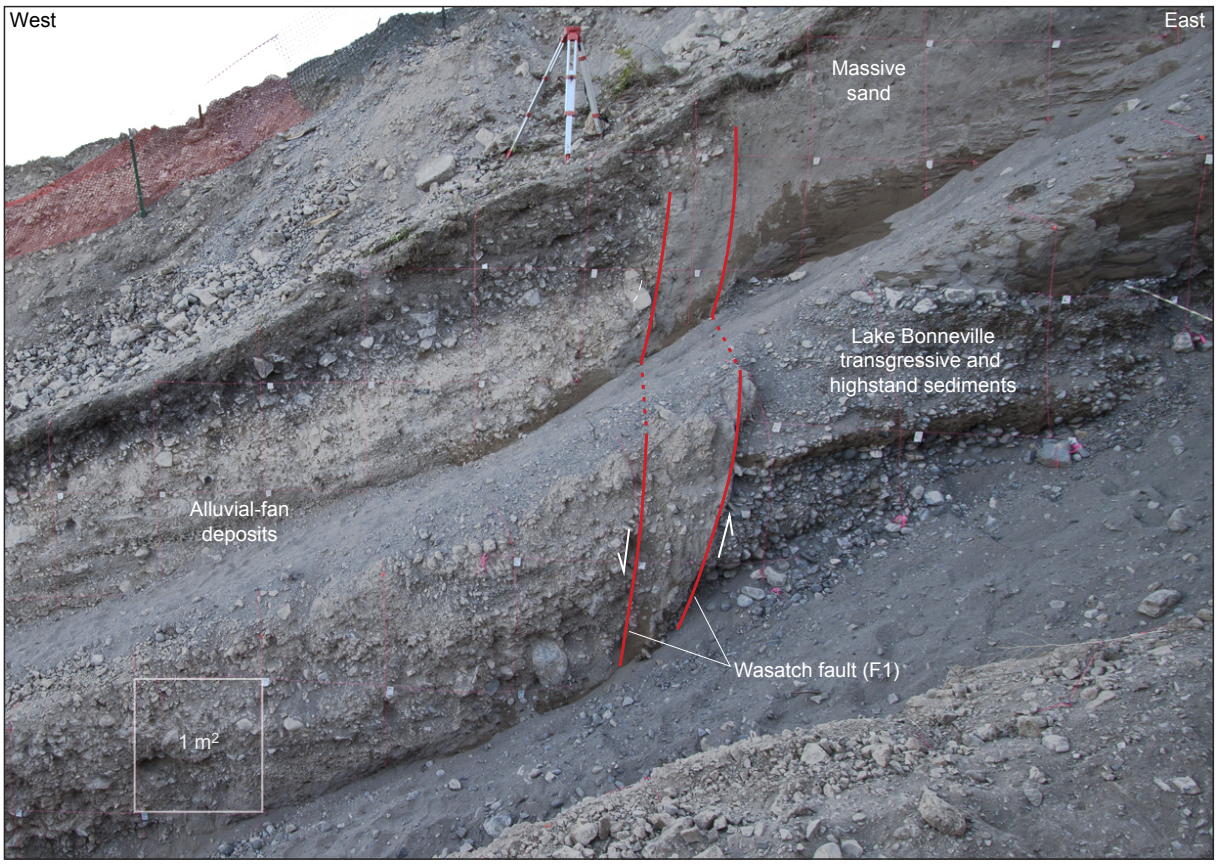

Figure 7. *North wall of the Spring Lake trench showing the main traces of the WFZ (fault F1) that juxtapose Lake Bonneville lacustrine sediments in the footwall with post-Bonneville alluvial-fan deposits in the hanging wall.*

N1a and S1a) overlain by thinly bedded medium- to fine-grained sand (units N1b1 and S1b1). The sand and gravel units are overlain by sand-rich units N1b2 and S1b2, which have remnants of bedding but are locally massive, and units N1c and S1c, which do not have preserved bedding. These units are overlain by a poorly sorted, boulder-rich deposit (units N1d and S1d). Although units N1b2/S1b2, N1c/S1c, and N1d/S1d were likely deposited in a subaerial environment (see discussion below), possibly thousands of years after the lacustrine package, these deposits are largely derived from the lacustrine units, and thus, we discuss them as part of the Lake Bonneville sedimentary package.

Units N1a/S1a and N1b1/S1b1 are sediments deposited during the transgression and highstand of Lake Bonneville. The units slope gently west, are each at least 2 m thick, and mostly consist of well-rounded gravel clasts and interbedded sand (units N1a/S1a) conformably overlain by continuous well-bedded sand (units N1b1/S1b1). These units are extensively faulted by west-dipping normal faults, which we could not trace into the generally more massive unit N1b2 in the north wall. However, in the south wall, these faults clearly displace units S1a and S1b1, but not S1c or S1d1. Units N1b1/S1b1 included a laterally continuous, 1–2-cm-thick clay interbed (blue lines at h-18–22 m, plates 1 and 2) that we used to measure fault displacement internal to the footwall. In the north wall, an OSL sample for the well-bedded fine sand (unit N1b1; sample SL-L9) yielded an age of 17.3 ± 1.9 ka (2σ). This age corresponds well with the age of the latest highstand occupation (Bonneville Flood) of 18 ka (Reheis and others, 2014; Oviatt, 2015).

Units N1b1/S1b1 are overlain by units N1b2/S1b2 and N1c/S1c, which include Bonneville lacustrine sand (of an origin similar to N1b1/S1b1) that has likely been remobilized by eolian or slope-wash processes or disturbed by bioturbation and weathering (e.g., soil creep and freeze-thaw processes) after Lake Bonneville fell below the elevation of the Spring Lake site. We do not consider remobilization by water (e.g., sheet flooding) likely due to the limited stratification. An OSL age of 10.0 ± 1.2 ka (sample SL-L8) for unit N1c indicates deposition in a subaerial (post-Bonneville) environment. A wind-blown origin for units N1b2/S1b2 and N1c/S1c is most likely considering the well-sorted and massive character of the unit and the unimodal distribution of OSL ages for grains in sample SL-L8, which does not show evidence of sediment mixing (e.g., multiple age populations from grains having inherited ages). Furthermore, the massive sand appears to have draped the local scarp-derived(?), erosional paleotopography based on the observation that units N1b2 and N1c and their basal contacts are subparallel to the modern-day scarp surface, rather than the gentle, west-sloping, undisturbed Bonneville unit contacts (N1a–N1b1 and within N1b1; h-19–25 m; plate 1). Units N1b2/S1b2 and N1c/S1c each have maximum thicknesses of about 1 m.

Units N1d/S1d likely represent a post-Bonneville debris flow sourced from nearshore (beach?) deposits originally deposited above the elevation of the site. Units N1d/S1d postdate the massive and possibly eolian sand of unit N1c in the north wall (h-19 m, v-11 m; plate 1), for which we have an OSL age of ~10 ka. The dramatic change in thickness from the south wall (~0.5 m; h-16 m, v-10.5 m, plate 2) to the north wall (~2.0 m; h-16 m, v-12 m, plate 1) also supports a debris-flow origin. Thus, units N1d/S1d postdate the Lake Bonneville transgressive sand (and period of bioturbation and erosion in the north wall possibly at about 10 ka) and predate the post-Bonneville alluvial-fan sediments exposed in the footwall of the fault (units N2 and S2).

We exposed massive sand—units N1c? and S1c?—in the hanging wall of the Wasatch fault that possibly corresponds with footwall units N1c and S1c, respectively (figure 8; plates 1 and 2). Units N1c?/S1c? consist of medium to coarse sand stratigraphically below colluvial-wedge unit C6 that is mostly massive, but locally has minor well-sorted sand lenses. Unit N1c? is possibly ~1.5 m thick, based on a discontinuous 1–2-cm-thick, subhorizontal clay bed that we exposed at the base of a temporary exposure below the unit N1c?/S1c?–C6 contact (figure 8). However, because of the short (~1-hour) duration of the exposure (excavated immediately prior to backfilling the trench), there is uncertainty in the thickness and origin of N1c?/S1c?. OSL ages for the top of units N1c? and S1c? are 7.0 ± 0.7 ka (SL-L5) and 7.8 ± 1.0 ka (SL-L3), respectively, and indicate subaerial (post-Bonneville) deposition. On the basis of their thickness (>1 m), texture (massive well-sorted sand), and age (>7–8 ka), we tentatively correlate units N1c?/S1c? with footwall units N1c/S1c. Although units N1c?/S1c? could have a colluvial origin—on the basis of scarp-parallel sand lenses thickening toward the Wasatch fault (figure 8)—we have low confidence in this interpretation. The slope-parallel lenses within N1c?/S1c? could simply represent eolian deposition on a preexisting fault scarp near the fault zone, similar to that on well-bedded lacustrine sand (e.g., unit N1b) outside of the fault zone. Further, the limited extent and duration of the exposure prevented a definitive evaluation of stratigraphic units. About 5 m west of the Wasatch fault, units N1c?/S1c? are interfingered with and overlain by alluvial-fan units N3/S3 and soils S3aA/S3bA. If the correlation of units N1c and N1c? is correct, the ~10-ka OSL age for unit N1c and the ~7.0–7.8-ka OSL ages for N1c?/S1c? (samples SL-L3 and SL-L5), which are similar to ~7.6–8.0-ka ages for soil S3bA (discussed below), provide a minimum range of time for deposition of this unit.

Post-Bonneville Alluvial-Fan Deposits

Alluvial-fan deposits exposed in the footwall and hanging wall of the WFZ consist of laterally discontinuous stream and debris-flow deposits. Footwall units include N2/S2 and subunits (e.g., N2a/S2a). Hanging-wall units include N3/S3 and subunits (e.g., N3a/S3a, N3b1). Alluvial-fan units in the footwall likely predate those in the hanging wall based on the interbedded nature of the hanging-wall alluvial-fan units with the colluvial wedges, indicating that hanging-wall fan deposition occurred in between surface-faulting earthquakes recorded in the Spring Lake trench.

Footwall alluvial-fan deposits: Footwall alluvial-fan units N2/S2 include gently west-dipping coarse gravel interbeds (subunits N2a-c/S2a-c). The units reach a maximum thickness of about 3.2 m in the south wall and are laterally continuous for at least 5 m in the north wall and 15 m in the south wall, where they are fully exposed in the footwall of the fault. In the north wall, unit N2b locally incised into debris-flow unit N1d (h-14.7 m, v-12 m, plate 1). N2b deposition east of N1d has resulted in a near-vertical contact between these units. Although the N2b-N1d contact is co-

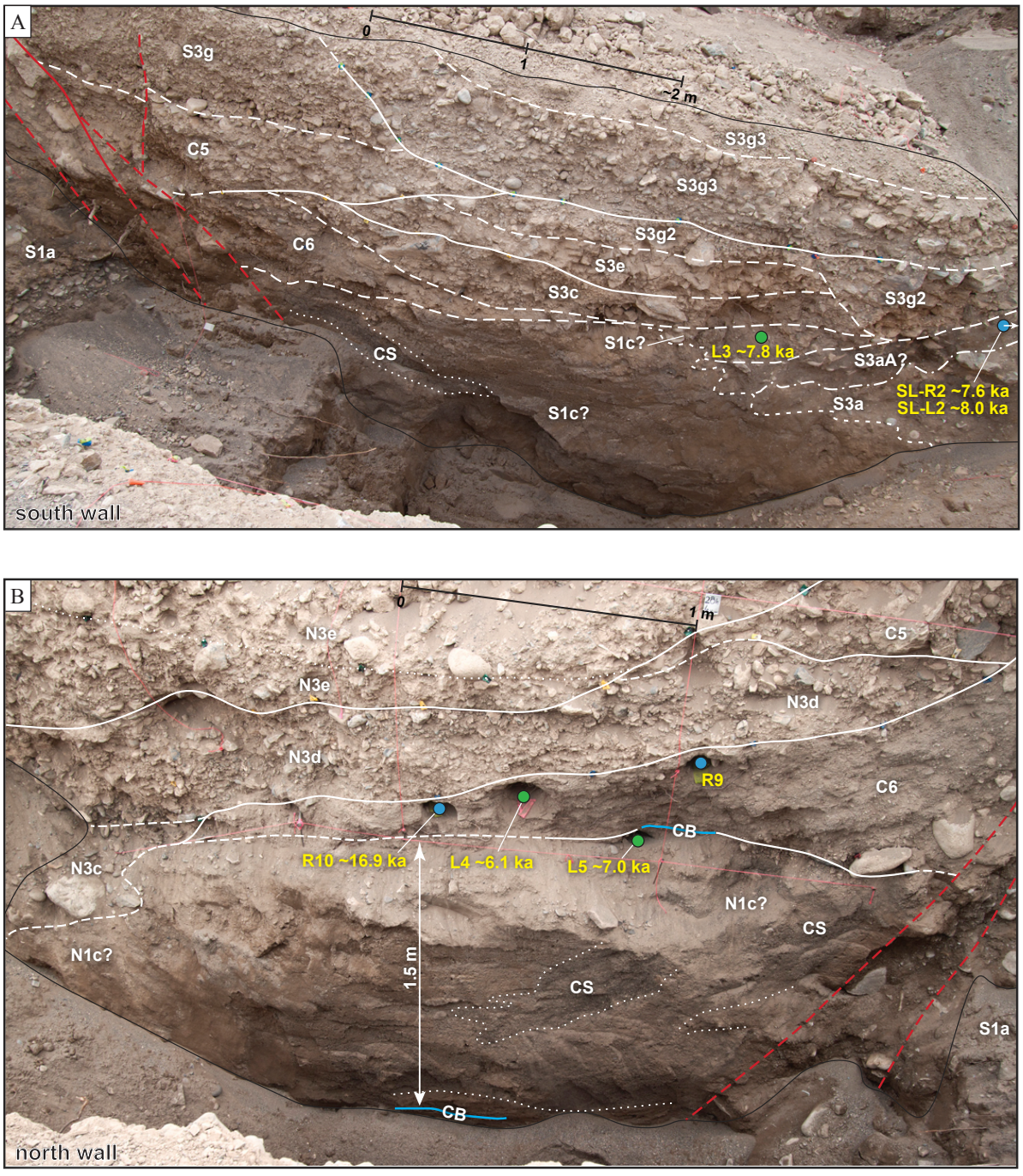

Figure 8. *Colluvial-wedge unit C6 exposed adjacent to the WFZ (red dashed lines). (A) South-wall exposure, showing unit C6, which overlies massive sand in unit S1c?, and is overlain by alluvial-fan deposits (S3). Unit C6 likely postdates the ~7.8 ka OSL age for unit S1c? (sample SL-L3), which is interfingered with soils S3aA and S3bA (dated to ~7.6–8.0 ka based on samples SL-L2 and SL-R2). (B) North-wall exposure, showing unit C6 unconformably overlying the subhorizontal sand and fine silt and 1-2-cm thick clay bed (CB) (upper blue line) in the uppermost part of unit N1c?. A lower clay bed in unit N1c? is the basis for a ~1.5-m minimum thickness of the unit. Unit C6 deposition predates the age for SL-L4 (~6.1 ka) and postdates the age for SL-L5 (~7.0 ka). CS indicates coarse, well-sorted sand.*

linear with faults in N1b1, we found no evidence for shear along the contact. The south-wall exposure suggests a similar relation: S2a/S2b postdate debris-flow unit S1d, and the majority of faults within S1b1 do not displace unit S1d or the S1d-S2a contact. Individual subunits are about 0.4 to 1.5 m thick. Units N2 and S2 are faulted by the easternmost trace of the Wasatch fault (fault F3) in both walls, and in the south wall, extensively faulted along the main trace of the Wasatch fault (fault F1; h-21–25 m; plate 2).

We mapped three soil A horizons within the footwall alluvial-fan units. Soil N2bA/S2bA is about 1 m below the ground surface and laterally discontinuous. Charcoal from soil S2bA (SL-R28) yielded an age of 13.7 ± 0.2 ka. However, charcoal from soil S2bA is older than the ~10-ka OSL age for unit N1c, which is stratigraphically lower, and is likely detrital in origin. Soils S2cA1 and S2cA2 are formed on unit S2c about 0.5–1.0 m above soil N2bA. We differentiated these soils in the south wall, where soil S2cA1 has been faulted down along fault F3 and buried by scarp colluvium (unit CF3). Soil S2cA2 is formed on the scarp colluvium and merges with soil S2cA1 outside of the area of colluvial-wedge deposition (h-13 m, v-14 m, plate 2). A soil A horizon below unit CF3 was not present in the north wall. Charcoal from soil S2cA1 yielded an age of 6.1 ± 0.1 ka (SL-R24). Although we did not extract charcoal from soil S2cA2, the soil must be younger than 3.6 ± 0.1 ka based on the charcoal sample from scarp colluvium unit CF3 (SL-R25).

Hanging-wall alluvial-fan deposits: The hanging-wall alluvial-fan units consist mostly of gently west-dipping coarse gravel interbeds and subhorizontal channel cuts and fills (subunits N3a to N3g and S3a to S3j). The deposits reach a thickness of at least 4 m in the south wall, and individual subunits are <0.1 m to about 1.5 m thick. Although some subunits (e.g., S3h and N3d) can be traced horizontally for as much as about 18 m, most subunits (especially those lower in the fan sequence) are less continuous and are observed laterally for only ~3–10 m. For this reason, there is significant uncertainty in the correlation of units along, and especially between, the north and south trench walls.

Soil horizons in units N3 and S3 include two buried soil A horizons and a modern soil A horizon. Soils N3aA and S3bA, which are likely correlative, mark the oldest buried soil—an A horizon developed in the oldest alluvial-fan sediments exposed on the hanging wall (e.g., h-32 m, v-2.5 m, plate 2). These soils are laterally continuous for about 6–7 m, and continue to within about 6–7 m of fault F1, where they have been locally removed by cross-cutting alluvial-fan channels (plate 1) or their exposure terminates into the floor of the trench (plate 2).

Concordant OSL and ^{14}C ages for soil S3bA indicate a soil burial time of about 7.6 ± 0.1 ka (SL-R2) to 8.0 ± 1.5 ka (SL-L2). About 2–3 m above S3bA, soil S3iA is developed in unit S3i and overlain by unit S3j and soil S3jA. In the north wall, a soil developed within fan units N3g1 (soil N3g1A) and N3g2 (soil N3f-gA) likely correlates with both soils S3iA and S3jA in the south wall. Because the relation of soil S3iA to surface faulting is unclear, and because S3jA and N3g-fA are modern soils, we did not sample them for ^{14}C dating.

Alluvial-fan units S3d, S3g, and S3h, all of which postdate soil S3bA, contained detrital charcoal fragments dispersed throughout them. Charcoal samples SL-R1 and SL-R3 indicate ages of 7.2 ± 0.2 ka (SL-R3) and 7.5 ± 0.2 ka (SL-R1) for unit S3d. In contrast, an OSL sample (SL-L1) of unit S3d yielded an age of 5.2 ± 0.3 ka. We have low confidence in these detrital-charcoal ages as they conflict with several soil-charcoal and OSL ages from above and below unit S3d. Below unit S3d, ^{14}C and OSL ages for soil S3bA and units C6 and N1c?/S1c? are between ~6.1 ± 1.2 ka (SL-L4) and 8.0 ± 1.5 ka (SL-L2). S3bA and C6 are stratigraphically below unit S3c (and thus S3d), which we exposed on both sides of a paleochannel within unit S3g. Above unit S3d, we have the most confidence in an OSL age of 5.7 ± 0.8 ka (SL-L6) for unit S3h. A charcoal fragment from unit S3h yielded an age of 7.1 ± 0.1 ka (SL-R11), which conflicts with the 5.7-ka OSL age; however, we have low confidence in the ^{14}C age because the detrital charcoal dated may have an inherited age component.

Scarp-Derived Colluvium

Scarp-derived colluvial wedges (units C1–C6 and CF1–CF3) at the Spring Lake site consist of lacustrine and alluvial-fan sediment eroded from scarps formed during surface-faulting earthquakes on the Nephi segment. The deposits have similar wedge-shaped geometries, horizontal extents (~2–5 m), and maximum thicknesses of 0.3–0.7 m where unaffected by synthetic or antithetic faulting (table 2). The mean maximum wedge thicknesses for colluvial wedges associated with the primary WFZ (F1) is 0.6 m. Colluvial wedge units C2–C6 have been faulted down to the west along fault F1. We group and discuss the colluvial wedges according to whether they (1) are interbedded with alluvial-fan deposits (units C4–C6), (2) postdate the majority of the alluvial-fan units (units C1–C3), or (3) formed as a result of rupture in the footwall of the fault (units CF1–CF3).

Units C4–C6 are the oldest colluvial wedges exposed at Spring Lake. These colluvial wedges are interbedded with alluvial-fan deposits, which indicate active fan deposition in between surface-faulting earthquakes. In addition, colluvial-wedge units C4–C6 mostly lack dispersed organics throughout them, likely reflecting the faulting and subsequent erosion of an active depositional surface rather than one that has been abandoned and has accumulated soil organics. For the youngest colluvial wedges (C1–C3 and CF1–CF3), organic A horizon soil matter is locally dispersed throughout the wedges, indicating cumulic A horizon development during wedge deposition.

Table 2. *Colluvial-wedge thickness and displacement at the Spring Lake site.*

Colluvial-wedge thickness[1]					Per-event displacement		
Unit	North wall (m)	South wall (m)	Preferred (m)	Revised[2] (m)	Maximum[3] (m)	Midpoint[4] (m)	Range[4] (m)
C1	0.7	0.7	0.7	0.8 (+0.1)	1.4	1.1	0.3
C2	0.5	0.5	0.5	0.6 (+0.1)	1.0	0.8	0.2
C3	0.5	0.5	0.5	0.8 (+0.3)	1.3	1.0	0.3
C4	0.3	~0.4†	0.4	0.7 (+0.3)	1.1	0.9	0.2
C5	0.5	0.6	0.6	0.7 (+0.1)	1.2	0.9	0.2
C6	0.7	>0.4†	0.7	0.8 (+0.1)	1.4	1.1	0.3
CF1	0.6	*NE*	0.6	-	-	-	-
CF2	*NE*	0.6	0.6	-	-	-	-
CF3	0.3	0.3	0.3	-	-	-	-

[1] Colluvial wedge thicknesses observed in the north and south wall. † Poor measurement because of bench (C4) or uncertainty in lower contact (C6). *NE* – not exposed. CF3 based on height of buried free face, rather than maximum wedge thickness.

[2] Revised colluvial-wedge thicknesses, which includes thickness increases in parentheses to account for colluvial wedges CF1, CF2, and CF3.

[3] Maximum per-event displacement based on individual colluvial-wedge thicknesses (e.g., 0.8 m for C1) scaled (increased by 70%; e.g., 1.4 m for C1) so that their sum equals the total stratigraphic displacement at the site (7.3 m).

[4] Midpoint and range displacements based on revised colluvial-wedge thicknesses and maximum per-event displacements.

The oldest colluvial wedge, C6, consists mostly of sand that is massive to weakly bedded, and locally has slope-parallel fabric that unconformably overlies the subhorizontal top of unit N1c?/S1c? (h-28 m, v-3.2 m, plate 1) (figure 8). Unit C6 is a maximum of 0.7 m thick based on the north wall exposure and is overlain by several alluvial-fan deposits (units S3c and N3d) that are laterally continuous for several meters and taper to the east, reflecting deposition on relatively steeper paleotopography (the base of the scarp). Unit C6 postdates unit N1c? (~7.0–7.8 ka) and soil S3bA (~7.6–8.0 ka). In the north wall, an OSL age for the uppermost part of unit C6 indicates that deposition occurred as late as 6.1 ± 1.2 ka (SL-L4). A ^{14}C age from the same stratigraphic position yielded an age of 16.9 ± 0.3 ka (SL-R10). This maximum age for C6 deposition likely reflects detrital charcoal eroded from unit N1.

Scarp colluvium of unit C5, which overlies unit C6 and alluvial-fan units N3d, S3c, S3e, and S3g2, is possibly evidence of a surface-faulting earthquake. Unit C5 is a maximum of 0.5–0.6 m thick, and has a horizontal extent of ~2.2–2.6 m. We did not sample unit C5 because of the lack of organic sediment for ^{14}C dating and well-sorted sand for OSL dating. However, unit C5 postdates the ~6.1-ka OSL age for C6, and predates an OSL age of ~5.7 ka and a ^{14}C age on charcoal of 7.1 ka (SL-R11) for unit S3h1. Considering the similarity of the detrital-charcoal age for S3h1 (~7.1 ka) to those from unit S3d, we have low confidence in the 7.1-ka age. Thus, C5 deposition likely occurred between about 6.1 and 5.7 ka.

Because unit C5 directly overlies the uppermost part of unit C6 (north wall, h-26.5 m, v-4.2 m) and has a limited lateral extent, C5 could be a younger pulse of unit C6 sedimentation. In this scenario, fan deposition (units N3d, S3c, S3e, and S3g) between units C6 and C5 would be contemporaneous with deposition of units C6 and C5. However, because these fan deposits are laterally continuous and nearly completely bury unit C6, they possibly indicate a period of scarp stabilization and fan deposition following C6 deposition. OSL ages, which show that C6 deposition occurred over a period of about ~1 kyr (based on mean ages of 7 ka for the uppermost part of N1c? [SL-L5] and 6 ka for the uppermost part of C6 [SL-L4]), support the near-complete deposition of unit C6 by the time of C5 deposition. Considering (1) the ~1-kyr time window in which C6 was likely deposited; (2) the distinct wedge geometry of C6

in the north wall; (3) the similar wedge geometries for C6 and C5, but stratigraphically separated by fan deposits that extend laterally for several meters in the hanging wall; and (4) the near-complete burial of the C6 wedge by the hanging-wall fan deposits, we infer that C5 is a separate colluvial wedge related to a younger surface rupture. However, deposition of units C5 and C6 occurred in a relatively short time (~1.3 kyr between the 7.0-ka age for uppermost unit N1c? and the 5.7-ka age for unit S3h1), and thus we cannot rule out the possibility that units C5 and C6 were deposited following a single earthquake.

Unit C4 postdates a period of alluvial-fan channel formation and gravel deposition (units S3g, S3h1, N3e, and basal N3f). Similar to C5, unit C4 has a lateral extent of ~2.5–4.3 m and a maximum thickness of ~0.3–0.4 m. In the south wall, unit C4 overlies a weak soil horizon developed in the uppermost parts of units S3h1 (h-29.5 m, v-5 m, plate 2) and S3g (h-26 m, v-5.3 m, plate 2). OSL and ^{14}C ages for unit S3h1 indicate that unit C4 deposition occurred after ~7.1 ka (^{14}C sample SL-R11) to ~5.7 ka (OSL sample SL-L6). ^{14}C and OSL ages suggest that C4 deposition occurred as late as 4.4–4.5 ka. A ^{14}C sample of charcoal from uppermost C4 colluvium in the south wall yielded an age of 4.4 ± 0.1 ka (SL-R20). An additional sample of unit C4 colluvium on the north wall consisted of sand eroded from the footwall (likely unit N1) and yielded an OSL age of 4.5 ± 0.5 ka (SL-L10). Unit C4 is overlain by a debris flow that is ~0.3 m thick in the south wall (unit S3h2) and ~0.2 m thick in the north wall (unit N3f3).

Unit C3 is the youngest wedge formed during the period of alternating alluvial-fan and colluvial-wedge deposition. Unit C3 has a lateral extent of 2.6–4.5 m and a maximum thickness of ~0.5 m, and is extensively faulted (h-26 m, v-6 m, plate 1). Unit C3 is overlain by a debris flow (unit N3g1) in the north wall and younger colluvial wedges (C2, C1) in the south wall. In the south wall, debris-flow unit S3i may correspond with N3g1 based on its stratigraphic position, thickness, and degree of soil development, and may similarly postdate unit C3. However, unit S3i is not in direct contact with unit C3, but is exposed at a broadly similar stratigraphic position as C3, overlying unit S3h2 (Plate 2). Unit C3 postdates the 4.4–4.5-ka ages for unit C4. Charcoal from uppermost C3 (SL-R19) suggests that C3 deposition occurred as late as 3.5 ± 0.1 ka (SL-R19). An OSL sample from C3 yielded an anomalously young age of >0.3 ka (SL-L7) and possibly included bioturbated sediment. Charcoal extracted from the overlying unit N3g1 yielded an age of 5.7 ± 0.1 ka (SL-R27). However, this age is stratigraphically inverted with several ages (e.g., SL-L10 in unit C3 and SL-R20 in unit C4). Thus, we consider the ~5.7-ka age for unit N3gi to be detrital in nature and consider it to be a maximum age for unit N3g1.

Considering the limited thickness of unit C4 (particularly in the north wall), we cannot rule out the possibility that C4 is an earlier phase of the unit C3 colluvial wedge. However, the limited (~0.3 m) thickness for unit C4 in the north wall may be related to a limited exposure as the unit crosses a ~1.5-m-wide horizontal bench in the trench excavation. In the south wall, C4 also has a limited thickness, and may not have been completely exposed, but has a wedge geometry that is more consistent with younger colluvial wedges C1–C3. Alternatively, the limited thickness for C4 may stem from alluvial-fan deposition (unit S3h2), which occurred between C4 and C3, and may have filled up part of the accommodation space made available by the scarp formed during the C4 earthquake. Finally, ^{14}C ages for units C4 and C3 indicate that a mean of 0.9 kyr (0.7–1.1 kyr at 2σ) elapsed between deposition of these colluvial-wedge units. Thus, we consider it likely that C3 and C4, which were deposited ~1 kyr apart and are separated by a distinct alluvial-fan unit, formed in response to separate surface-faulting earthquakes.

Unit C2, which overlies unit C3 in the south wall and units C3 and N3g1 in the north wall, is the youngest faulted colluvial wedge along the main fault zone (fault F1). The colluvial wedge continues laterally for 5.1–5.4 m, and has a maximum thickness of ~0.5 m. Fault-related evidence for C2 includes F1 faults splays/strands that displace the C3 wedge, but do not continue into unit C2 (h-26 m, v-6.8 m, plate 1). Unit C2 postdates the 3.5-ka age for unit C3. C2 deposition occurred as late as 4.1 ± 0.1 ka (SL-R18) to 2.3 ± 0.1 (SL-R17), based on charcoal ages for the uppermost part of the wedge in the south wall. However, we dismiss the 4.1-ka age for SL-R18 as it is stratigraphically inverted with the 3.5-ka age (SL-R19) for soil organics within unit C3, and buried by unit C2. Sample SL-R18 likely contained charcoal eroded from the faulted soil within unit C3, as its age is similar to the ~3.5–4.5-ka age constraints for unit C3. In the north wall, charcoal from uppermost unit C2 suggests that deposition occurred as late as 1.1 ± 0.04 ka (SL-R22).

Unit C1 consists of unfaulted scarp colluvium that overlies unit C2 in the north and south walls. Unit C1 is exposed laterally for about 4.7–5.6 m and has a maximum thickness of 0.7 m. Scarp-derived colluvium in C1 includes silt, sand, and gravel that locally forms slope-parallel fabric and along the western base of the unit, has buried a shear zone and eroded scarp free face. The timing of unit C1 deposition is complicated by poor agreement between the north- and south-wall ^{14}C ages. In the north wall, charcoal derived from C1 soil organics suggest that deposition occurred at 0.7 ± 0.04 ka (SL-R21). In the south wall, two charcoal samples from C1 indicate deposition at 0.7 ± 0.04 ka (SL-R15) and 2.4 ± 0.1 ka (SL-R16). However, we dismiss the 2.4-ka age, which is for charcoal likely derived from the underlying ~2.3-ka soil sediment (SL-R17) in the faulted C2 wedge. Maximum times of unit C1 deposition are 1.1 ± 0.1 ka based on north-wall sample SL-R22 and 2.3 ± 0.1 ka based on south-wall sample SL-R17. Based on these ages, unit C1 was likely deposited after ~1.1 ka, and possibly as late as ~0.7 ka.

Colluvial wedges CF1–CF3 were deposited following movement on faults F1 (CF1 and CF2) and F3 (CF3). Unit CF1 is only present in the north wall where it overlies sheared sediment near the top of the complex F1 fault zone, and is east of the buried free face adjacent to colluvial wedge C1 (h-25 m, v-8 m, plate 1). CF1 has a maximum thickness of 0.6 m; however, this is a poor estimate due to its limited exposure (~0.6-m lateral extent). CF1 predates unit C1 and is likely a faulted remnant of an older colluvial wedge deposited adjacent to fault F1 in the north wall (i.e., C2 or older). We also exposed a colluvial wedge, unit CF2, which formed in response to movement of the easternmost splay faults in F1 (h-22 m, v-9.5 m, plate 2). CF2 has a lateral extent of 3.0 m and a maximum thickness of 0.6 m, but is not in stratigraphic contact with units C6 to C1, and is only exposed in the south wall. Thus, CF2 likely represents wedge deposition following distributed faulting contemporaneous with one of the events associated with the C6 to C1 colluvial wedges. Unit CF2 postdates deposition of units S2 and N2 (both younger than ~10 ka), but otherwise, does not have closely constraining ages. Unit CF3 is exposed on the downthrown (west) side of fault F3 in both the north and south walls (h-11 m, v-14 m, plates 1 and 2). The CF3 colluvial wedge has a lateral extent of ~2.6–3.3 m and a maximum thickness of ~0.3 m. Unit CF3 was deposited after a 6.1 ± 0.1-ka age (SL-R24) for soil S2cA1 (beneath unit CF3) and before a 3.6 ± 0.1-ka age (SL-R25) for the basal part of CF3.

Wasatch Fault Zone

The WFZ at the Spring Lake site is characterized by (1) a main and westernmost shear zone (F1), (2) a central zone of complex faulting primarily in Lake Bonneville lacustrine sediments (F2), and (3) an easternmost fault trace (F3) (plates 1 and 2).

Fault zone F1 comprises about four to six traces that juxtapose Lake Bonneville lacustrine and post-Bonneville alluvial-fan sediments in the footwall with alluvial-fan sediments and scarp-derived colluvium in the hanging wall (figure 7). These traces form a complex, upward-diverging fault zone about 0.3–1.2 m wide in the north wall and 0.4–2.1 m wide in the south wall. This fault zone consists of sheared silt, sand, and gravel containing clasts rotated parallel to one of several fault planes. In the south wall, the main shear zone (h-25.1 m, v-5.0 m; plate 2) dips about 65° west; within the shear zone, fault trace dips range from about 50° west to near vertical and locally as much as about 20° overturned (east dipping). In the north wall, the main shear zone (h-25.7 m, v-5.0 m; plate 1) dips about 70°–80° west (h-25 m, v-5 m, plate 2) and fault trace dips range from about 60° west to near vertical (locally 10° overturned).

The F2 fault zone consists of a 6.5–8.0-m-wide zone of complex and diffuse faulting primarily within Lake Bonneville lacustrine sediments (units S1, S2, and N1). In both walls, the faults primarily dip 55° to 75° west. Locally, some faults have shallow (~35°–50°) west or moderate (~60°–75°) east dips. In the north wall, several minor-displacement faults in the F2 fault zone terminate near the top of well-bedded unit N1b1 (e.g., h-18 m, v-10 m, plate 1). We did not observe faulting in overlying units N1b2, N1c, or N1d, although the mostly massive character of these units could have obscured evidence of faulting. We also observed faults that displace unit N1b1, but are truncated by post-Bonneville alluvial-fan unit N2b (h-15 m, v-11.4 m, plate 1). In the south wall, several faults displace well-bedded unit S1b1, but not the overlying units S1c, S1d, or S2a. These fault terminations indicate at least one earthquake postdating the Bonneville highstand, but predating the post-Bonneville alluvial fan (units N1d/S1d and N2/S2). Although most faults within F2 terminate within unit S1, at least one fault truncates unit S2 (e.g., h-21.6 m, v-8.5 m, plate 2), and thus is likely contemporaneous with faulting along F1.

At the eastern end of the trench exposure, fault F3 consists of a single, west-dipping strand that displaces alluvial-fan units N2 (h-11.2 m, v-14 m, plate 1) and S2 (h-11 m, v-14 m, plate 2). Fault F3 dips about 55° to 70° and vertically offsets S2 subunit contacts about 0.2 m and N2 subunit contacts about 0.2–0.4 m. We infer that movement of fault F3 has only occurred in a single surface-faulting earthquake based on the minor displacement and single associated colluvial wedge (unit CF3).

We observed only minor rotation (shallowing) of unit contacts in the hanging wall of fault F1. For example, in the north and south walls, the bases of lowermost colluvial wedges C5 and C6 are subhorizontal, whereas the base of the uppermost colluvial wedge C1 dips about 15° to 20° west. We did not observe significant fault rotation or drag (steepening of unit contacts on either the hanging-wall or footwall) along faults F2 or F3.

The total vertical displacement at the Spring Lake site is uncertain because of alluvial-fan units deposited on the hanging wall following several surface-faulting earthquakes. As a result, footwall and hanging-wall alluvial-fan sediments and soils are non-contemporaneous, which complicates both the measurement of total site displacement and the period of time over which that displacement occurred. However, we surmise that the lowermost soil (S3bA/N3aA) in the hanging wall, which has ages of ~7.6–8.0 ka (SL-R2 and SL-L2), is approximately contemporaneous with the soils (N2bA/S2bA or N2cA/S2cA) exposed within ~1 m below the ground surface in the fault footwall. The footwall soils are broadly dated from ~6.1 ka (S2cA) to ~13.7 ka (S2bA). However, we have more confidence in the younger (~6.1 ka) soil age, which corresponds well with the post-7–8-ka ages for colluvial wedges C6 to C1 (which postdate formation of S2bA), and is stratigraphically consistent with the early Holocene (~10 ka; SL-L8) age for underlying post-Bonneville unit N1c. Accounting for the deposition time of units N1d/S1d and N2a-c/S2a-c that postdate the ~10-ka-unit N1c, an approximate age of ~6–9 ka for N2bA/S2bA and N2cA/S2cA is permissible. Furthermore, the footwall (e.g., N2bA) and

hanging-wall (e.g., N3aA) soils were both formed within a period of alluvial erosion and deposition (units N2/S2 in the footwall and N3/S3 in the hanging wall) that occurred after deposition of massive (possibly eolian or slope-wash-derived) sand across the site (units N1c/S1c in the footwall and N1c?/S1c? in the hanging wall). If these footwall and hanging-wall soils are contemporaneous, then the total displacement at the site is 6.0–7.3 m, based on 6.0–7.1 m measured in the south wall and 6.6–7.3 m in the north wall (appendix I). The range in these displacement values results from the limited exposures of these soils and their consequent uncertain projections into the F1 fault zone.

We estimate the minimum site displacement by summing the individual colluvial-wedge maximum thicknesses, which represent the minimum displacement in each earthquake (after DuRoss, 2008). Cumulative thickness of the C6 to C1 colluvial wedges exposed along fault F1 is 3.4 m (using the preferred values in table 2); including the footwall colluvial wedges (CF1/CF2 and CF3), the minimum site displacement is 4.3 m. The total minimum displacement based on colluvial wedges C6–C1 (4.3 m) is 1.7–3.0 m less than the stratigraphic offset of the soils (6.0–7.3 m). We have less confidence in the wedge-based value because of the alluvial-fan deposition on the hanging wall and adjacent to the fault zone that occurred between several of the faulting events. Fan deposition along the fault occurred partly in response to surface faulting (the creation of accommodation space), which would have limited the amount of space available for colluvial-wedge sedimentation.

Per-event vertical displacements for the Spring Lake site are based on the assumption that (1) each colluvial wedge along fault F1 represents a separate surface-faulting earthquake (table 3), (2) the maximum colluvial-wedge thickness represents the minimum fault displacement, and (3) the maximum total displacement based on the stratigraphic offset of soils S3bA/N3bA represents a reasonable upper-bound displacement. To estimate the upper-bound displacement per event, we took the individual wedge thicknesses and increased them so that their sum equaled the maximum stratigraphic offset at the site (7.3 m) (following DuRoss and others, 2014). To account for the offset in footwall colluvial wedges CF1 (~0.6 m; north wall) and CF2 (~0.6 m; south wall), which are exposed in opposite trench walls, we allocated a total of 0.6 m for these wedges equally to main-fault colluvial wedges C1–C6 prior to scaling. That is, individual displacements for C1 to C6 were each increased by 0.1 m (table 4). To account for colluvial wedge CF3, we added one-half of its 0.3-m height to colluvial wedges C4 and C3 (on the basis of their numerical constraints; discussed below) prior to the scaling. The revised heights for C1–C6 have a mean of 0.7 m, which we increased by 70%, yielding a scaled mean height of 1.2 m. Using the revised height as the lower bound and the scaled height as the upper bound, the midpoint and range displacements for C1–C6 have a mean of 1.0 ± 0.3 m. Individual displacements range from 0.8 ± 0.2 m (C2) to 1.1 ± 0.3 m (C1 and C6) (table 4). These displacements are similar to a mean per-event vertical displacement of 1.0–1.2 m determined by dividing the total site displacement (6.0–7.3 m) by six surface-faulting earthquakes (colluvial wedges C1–C6 that postdate soils S3bA and N3bA).

Table 3. *Earthquake timing and recurrence at the Spring Lake site.*

	Earthquake timing		**Earthquake recurrence**	
Event[1]	**Mean ± 2σ**[2] (ka)	**Central 95%**[3](ka)	**Inter-event** (kyr)	**Mean** (kyr)
SL1	0.9 ± 0.2	0.7–1.1	-	-
SL2	2.9 ± 0.7	2.3–3.5	SL2–SL1: 2.1	-
SL3	4.0 ± 0.5	3.5–4.4	SL3–SL2: 1.0	SL3–SL1: 1.5
SL4	4.8 ± 0.8	4.3–5.6	SL4–SL3: 0.8	SL4–SL1: 1.3
SL5	5.7 ± 0.8	5.0–6.5	SL5–SL4: 1.0	SL5–SL1: 1.2
SL6	6.6 ± 0.7	5.9–7.3	SL6–SL5: 0.9	SL6–SL1: 1.2
SL7	13.1 ± 4.0	9.6–16.8	SL7–SL6: 6.5	SL7–SL1: 2.0

[1] Spring Lake earthquakes; color shading indicates events that could possibly be grouped (e.g., SL6 and SL5 could be related to single earthquake); see text for discussion.

[2] Mean ± 2σ based on OxCal model results (model v. 5; appendix H).

[3] Earthquake time range including 95.4% of the total area of the time distribution having the highest probability density (Bronk Ramsey, 2013).

Table 4. *Vertical slip rates at the Spring Lake site.*

Event[1]	Displacement[2] (m)	Total Displacement[3] (m)	Elapsed Time[4] (kyr)	Slip Rate[5] (mm/yr)
SL1	1.1 (0.8–1.4)	1.1 (0.8–1.4) [SL1]	2.1 (1.4–2.7) [SL2–SL1]	0.5 (0.3–1.0)
SL2	0.8 (0.6–1.0)	1.9 (1.4–2.4) [SL2–SL1]	3.1 (2.6–3.6) [SL3–SL1]	0.6 (0.4–0.9)
SL3	1.0 (0.8–1.3)	2.9 (2.2–3.7) [SL3–SL1]	3.9 (3.3–4.7) [SL4–SL1]	0.7 (0.5–1.1)
SL4	0.9 (0.7–1.1)	3.8 (2.9–4.8) [SL4–SL1]	4.9 (4.1–5.6) [SL5–SL1]	0.8 (0.5¬–1.2)
SL5	1.0 (0.7–1.2)	4.8 (3.6–6.0) [SL5–SL1]	5.8 (5.0–6.5) [SL6–SL1]	0.8 (0.6–1.2)
SL6	1.1 (0.8–1.4)	5.9 (4.4–7.4) [SL6–SL1]	12.3 (8.7–15.9) [SL7–SL1]	0.5 (0.3–0.9)
SL7	unknown	-	-	-

[1] Earthquakes identified at the Spring Lake site and modeled in OxCal model v. 5 (appendix H).

[2] Vertical displacement per earthquake, reported as the midpoint and range (in parentheses); see table 2 and text for description.

[3] Total displacement is the sum of the per-event displacements (reported as the midpoint and range in parentheses) for earthquakes included in brackets.

[4] Mean elapsed time (with 95% ranges included in parentheses) between earthquakes included in brackets (e.g., 12.3 kyr between earthquakes SL7 and SL1).

[5] Vertical slip rate, based on total displacement divided by elapsed time. Ranges in parentheses approximate 95% uncertainty.

Because we did not expose lacustrine sediments on the hanging wall of the fault, we were unable to constrain the total (post-18 ka) vertical displacement of the Lake Bonneville transgressive and highstand units. Although units S1c and N1c are possibly exposed on both the hanging-wall and footwall sides of F1, we did not measure their total offset on account of their limited hanging-wall extents and remaining uncertainty in the origin of units S1c? and N1c?.

Paleoseismology of the Spring Lake Site

Chronology of Surface-Faulting Earthquakes

OxCal models for the Spring Lake site constrain the timing of five to seven surface-faulting earthquakes that postdate the highstand of Lake Bonneville (~18 ka) (table 3). We interpret that a surface-faulting earthquake correlates with each of the six, distinct colluvial-wedge units C1–C6 exposed along the main fault F1 and a seventh earthquake correlates with the set of upward terminations of faults (F2) in the footwall of fault F1 (figure 9). We constructed several OxCal models for the Spring Lake site to account for (1) possibly erroneous ^{14}C and OSL ages (e.g., SL-L1 and SL-R11), (2) the possibility that the detrital-charcoal ages (for SL-R1, SL-R3, and SL-R11) are older than the time of fan deposition, and (3) uncertainty in the context of samples SL-L3 and SL-L5 in unit N1c?/S1c?. These models have agreement indices, or the overall agreement of the ages in the stratigraphic model, which vary from low (~30–40) to high (>100). We found the best agreement for models that excluded OSL sample SL-L1 in unit S3d and the detrital charcoal samples SL-R1, SL-R3, and SL-R11 in units S3d and S3h1. Our preferred model (version 5; appendix H) excludes these ages, but includes the ages for SL-L3 and SL-L5, and has a high model agreement index of 107. Alternative models having high agreement indices exclude SL-L3 and (or) SL-L5, but we have less confidence in these results. After consideration of the SL-L3 and SL-L5 OSL-sample equivalent-dose populations as well as the context of the samples (using the photomosaics), we consider SL-L3 and SL-L5 to be good ages for units S1c? and C6, respectively.

SL7, the oldest earthquake at the site, occurred at 13.1 ± 4.0 ka based on our preferred OxCal model (appendix H). Several faults within the F2 fault zone complexly displace the Lake Bonneville highstand lacustrine sediments (unit N1b/S1b), but not overlying loess (unit N1c/S1c), debris-flow (N1d/S1d), or alluvial-fan sediments (N2/S2), and provide evidence of earthquake SL7. Thus, earthquake SL7 has a maximum constraint of ~17.3 ka (OSL sample SL-L9 for unit N1b) and a minimum of ~10.0 ka (OSL sample SL-L8 for unit N1c). Earthquake SL7 also predates the ~7.0-ka OSL age for uppermost unit N1c? on the hanging wall as well as the ^{14}C and OSL ages for soil S3bA and unit N1c?/S1c? that range from 7.0 to 8.0 ka (SL-L5, SL-L3, SL-L2, and SL-R2).

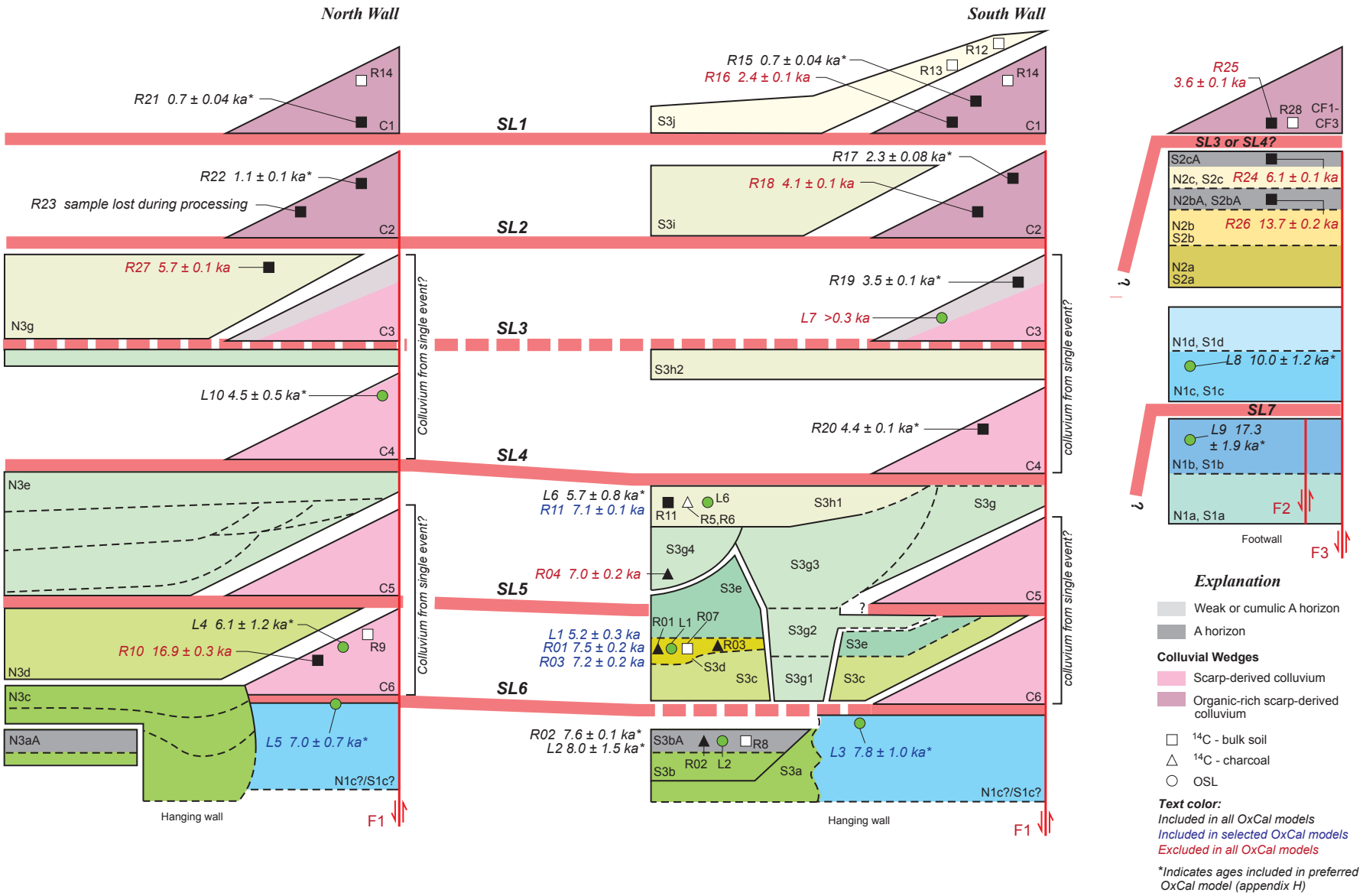

Figure 9. *Summary of colluvial wedges exposed at the Spring Lake site and their relation to alluvial-fan and lacustrine sediments and ^{14}C and OSL ages. Text color for numerical ages indicates placement in several OxCal models constructed for the site (appendix H). Horizontal red bars indicate surface-faulting earthquakes in the context of the sedimentary deposits and numerical ages.*

Earthquake SL6 occurred at 6.6 ± 0.7 ka. SL6 postdates the 7.0–8.0 ka ages for N1c?/S1c? and S3bA (samples SL-L5, SL-L3, SL-L2, and SL-R2) and predates an OSL age for C6 colluvium of 6.1 ± 1.2 ka (SL-L4). Because we consider the sample of uppermost unit N1c?/S1c?, where buried by unit C6, to be a better approximation of the earthquake SL6 time than the minimum age of 6.1 ka from the uppermost part of unit C6, we used a Zero_Boundary grouping in OxCal (appendix H-1) to implement this interpretation. Pairing a Zero_Boundary distribution with an earthquake time distribution yields an earthquake distribution that is skewed toward the closest limiting age(s) (in this case, the 7–8 ka ages; see DuRoss and others [2011] for additional discussion). As discussed above, we excluded detrital charcoal ages (~7.2–7.5 ka for SL-R1 and SL-R3) for the overlying alluvial-fan unit S3d because they are stratigraphically inverted with samples SL-L5 and SL-L4 (~6.1–7.0 ka). If included, these ages result in an OxCal model having low agreement indices.

Earthquake SL5 occurred at 5.7 ± 0.8 ka. SL5 has a maximum age constraint of 6.1 ka (SL-L4) for uppermost unit C6, and a minimum age constraint of ~5.7 ka (SL-L6) for alluvial-fan unit S3h. We excluded the detrital charcoal ages for units S3d (~7.2–7.5 ka; SL-R3 and SL-R1) and S3h (7.1 ka; SL-R11). Although the ^{14}C ages for the alluvial-fan sediment are stratigraphically consistent, they are stratigraphically inverted with the OSL ages and yield a low model agreement index if included. Thus, we consider OSL ages for samples SL-L4 (~6.1 ka) and SL-L6 (~5.7 ka) to best constrain the time of earthquake SL5. As discussed previously, we are uncertain whether colluvial wedges C6 (SL6) and C5 (SL5) represent one or two earthquakes. Earthquakes SL6 and SL5 have mean times that are ~0.9 kyr apart and 95% ranges that have ~0.6 kyr of overlap (between 5.9 and 6.5 ka). Although we prefer a model of separate earthquakes for SL6 and SL5, considering the overlap in the earthquake times and the limited extent of the C5 colluvial wedge, we cannot rule out the possibility that these units represent separate pulses of colluvium deposited following the same earthquake.

Earthquake SL4 occurred at 4.8 ± 0.8 ka. SL4 postdates the ~5.7-ka OSL age for alluvial-fan unit S3h, and predates ~4.4–4.5 ka ^{14}C (SL-R20) and OSL (SL-L10) ages for uppermost C4 colluvium. Based on the maximum limiting age, colluvium related to earthquake SL4 (C4) could also correspond with footwall colluvial wedge CF3 along fault F3 (figure 9). However, CF3 is broadly constrained to ~3.6–6.1 ka based on maximum and minimum limiting ^{14}C ages (SL-R24 and SL-R25) and could also correspond with earthquake SL3. Displacement in SL4 divided between faults F1 and F3 could help explain why the C4 colluvial wedge is poorly expressed (thickness of ~0.4 m) along the main fault (F1).

Earthquake SL3 occurred at 4.0 ± 0.5 ka using the 4.4–4.5-ka ages for C4 colluvium as a maximum timing constraint and a 3.5-ka ^{14}C age (SL-R19) for C3 colluvium as a minimum. Using its minimum limiting age (3.5 ka), SL3 (and C3 colluvium) could correspond with footwall colluvial wedge CF3 (~3.6–6.1 ka). The 0.8-kyr difference in the mean times for SL4 (~4.8 ka) and SL3 (~4.0 ka) and the minimal (~0.1 kyr) overlap in their 95% ranges support our interpretation of two separate earthquakes; however, we cannot rule out a single-earthquake model.

The penultimate earthquake (SL2) occurred at 2.9 ± 0.7 ka. The timing of earthquake SL2 is based on the 3.5-ka ^{14}C age (SL-R19) for C3 colluvium that provides a maximum constraint, and two ^{14}C ages of 1.1 and 2.3 ka (SL-R22 and SL-R17) for C2 colluvium that provide a minimum constraint. We excluded an additional age for the C2 colluvium of 4.1 ka (SL-R18) because it is stratigraphically inconsistent with SL-R17, SL-R22, and SL-R19. Sample SL-R18 likely included charcoal derived from the soil developed in unit C3.

The most recent earthquake (SL1) occurred at 0.9 ± 0.2 ka, postdating the 1.1–2.3-ka ^{14}C ages for C2 colluvium and predating two nearly identical 0.7-ka ^{14}C ages (SL-R15 and -R21) for C1 colluvium. Samples R15 and R21 are from opposite walls and from both the basal (R21) and uppermost (R15) parts of the C1 wedge. An additional sample of C1 colluvium yielded an age of 2.4 ka (SL-R16), which is significantly older than the 0.7-ka minimum ages and stratigraphically inverted with the 2.3-ka age for C2. We excluded the 2.4-ka age for SL-R16 from the OxCal model as the charcoal dated is likely derived from the faulted soil in the C2 colluvial wedge.

Earthquake Recurrence and Fault Slip Rate

We calculated inter-event and mean recurrence intervals between individual Spring Lake earthquakes SL7 and SL1 using the mean earthquake times (table 3; appendix K). Inter-event recurrence is the elapsed time between two successive earthquakes (e.g., SL7–SL6); mean recurrence is the mean over several seismic cycles based on the elapsed time between the oldest and youngest earthquakes (e.g., SL7–SL1) divided by the number of closed inter-event intervals.

Inter-event recurrence intervals between earthquakes SL7 and SL1 have a broad range, varying from ~0.8 kyr for SL4–SL3 to ~6.5 kyr for SL7–SL6 (table 3). The relatively long interval between SL7 and SL6 is related to the poorly resolved time of earthquake SL7 (~4-kyr uncertainty at 2σ). In addition, we consider the SL7–SL6 interval a maximum value because of the limited exposure of units N1c?/S1c? in the fault zone, a low post-Bonneville sedimentation rate (between deposition of units S1a-b/N1a-b and S2/N2), uncertainty in the correlation of these units with footwall units N1c/S1c, and the well-sorted and massive texture of units N1c?/S1c? that could mask evidence of individual surface-faulting earthquakes. We also report a long, ~2.1-kyr elapsed time between earthquakes SL2 and SL1. However, as opposed to the SL7–SL6 interval, we do not consider the SL2–SL1 interval poorly constrained due to limited stratigraphy or limiting ages. Excluding the SL7–SL6 interval,

the inter-event intervals are less than 2.1 kyr (table 3) and yield a coefficient of variation (COV) on recurrence—the standard deviation of the inter-event recurrence values divided by their mean—of 0.45 (0.52 kyr divided by 1.15 kyr).

To account for the long (~6.5 kyr) elapsed time between earthquakes SL7 and SL6, we considered the possibility that slope-parallel sand lenses in units N1c? and S1c? are related to at least one earthquake between about 10 and 7 ka. The earthquake(s) would predate formation of hanging-wall soil N3aA/S3bA (~7.6–8.0 ka) and deposition of colluvial-wedge unit C6 (~6.1 ka). Although earthquakes in this period would help explain the long gap in surface faulting between SL7 and SL6, we have low confidence in this interpretation because of the thick, massive character of units N1c/N1c? and S1c/S1c?. That is, without local changes in sedimentary texture or the presence of buried soils, colluvial wedges derived primarily from sandy unit N1c/S1c in the fault footwall would be difficult to discern from units N1c?/S1c? in the hanging wall.

Mean recurrence intervals measured between earthquakes SL7 and SL1 (i.e., SL7–SL1 to SL3–SL1) range from ~1.2 to ~2.0 kyr (table 3). Excluding the longest interval (~2.0 kyr for SL7–SL1), which is poorly constrained and possibly a maximum value, the mean intervals are between ~1.2 and 1.5 kyr, indicating a relatively constant rate of earthquakes when averaged over thousands of years. The best-constrained mean recurrence for the Spring Lake site is ~1.2 kyr for SL6–SL1, which excludes the SL7–SL6 interval, but includes five closed intervals between SL6 and SL1.

We calculated closed-seismic-interval vertical slip rates for the Spring Lake site using the individual earthquake displacements and time ranges between events (table 4; appendix K). For example, ~4.8 m of displacement occurred in earthquakes SL5–SL1, and thus, using the total elapsed time of ~5.8 kyr between earthquakes SL6 and SL1 (excluding the elapsed time for SL7–SL6 and the time between SL1 and the present), we calculate a slip rate of ~0.8 mm/yr. Slip rates for the Spring Lake site vary from ~0.5 to 0.8 mm/yr. The lower-bound slip rates are ~0.5–0.6 mm/yr for the total displacement in earthquakes SL6–SL1 (which includes the poorly constrained total time interval for SL7–SL1) and SL2–SL1, and the individual displacement for earthquake SL1. The upper-bound slip rate is ~0.8 mm/yr using the total displacements in SL5–SL1, SL4–SL1, and SL3–SL1. We have the most confidence in the slip-rate values between ~0.6 and 0.8 mm/yr, which account for several earthquake cycles and exclude the poorly constrained time interval for SL7–SL1.

NORTH CREEK TRENCH SITE

Surface Faulting and Geology

The North Creek site is on the north-central part of the southern Nephi strand, at the north end of a series of prominent, continuous scarps on late Pleistocene to Holocene alluvial-fan surfaces and bedrock that form the linear range front below Mount Nebo (Harty and others, 2007) (figure 10). To the north, less prominent (more degraded) and discontinuous scarps continue on trend with the southern strand (Machette and others, 1992), but also bifurcate to the northwest and north-northeast. About 1 km north of North Creek, discontinuous scarps associated with the Mendenhall fault branch to the northwest (DuRoss and Bruhn, 2005); about 2 km north of North Creek, large prominent scarps trend north-northeast into bedrock (Machette and others, 1992). The North Creek site is at ~1735 m (5690 ft) elevation, above the highstand shoreline of Lake Bonneville (Felger and others, 2004).

Surficial deposits at the North Creek site are mostly stream and debris-flow deposits sourced from two drainages in Cambrian to Pennsylvanian sedimentary bedrock (Witkind and Weiss, 1985; Felger and others, 2004) of the Wasatch Range to the east: (1) the large (~3.7 km^2) North Creek drainage, and (2) a smaller (~0.3 km^2) drainage to the southeast ("South Creek" of Hanson and others, 1981) (figure 11). To the east, on the upthrown side of the WFZ, a ~0.01 km^2, mid-Holocene (Bucknam, 1978; included in Bowman and Lund, 2013) alluvial-fan surface has been uplifted and incised (figure 12). To the west, on the downthrown side of the fault, alluvial-fan surfaces coalesce to form a broad, west-sloping apron.

Holocene movement on the southern strand of the Nephi segment has created a single, prominent, ~150-m-long by ~8–9-m-high, west-facing fault scarp bounding the uplifted fan remnant (figure 12). Uplift of the footwall fan surface above the elevation of the fault scarp has led to surface abandonment and incision east of the fault and shifted the locus of deposition entirely to the hanging wall west of the WFZ. We estimate 7.7 m of vertical offset across the scarp based on a 75-m-long profile (figure 13). However, this offset represents a minimum mid-Holocene displacement because of several meters of younger alluvial-fan deposits on the fault hanging wall (based on the trench stratigraphy discussed below).

Trench Stratigraphy and Structure

The North Creek trench exposed the WFZ and three distinct sedimentary packages: alluvial-fan deposits sourced from the North Creek drainage to the east, alluvial-fan deposits sourced from the South Creek drainage to the southeast, and scarp-derived colluvium (colluvial wedges). Alluvial-fan sediments derived from the North Creek drainage are mostly exposed in the fault footwall, whereas fan deposits from South Creek are interfingered with scarp-derived colluvial wedges in the fault hanging wall (figure 14; plates 3 and 4). We also describe an exposure of cultural fill on the fault hanging wall related to the Hansen and others (1981) trench investigation.

Footwall Alluvial-Fan Sediments

Alluvial-fan sediments exposed in the footwall of the main trace of the fault (F1; e.g., h-22.2 m, v-2.0 m; plate 3)

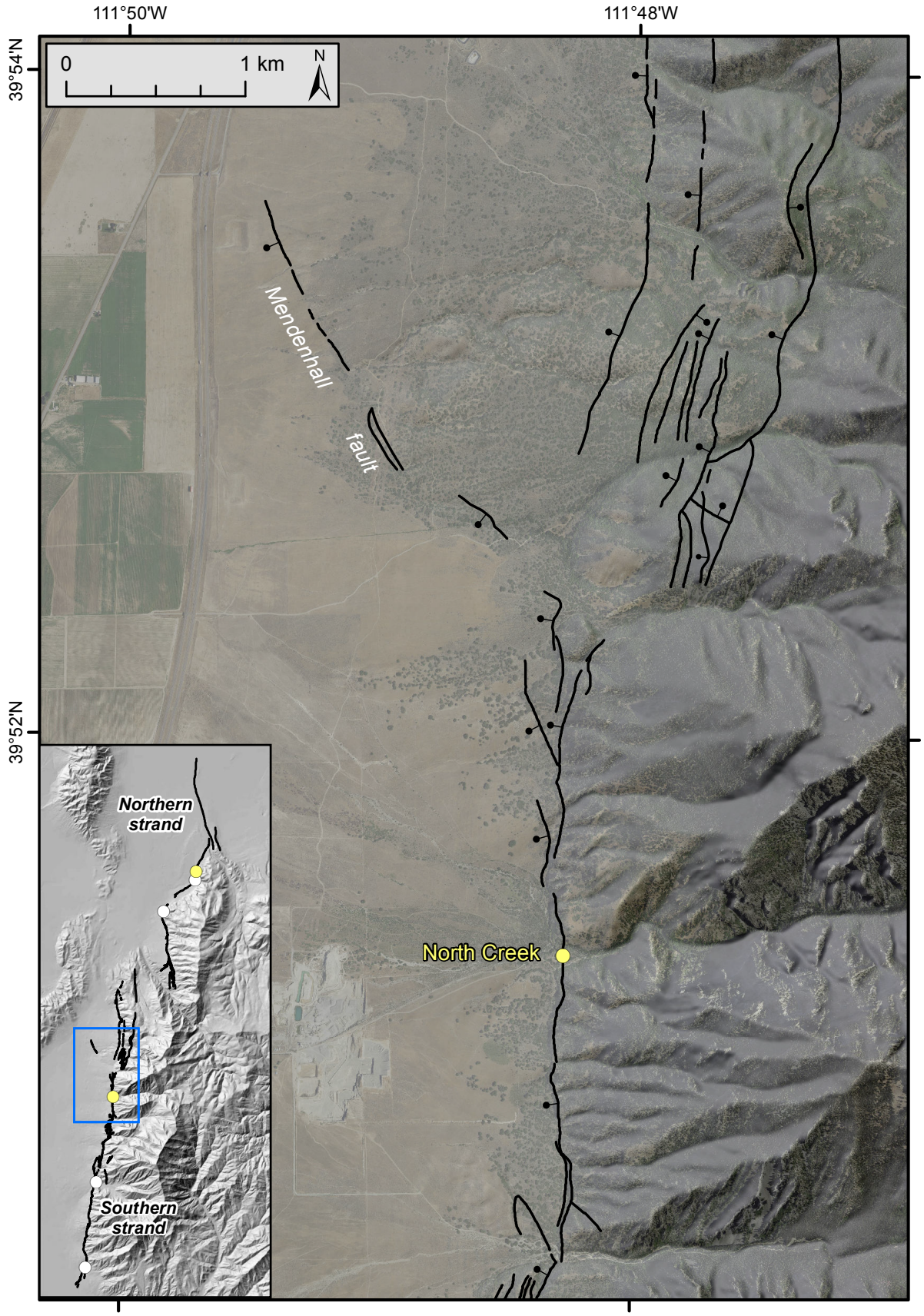

Figure 10. *Southern strand of the Nephi segment showing the North Creek trench site. Ball and bar indicates downthrown side of fault. Fault traces from Black and others (2003) show the approximate location of the WFZ. Trace of the Mendenhall fault from Black and others (2003) and DuRoss (2004). Base map is 2014 NAIP aerial photographs (USDA, 2017) overlain on a 10-m DEM with hillshade (Utah AGRC, 2017).*

Figure 11. *North Creek site on the southern strand of the Nephi fault segment. (A) View to the northeast of the North Creek drainage (photo taken on distal alluvial-fan sediments derived from North Creek). South Creek is a minor drainage to the south (after Hanson and others, 1981); alluvial-fan sediments from South Creek have partially buried North Creek alluvial-fan sediments on the hanging wall of the WFZ. Red line indicates mapped trace of the WFZ. (B) Excavation of the North Creek site. The scarp shown is approximately 8 m high. View is to the southeast.*

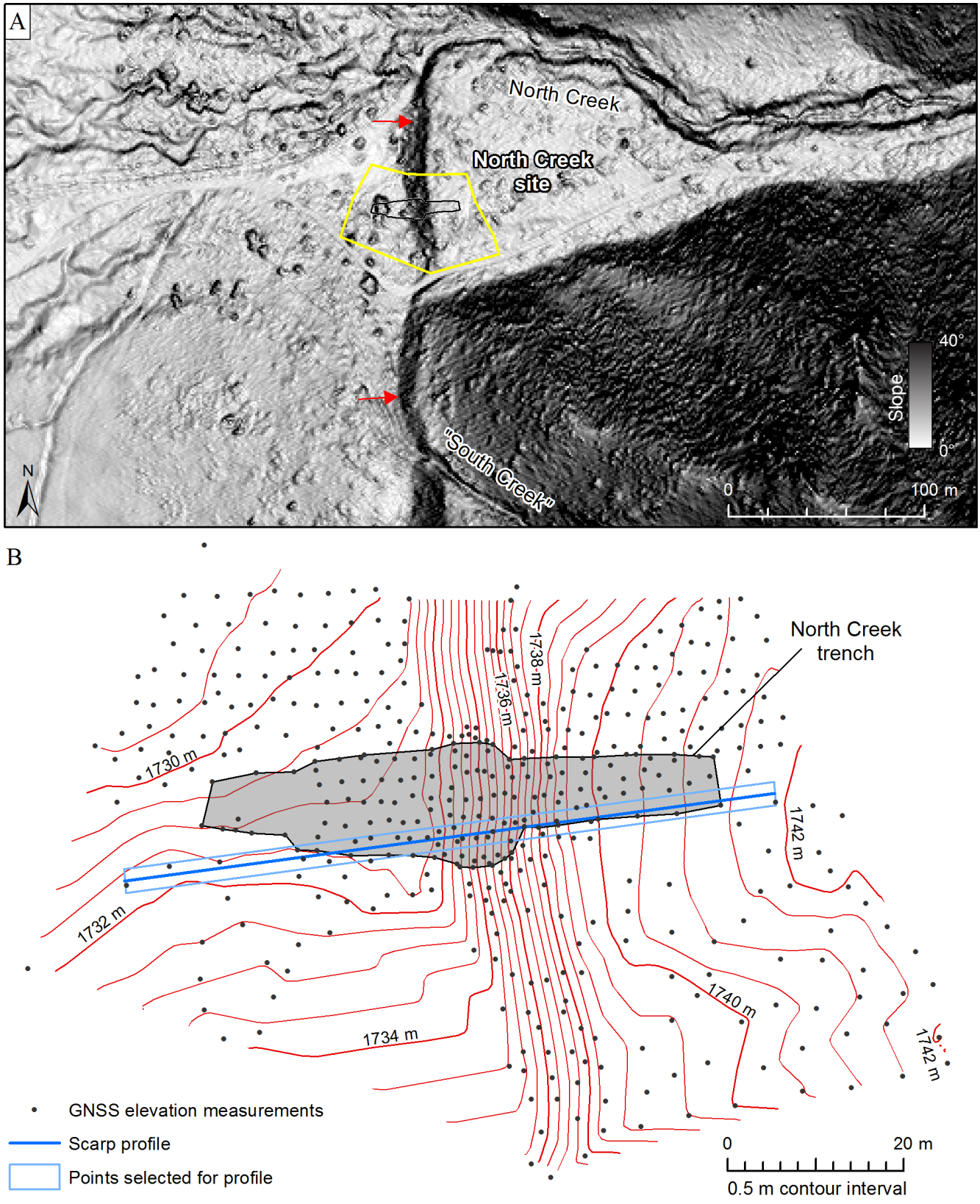

Figure 12. *North Creek site shown on (A) 2008 lidar slopeshade map, and (B) topographic map based on high-precision GNSS data measured prior to trench excavation. Red arrows indicate Wasatch fault scarps. Gray-filled polygon indicates extent of the North Creek trench; blue line indicates scarp profile (figure 13). Contours interpolated from a TIN generated using the point elevation data.*

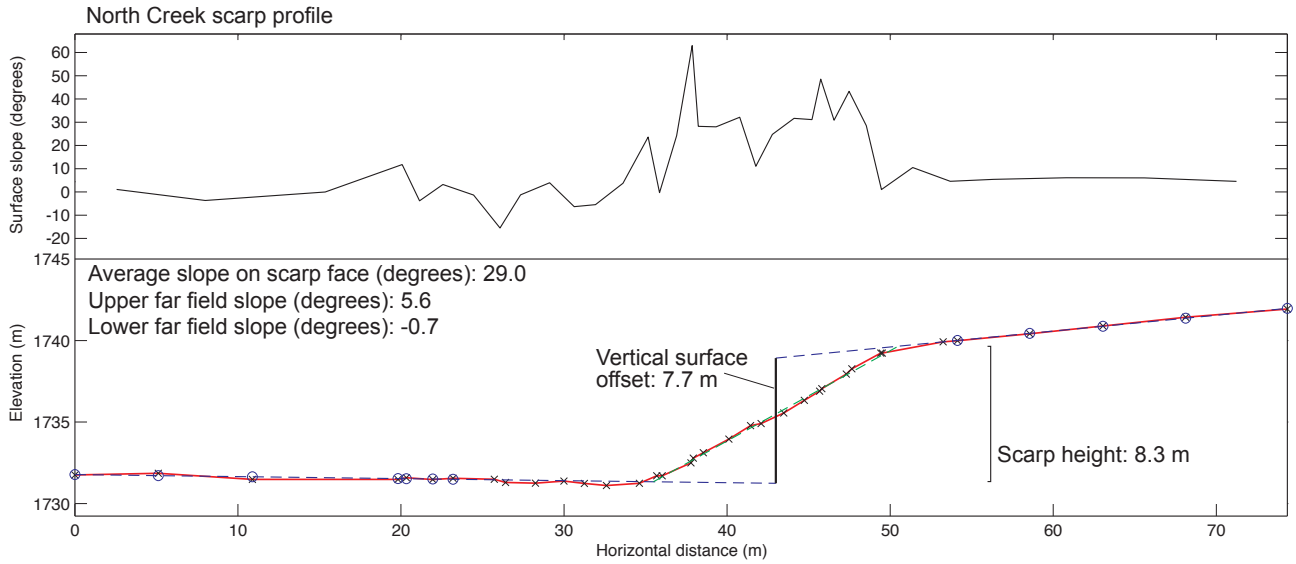

Figure 13. *Scarp profile measured across the North Creek site. Profile points (blue X's) measured using high-precision GNSS; elevation is relative to mean sea level. Upper panel shows surface slope measured at midpoint distances between profile points. On lower panel, blue circles indicate profile points selected for footwall and hanging wall surface-slope measurements. Vertical surface offset is the vertical separation of these surfaces, measured at the horizontal midpoint of the maximum scarp slope (green dashed line). Scarp height is the vertical distance between the intersections of the maximum scarp slope (green dashed line) with the footwall and hanging wall surface-slope projections (blue dashed lines).*

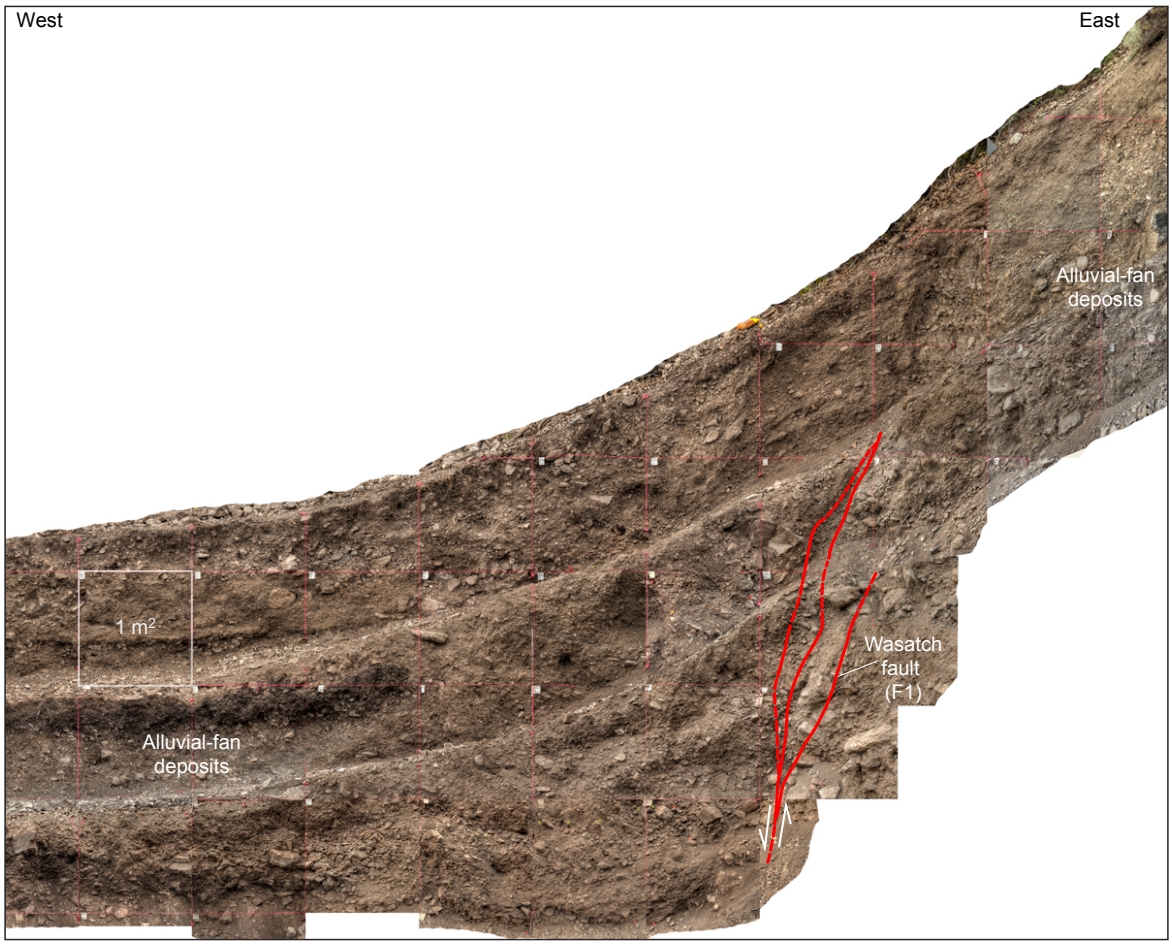

Figure 14. *Subset of the photomosaic of the north wall of the North Creek trench showing the main traces of the WFZ (fault F1), which juxtapose alluvial-fan deposits sourced from the North Creek drainage in the footwall with younger alluvial-fan deposits likely sourced from a minor drainage to the south (South Creek) in the hanging wall.*

consist of a 12-m-thick package of vertically aggraded stream and debris-flow deposits, which we subdivided into three units: 1a, 1b, and 1c. These units are sourced from the North Creek drainage based on their gentle west dip and exposure at the east end of the trench, east of the mouth of the North Creek drainage, which rules out South Creek as a possible source area. East of the trench, the alluvial-fan surface (and likely soil 1cA) continues east into the canyon. Units 1a–1c consist of coarse, poorly sorted gravel; are individually 2–6 m thick; and can be traced laterally for a minimum of 1–12 m. Within units 1b and 1c, subunits include individual deposits (stream and debris flows) that are a few centimeters (e.g., 1b-2) to a few meters (e.g., 1b-1) thick.

A thin (~0.1–0.2 m thick) but prominent soil A horizon (1bA), which includes abundant charcoal that may have formed in situ (i.e., as part of a widespread "burn horizon"), is developed in the uppermost part of unit 1b and is buried by unit 1c (h-28 m, v-9.75 m, plate 3). Charcoal derived from soil 1bA yielded ages of 5.3 ± 0.1 ka (NC-R9) and 7.9 ± 0.1 ka (NC-R7). We prefer the 5.3-ka age to characterize the age of soil 1bA at burial, because charcoal sampled from several colluvial wedges, but likely sourced in part from soil 1bA, yielded ages of 5.4 ± 0.2 ka (NC-R13), 6.0 ± 0.1 ka (NC-R15), and 6.2 ± 0.1 ka (NC-R28). Furthermore, this 5.3 ka age is nearly identical to an age of 5.2 ± 0.6 ka (appendix E) for charcoal sampled and dated from the North Creek footwall by Bucknam (1978).

Hanging-Wall Alluvial-Fan Sediments

Alluvial-fan sediments exposed in the fault hanging wall consist of subhorizontal, well- to poorly sorted silt, sand, and gravel deposits (units 2a–e and 3) that are locally interbedded with scarp-derived colluvial wedges (units C5 to C1) near fault F1. Units 2a–e and 3 are likely derived from South Creek based on local site topography, which includes a minor alluvial fan sourced from South Creek that has partially buried North Creek-derived fan sediments on the downthrown side of the fault scarp (surface contours decrease in elevation and are convex to the north; figure 12). However, we cannot rule out North Creek (which is incised into the footwall fan units immediately north of the trench site) as an origin for these deposits. The exposed hanging-wall fan sediments reach a thickness of at least 4 m in the south wall of the trench and include individual subunits that are <0.1 m (unit 2d2) to about 1.5 m thick (unit 2c). The fan units are laterally continuous for as much as 17 m (e.g., unit 2c). The majority of the hanging-wall fan units are faulted by a series of antithetic and synthetic faults (F2–F7; h-5.6 to 14.2 m; plates 3 and 4) in an ~13-m-wide graben (measured between F1 and the most prominent graben-bounding antithetic fault, F6).

Deposition of units 2a–e and 3 occurred after about 6 ka based on an OSL age of 6.0 ± 0.3 ka (NC-L1) for the oldest unit, a subhorizontal silt bed (unit 2a) exposed in the footwall of graben-bounding fault F6 (h-8 m, v-1.7 m, plate 4). The youngest silt beds (units 2d and 2e) bury soil 2cA (e.g., h-18.0 m, v-3.0 m, plate 3) and are locally interfingered with colluvial wedge C1 (e.g., h-19.0 m, v-3.7 m, plate 3; h-17.0 m, v-3.7 m, plate 4), indicating deposition after the youngest North Creek earthquake. An OSL age for unit 2d2 on the northern trench wall, a <10-cm-thick silt lens that overlies most of the hanging-wall fan gravels, yielded an age of 1.5 ± 0.8 ka (NC-L2). However, this age is significantly older than an age of 0.2 ± 0.2 ka (NC-R22) for charcoal derived from the unit (nearly identical sample location within unit 2d2) and stratigraphically inverted with several <1-ka radiocarbon ages for soils that are stratigraphically below unit 2d2 (e.g., soil 2cA). The youngest hanging-wall deposit (unit 3) is a coarse, poorly sorted historical debris flow containing fragments of metal fencing materials.

Three distinct buried soils (h-9 m, v-2–4 m, plate 4) within the hanging-wall fan units also help constrain the ages of units 2a–e and 3. Soil 2bA is developed within the uppermost gravel of unit 2b and is laterally continuous for about 14–17 m. However, between faults F1 and F2, soil 2bA is overlain by soil 2b2A (h-15 m, v-1.5 m, plate 4), which may represent a younger part of soil 2bA formation east of fault F2. Sample NC-R19, which sampled charcoal from soil 2b2A, yielded an age of 4.1 ± 0.1 ka. Thus, soil 2bA (between faults F1 and F2) must be older than ~4.1 ka and may be approximately contemporaneous with deposition of the oldest colluvial wedge (unit C5), which predates a 4.0 ± 0.1-ka age (NC-R12) for charcoal derived from an A horizon developed within the uppermost part of C5 (soil C5A; h-20.5 m, v-1.3 m; plate 4). The similar stratigraphic positions (depth below a younger soil 2cA) of soil 2bA and soil C5A support this inference. Soil 2cA is formed in the uppermost gravel of unit 2c and is laterally continuous for about 17–19 m. Charcoal derived from soil 2cA yielded ages of 0.4 ± 0.1 ka (NC-R31) where buried by colluvial wedge Cg2 in the graben, to 0.6 ± 0.1 ka (NC-R23) to 1.2 ± 0.1 ka (NC-R16) where buried by colluvial wedge C2 adjacent to the main fault zone. The youngest buried soil in the graben fan sequence is soil 2cA2/CgA, which is developed within the uppermost parts of colluvial wedges Cg1 and Cg2 in the graben (e.g., h-9 m, v-3.5 m, plate 4), and overlies soil 2cA beyond the extent of Cg1 and Cg2 (east of fault F3 and west of fault F6). Charcoal derived from soil 2cA2/CgA, where developed within unit Cg1, yielded an age of 0.9 ± 0.1 ka (NC-R2).

Scarp-Derived Colluvium

Colluvial wedges (e.g., C1–C5) at the North Creek site consist of silt, sand, and gravel eroded from fault scarps formed in the footwall and hanging-wall alluvial-fan sediments during separate surface-faulting earthquakes on the Nephi segment. These units range from about 0.8 m to 1.5 m thick (table 5) and continue laterally for about 2–6 m. Units C1–C4 are colluvial wedges that have similar wedge-shaped geometries, texture and sorting, and soil development. Unit C5 is likely an older colluvial wedge exposed below C4 near fault F1. We

Table 5. *Colluvial-wedge thickness at the North Creek site.*

Unit	North wall (m)	South wall (m)	Preferred (m)
C1	1.5	1.3	1.4
C2	1.2	0.9	1.1
C3	0.8†	1.0†	0.9
C4	1.3	1.4	1.4
C5	*NE*	*NE*	-
Cg1	0.2–0.3	0.3–0.4	0.2–0.4
Cg2	0.3–0.5	0.4–0.6	0.3–0.6
Cg3	0.3–0.5	*NE*	0.3–0.5

† Poor measurement because unit crosses a horizontal bench and has been modified by fan unit 2c.

NE – not fully exposed.

For C5, the base of the colluvial wedge was not exposed.

Range in Cg1–3 measurements based on values including and excluding soil 2cA2/CgA.

also describe colluvial wedges formed along synthetic and antithetic faults in the faulted graben between faults F1 and F6 (Cg1–Cg3). The youngest colluvial wedges (e.g., C1 along fault F1) are not faulted, but units C2–C5 have been faulted down to the west on the fault hanging wall.

Unit C5 is the oldest colluvial wedge at the site. However, there is uncertainty in the origin of this unit because of its limited exposure at the base of the trench in the hanging wall of fault F1 (h-20.5 m, v-1 m, plate 4). Evidence for a colluvial origin of unit C5 includes its proximity to fault F1 (all stream and debris-flow deposits exposed in the hanging wall are several meters west of fault F1) and the poorly sorted texture of the unit, which locally includes mixed soil matter and gravel. C5 includes a soil A horizon formed within its uppermost ~0.2 m (C5A; h-20.5 m, v-1.4 m, plate 4) as well as a basal lens of soil organics that is ~0.5 m below the top of the unit (C5A; h-20.5 m, v-0.8 m, plate 4). The interfingered gravel and soil matter of C5 is more consistent with scarp-derived colluvium (e.g., similar to that found within C4 at h-20.5 m, v-1.6 m, plate 4) than the well-sorted gravel in footwall units 1c-3 and 1c-4 or hanging-wall units 2b and 2c. A ^{14}C age for the uppermost part of C5A is ~4 ka (NC-R12), which indicates that soil development in C5 postdates the deposition of hanging-wall loess unit 2a at ~6 ka and the formation of footwall soil 1bA at ~5–6 ka. We disregard a younger C5A age of ~2 ka (NC-R11), which is stratigraphically inconsistent with the ages for soil 2bA2 (~4.1 ka; NC-R19) and overlying unit C3. Unit C5 and soil C5A may be contemporaneous with soil 2bA, formed in the uppermost part of hanging-wall gravel unit 2b. Soil 2bA, which is overlain by soil 2b2A and colluvial wedge C4, is older than ~4 ka based on a ^{14}C age for 2b2A. Using a unit 2b thickness of 1.4–1.5 m (where completely exposed west of fault F4) and based on the similar stratigraphic position of soil 2bA adjacent to C5A (at v-1.0-1.5 m, plate 4), we infer that units 2b and C5 interfinger (possibly similar to the relation between colluvial wedge C3 and alluvial-fan gravel unit 2c) and postdate unit 2a. If the vertical accommodation space for unit 2b is approximately equal to the thickness of C5, then the C5 thickness would be ~1.5 m, which is consistent with that for colluvial wedges C1–C4 (~1–1.5 m). The age of unit C5 is thus bracketed between ~5–6 and ~4 ka, postdating footwall fan deposition, but contemporaneous with early alluvial-fan sedimentation on the hanging wall.

Unit C4 is the oldest colluvial wedge for which we exposed a basal contact. The wedge continues laterally ~3.2–5.0 m and has a maximum thickness of 1.3–1.4 m. Evidence for C4 includes a fault termination at the C5A–C4 contact (h-21 m, v-1.4 m, plate 4), slope-parallel clast fabric, and an intra-wedge soil lens (soil C4A; h-20.7 m, v-1.6 m, plate 4). Unit C4 overlies soil C5A and likely 2bA, is interfingered with soil 2b2A (h-19 m, v-1.5 m, plate 4), and predates formation of an A horizon developed within the uppermost part of the unit (soil C4A; h-21.0 m, v-2.4 m; plate 3). Charcoal from soil C5A (NC-R12) yields a maximum age of 4.0 ± 0.1 ka for C4. Charcoal (charred floral remains) from 2b2A, an alluvial-fan unit coeval with C4, yielded an age of 4.1 ± 0.1 ka (NC-R19). A charcoal sample from soil C4A (intra-wedge soil lens) yielded an age of 5.4 ± 0.2 ka (NC-R13); however, this sample likely contained charcoal fragments eroded from soil 1bA (~5 ka) exposed in the fault footwall. The age of unit C4 is thus about 4 ka.

Unit C3 consists of scarp colluvium interbedded with hanging-wall gravel unit 2c (h-18 m, v-2.2 m, plate 4). The colluvial wedge continues laterally 5.2–6.3 m and has a maximum thickness of about 0.8–1.0 m; however, considerable uncertainty exists in the thickness of C3 because it is locally interfingered with unit 2c. Although we consider unit C3 a probable colluvial wedge, evidence in support of this interpretation is weaker than for C1, C2, and C4. Although C3 has a geometry that shows a minor degree of thickening toward fault F1 (h-18–20, plate 3; h-18–19, plate 4), colluvial deposition in the unit may have been impeded by fan-gravel deposition in unit 2c on the hanging wall. Further, the exposure of C3 adjacent to fault F1 was limited because of a short trench-wall height, which may not have completely exposed the unit. Regardless of the origin for C3, the unit includes sediment that unconformably overlies minor faults and fissures formed in unit C4 and soil C4A. Locally, an A horizon is developed within the uppermost part of C3 (soil C3A; h-22.0 m, v-3.3 m; plate 3). In the south wall, unit C3 postdates the ~4-ka age for soil 2b2A. Colluvial deposition in C3 occurred as late as

~2.1 ka (NC-R18) based on charcoal extracted from the uppermost part of the unit. Charcoal from soil 2cA, developed within the uppermost part of unit 2c, yields a minimum age of 1.2 ± 0.1 ka (NC-R16) for C3 deposition. In the north wall, unit C3 is bracketed by ages of 0.2 ± 0.2 ka (NC-R29) and 0.6 ± 0.1 ka (NC-R23) for C4A and C3A, respectively; however, these anomalously younger ages are stratigraphically inverted with each other and overlying units (e.g., C2A), and may be indicative of burrowed sediment. The age of unit C3 is thus bracketed between ~4 ka and ~2 ka.

Scarp colluvium in unit C2 postdates units C3 and 2c, as well as soils C3A and 2cA, and is the youngest faulted colluvial wedge along fault F1. Evidence for C2 includes slope-parallel clast fabric and silt, sand, and gravel that have partially buried soil 2cA. Unit C2 has a maximum thickness of 0.9–1.2 m and a horizontal extent of about 1.9–2.8 m. Unit C2 is bracketed by soils 2cA (below) and C2A (above), which merge into a single soil (2cA) beyond the extent of C2. This relation is similar to that for colluvial wedge Cg1 in the graben (south wall; near fault F6), which is bracketed by soils 2cA (below) and 2cA2/CgA (above). A maximum age constraint for unit C2 deposition is 1.2 ± 0.1 ka (NC-R16) based on charcoal derived from the underlying soil 2cA. Charcoal from the overlying soil C2A yielded ages of 0.3 ± 0.2 ka (NC-R21) and 6.0 ± 0.1 ka (NC-R15); however, charcoal in sample NC-R15 is likely derived from the unit 1bA burn horizon (~5 ka) in the footwall. An additional minimum age for C2 deposition is from the soil on unit Cg1 (2cA2/CgA; 0.9 ± 0.1 ka for NC-R2; h-8.4, v-3.6; plate 4). Considering the similar soil and stratigraphic relations for colluvial wedges C2 and Cg1 (both deposited on the unit 2c A horizon) and similar ages (~1.2 ka for soil 2cA and ~0.9 ka for soil 2cA2/CgA), we consider it likely that unit Cg1 was deposited contemporaneously with C2. Thus, unit C2 deposition occurred between about 1.2 and 0.3–0.9 ka.

Unit C1 is the youngest colluvial wedge adjacent to fault F1 and is unfaulted. The colluvium has a maximum thickness of 1.3–1.5 m and continues laterally for 5.4–5.5 m. Evidence for C1 includes silt, sand, and gravel that form a slope-parallel fabric (lenses) that has buried a shear zone and 1.4–2.3-m-high eroded scarp free face. Deposition of unit C1 occurred after the formation of soil C2A at about 0.3 ± 0.2 ka (NC-R21) in the north wall, and as late as 0.4 ± 0.1 based on a charcoal age for an intra-wedge soil lens (NC-R20). A second intra-wedge soil lens in unit C1 yielded an anomalously old age of 6.3 ± 0.1 ka, which likely is for charcoal derived from footwall soil 1bA. Age constraints for unit 2d2—a thin silt horizon interfingered with C1—provide additional constraints on the timing of C1 deposition. Charcoal from unit 2d2 yielded an age of 0.2 ± 0.2 ka (NC-R22) and an OSL age for the silt is 1.5 ± 0.3 ka (NC-L2). We discount the OSL age considering the numerous young (<1 ka) ages for soil charcoal sampled from units stratigraphically below unit 2d2. Considering these ages, C1 deposition occurred at ~0.2–0.4 ka. In the graben, C1 postdates soil 2cA, which formed at about 0.4 ka (NC-R31), and may be contemporaneous with colluvial wedges Cg2 and Cg3, which partially bury soil 2cA and were deposited as late as about 0.2 ka (NC-R32). However, the relation of C1 to Cg1 is less clear as Cg1 deposition predates soil formation in 2cA2/CgA at ~0.9 ka (NC-R02).

Colluvial wedges formed by movement on graben faults F2–F7 include units Cg1–3. These colluvial wedges have limited (less than ~1.5-m-wide) horizontal extents and have maximum thicknesses of 0.2–0.6 m (table 5). Colluvium in unit Cg1 is adjacent to antithetic fault F6 and buries soil 2cA in both the north and south walls. Similarly, unit Cg2 is formed adjacent to synthetic fault F3 and buries soil 2cA in both walls. Unit Cg3 postdates faulting on antithetic fault F2; sediment in Cg3 overlies soil 2cA in the north wall. Although we did not map unit Cg3 in the south wall, we note that soil 2cA is overthickened adjacent to fault F2, and thus, colluvium postdating soil 2cA may be present.

Cultural Fill

We exposed cultural fill (unit 4; plates 3 and 4) related to the backfill of a fault-parallel trench excavated by Hansen and others (1981) in 1978. Unit 4 is massive and consists of a poorly sorted mixture of silt, sand, gravel, and organics, and near the base of the deposit, locally includes flagging, nails, and string line. Where best preserved in the south wall, unit 4 is exposed to a maximum depth of about 2.9 m below the surface and is about 1.3 m wide. Based on the position of unit 4 on the fault hanging wall, its north-south orientation, and decrease in depth to the north, we likely exposed the northernmost part of trench NC-1A of Hansen and others (1981).

Wasatch Fault Zone

The WFZ at the North Creek site consists of (1) a main, down-to-the-west shear zone (F1), and (2) a graben between faults F1 and F6. The graben includes both synthetic (F3 and F5) and antithetic (F2, F4, and F6) faults. F6 is the most prominent, westernmost graben-bounding antithetic fault; an additional antithetic fault (F7) is present west of F6, but this fault has only minor vertical displacement (<0.2 m) and is not used to define the graben.

Fault F1 consists of one to three fault traces (figure 14; plates 3 and 4) that juxtapose the footwall alluvial-fan gravel (units 1a and 1b) and hanging-wall colluvial wedges (C2–C5). The relatively simple fault zone is <0.5 m wide and includes sheared silt, sand, and gravel containing clasts rotated parallel to the general plane of faulting. In the north wall, fault F1 dips about 67° to 80° west, and in the south wall, about 77° to 85° west.

Faults F1 to F6 form a ~13-m-wide graben in hanging-wall alluvial-fan units 2a–2c. The bulk of graben deformation is within the 5.3–6.1 m between faults F2 and F6, where both down-to-the-east and -west faults define narrow (<2 m wide) fault-bounded blocks. Antithetic fault F7 is 2.6–3.1 m west

of fault F6 (h-5.5 m, v-3 m, plate 4) and has ~0.1–0.2 m of vertical displacement. Faults F2–F6 displace soil 2cA, but not 2cA2/CgA or overlying units 2d–e or 3. In the north wall, faults F2–F7 dip 80° to 83° west and 74° to 83° east, compared to 71° to 84° west and 69° to 87° east in the south wall.

The differential displacement of soils 2bA and 2cA across the graben provide evidence of at least two surface-faulting earthquakes (appendix J). Using horizontal projections, soil 2bA is vertically displaced 1.5–2.0 m across faults F2–F6 (e.g., v-~2.8 m west of F6 to v-~1.3 m east of F2; plate 3). In contrast, soil 2cA is vertically displaced 0.7–0.9 m (e.g., v-~3.5 m west of F6 to v-~2.7 m east of F2; plate 3). This implies an initial event that displaced soil 2bA down to the east 0.7–1.1 m. Fault F2 provides good evidence of these two events, as soil 2bA is displaced 0.6–0.8 m and soil 2cA is displaced only 0.3–0.5 m. We infer that the earlier earthquake predates soil 2b2A and also C4, which interfingers. Soil 2b2A, which is likely contemporaneous with soil 2bA west of fault F2, has a vertical displacement of ~0.3–0.5 m, consistent with the displacement for soil 2cA. Thus, the earlier graben-faulting event could correspond with the event responsible for C4 deposition. Alluvial-fan deposition in the graben (unit 2c) and subsequent soil development (soil 2cA) postdate the earlier graben event and predate the second graben event. Soil 2cA is continuous beneath units C2, Cg1, and Cg2 and thus, the younger graben event may correspond with the main-fault (F1) surface rupture responsible for C2 deposition. However, more than one event could be recorded in the distributed faulting of 2cA. For example, based on the timing of Cg2 deposition (~0.4 ka), the earlier graben event could also correspond with the event that occurred immediately prior to C1 deposition.

The total displacement across the main fault (F1) is difficult to assess, as we did not expose alluvial-fan deposits on the hanging wall that are correlative with those in the footwall. However, our stratigraphic observations and geochronologic results indicate that hanging-wall alluvial-fan unit 2c is contemporaneous with colluvial wedges C4 and C3 and that these fan and colluvial-wedge units postdate the footwall fan stratigraphy (unit 1). We also infer that units 2b and C5 postdate the footwall fan units. This inference is based on the character of the alluvial-fan sediments in 2b (similar to 2c) and the inferred thickness of units 2b and C5, which likely overlie hanging-wall silt unit 2a if projected horizontally toward fault F1. Further, the similar ages for units 2a (~6 ka) and 1bA (~5–6 ka) suggest that the basal hanging-wall and uppermost footwall units are approximately contemporaneous. Assuming that the footwall fan surface (top of unit 1c) and the top of unit 2a in the hanging wall are correlative surfaces, we estimate a total vertical displacement, accounting for graben deformation in faults F2 to F7, of 10.4 m (appendix J).

We also estimate the total displacement post ~5–6 ka using the sum of the individual colluvial wedge maximum thicknesses. The cumulative thickness for C1 to C4 is 4.8 m, or an average thickness of 1.2 m. Assuming that the thickness of C5 is similar to the C1–C4 average, the total thickness is 6.0 m. However, we have lower confidence in the total wedge thickness because of the extensive graben faulting, which occurred in some, but not all earthquakes (we have evidence of at least two graben events, compared to five main-fault events). The formation of a sediment trap through graben formation could result in an exaggerated colluvial-wedge thickness compared to events without graben faulting. Despite the uncertainty in the relation between colluvial-wedge thickness and displacement at North Creek, we still consider the values to be a good proxy for minimum fault displacement.

Estimating vertical displacement per event at the North Creek site is problematic because of uncertainties in relating colluvial-wedge thicknesses to displacement, and is compounded by the graben formation in some events. Thus, we do not scale the individual wedge thicknesses to reach the maximum displacement for the site as we did for the Spring Lake site. Although the wedge thicknesses may represent minimum per-event displacements ranging from 0.9 to 1.4 m (average of 1.2 m), we have low confidence in these values. Alternatively, the average per-event displacement at the site is 2.1 m, based on the total displacement at the site (10.4 m) divided by the number of events (five). To approximate the maximum per-event displacements, we added the difference (0.9 m) between the mean displacement (2.1 m) and the mean colluvial-wedge thickness (1.2 m) to the mean displacement (2.1 m). This yields an estimated maximum displacement of 3.0 m per event. These displacement values require several assumptions regarding wedge formation and total displacement, and thus we consider per-event displacement at North Creek poorly constrained.

Paleoseismology of the North Creek Site

Chronology of Surface-Faulting Earthquakes

We used stratigraphic and geochronologic data from the North Creek site, including our observation of five separate colluvial wedges (C1 to C5), to construct several OxCal models for the North Creek site. These models constrain the timing of five surface-faulting earthquakes in the mid- to late Holocene (figure 15, table 6).

We constructed several OxCal models for the North Creek site, but ultimately preferred a model (v3d; appendix H) that (1) excluded near-modern ages likely derived from burrowed sediment, (2) excluded the ~5–6-ka ages for possibly recycled charcoal in the main-fault colluvial wedges, and (3) included several ages from the 1978 Hanson and others (1981) investigation. We excluded several ages from the OxCal model that are clustered around 0.2–0.6 ka (NC-R29, NC-R23, and NC-R20). The anomalously young ages for these charcoal samples may reflect recent burrowing in the sampled sediment. Several charcoal ages are also clustered around 5.4–6.2 ka (NC-R13, NC-R15, and NC-R28). The anomalously old ages for these samples likely reflect charcoal derived from footwall soil (burn

horizon) 1bA (~5.3 ka), which contains abundant charcoal. Our North Creek investigation reoccupied the site of the original trench investigation by Hanson and others (1981). Because of similar stratigraphy exposed in these investigations, we chose to incorporate several ^{14}C ages from Hanson and others (1981) as well as one ^{14}C age from Bucknam (1978), who investigated a natural exposure of the footwall alluvial-fan sediments. We identified samples for which (1) there is minimal uncertainty in their stratigraphic context, especially when compared to our trench interpretation, and (2) the original ages were deemed reliable and used in an OxCal model constructed for a recent reevaluation of the original North Creek data by Crone and others (2014). The original North Creek ages include a 5.2-ka age for the footwall burn horizon (sampled and dated by Bucknam,

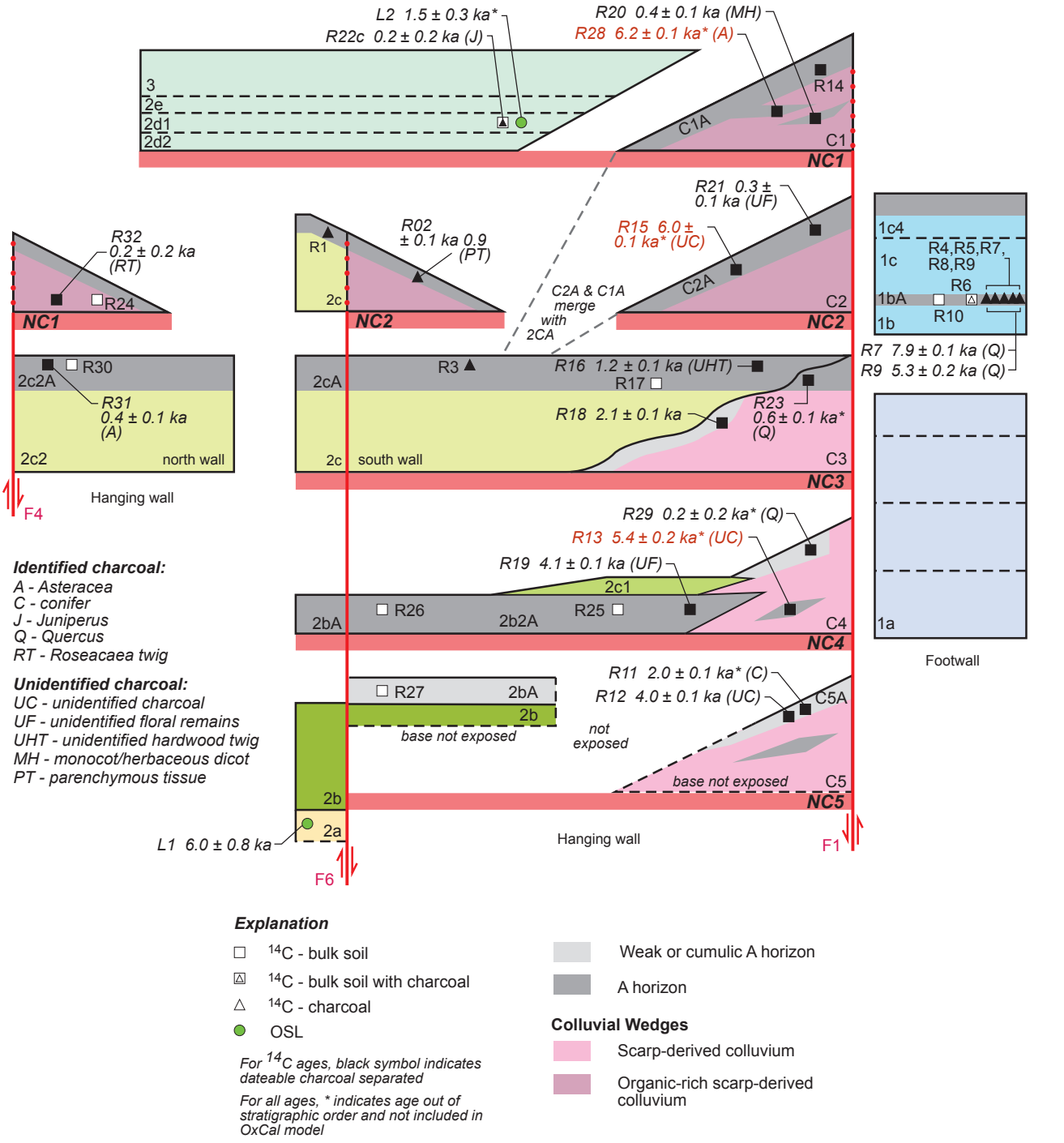

Figure 15. *Summary of colluvial wedges exposed at the North Creek site and their relation to alluvial-fan sediments and ^{14}C and OSL ages. Red text for numerical ages indicates ^{14}C samples likely containing charcoal derived from soil 1bA in the footwall. Horizontal red bars indicate surface-faulting earthquakes in the context of the sedimentary deposits and numerical ages.*

Table 6. *Earthquake timing and recurrence at the North Creek site.*

	Earthquake timing		Earthquake recurrence	
Event	**Mean ± 2σ**[1] *[mode]* (ka)	**Central 95%**[2] (ka)	**Inter-event** *[mode]* (kyr)	**Mean** *[mode]* (kyr)
NC1	0.2 ± 0.1	0.2–0.3	-	-
NC2	1.2 ± 0.1	1.0–1.3	NC2–NC1: 0.9	-
NC3	2.6 ± 0.9 *[2.2]*	2.0–2.5	NC3–NC2: 1.4 *[1.0]*	NC3–NC1: 1.2 *[1.0]*
NC4	4.0 ± 0.1	3.9–4.1	NC4–NC3: 1.4 *[1.8]*	NC4–NC1: 1.3
NC5	4.7 ± 0.7	4.1–5.3	NC5–NC4: 0.6	NC5–NC1: 1.1

[1] Mean ± 2σ based on the OxCal model (model v3f) results. Modal age included in brackets for earthquake NC3.

[2] Earthquake time range including 95.4% of the total area of the time distribution having the highest probability density (Bronk Ramsey, 2013).

1978) and samples WC-12-80-6, WC-12-80-8, and WC-12-80-9 (~1.0–1.3 ka), which provide minimum constraints for the timing of earthquake NC2, and WC-12-80-4 that provides a minimum time for NC1. These ages are in good agreement with ages from our investigation (at similar stratigraphic positions) and help constrain the North Creek earthquake times.

The oldest earthquake observed in our North Creek excavation, NC5, occurred at 4.7 ± 0.7 ka, based on our preferred OxCal model. This earthquake timing assumes that interbedded gravel and organic sediment below unit C4 are related to a colluvial wedge, which likely postdates the youngest footwall alluvial-fan units (e.g., burn horizon 1bA). However, because of the limited exposure of unit C5, we have less confidence in this event. Earthquake NC5 postdates the ~5.3-ka age for the footwall burn horizon (unit 1bA) and predates ~2.0-ka (NC-R11) to ~4.0-ka (NC-R12) ages for charcoal derived from soil C5A. We disregard the ~2.0-ka age, which is anomalously young and stratigraphically inverted with ^{14}C ages for overlying units (e.g., NC-R19 for soil 2b2A).

Earthquake NC4 occurred at 4.0 ± 0.1 ka. The timing of this earthquake is well constrained as it postdates the 4.0 ± 0.1 ka age (NC-R12) for soil C5A and predates the 4.1 ± 0.1 ka age (NC-R19) for soil 2b2A, which likely formed contemporaneously with the deposition of unit C4. Although we considered the possibility that the 4.1-ka charcoal in soil 2b2A is derived from unit C5A, the charcoal consisted of floral remains, which were more likely burned in place than transported. Furthermore, the NC-12 and NC-19 mean ages are only 30 years apart (appendix E), which is less than their average 1σ uncertainty (~60 yr). We excluded two potential minimum age constraints, including a presumably burrowed charcoal from soil C4A, which yielded an age of ~0.2 ka (NC-R29), as well as the anomalously old age for an intra-wedge soil lens within unit C4 of ~5.4 ka (NC-R13), which likely is for charcoal derived from footwall soil 1bA.

Earthquake NC3 occurred between ~4 and 2 ka. Earthquake NC3 is poorly constrained to a maximum by the 4.1-ka age for soil 2b2A, which formed during rather than following C4 deposition (e.g., C4A). Charcoal derived from a soil developed within the uppermost part of unit C3 provides a minimum age of 2.1 ± 0.1 (NC-R18). An additional minimum age is 1.2 ± 0.1 ka (NC-R16) for soil 2cA, which postdates deposition of units C3 and 2c. These limiting ages yield an earthquake time of 2.6 ± 0.9 ka. However, because of the unknown elapsed time between C4 deposition, soil development (C4A), and early C3 colluvial-wedge deposition, we consider the ~2.1-ka minimum age (from C3) to be a better approximation of the NC3 time than the 4-ka maximum age (from C4). Thus, we used a Zero_Boundary grouping in OxCal to implement this interpretation (see discussions above and in DuRoss and others [2011]). This results in an earthquake NC3 time distribution that has a mode of 2.2 ka, closer to the younger end of its 95% range (2.0–2.5 ka); we prefer the modal time (peak of the probability density function) because the Zero_Boundary command produces a highly skewed distribution. In constructing the OxCal model, we also evaluated ^{14}C ages for charcoal and bulk-soil samples that were part of the original North Creek trench investigation. Hanson and others (1981) reported a ~2.0-ka age (WC-12-80-3) for a soil sampled 2.0–2.5 m below the ground surface in their trench NC-1A. Based on the depth of the sample location and its age, we suspect that Hanson and others (1981) sampled our soil 2bA, which is 1.8–2.4 m below the surface where we exposed the Hanson and others (1981) trench (unit 4). However, because of uncertainty in whether the soil sampled in WC-12-80-3 predates or postdates colluvial wedge C3, we excluded the age in our OxCal model.

Earthquake NC2 occurred at 1.2 ± 0.1 ka, following deposition of extensive alluvial-fan unit 2c. The ages for soil C3A and soil 2cA provide maximum constraints of 2.1 ka and 1.2 ka, respectively. An age of 0.9 ka (NC-R02) for soil 2cA2/CgA, which postdates antithetic faulting along graben fault F6a, possibly provides a minimum constraint on the timing of earthquake NC2. This inference is based on the interpretation that between faults F1 and F2, soil 2cA splits to soil 2cA below unit C2 and soil C2A above it. This relation is similar to soils 2cA below colluvial wedges in the graben and 2cA2/CgA above. Although we suspect soil 2cA in the graben continued forming after earthquake NC2 (as suggested by the <0.5-ka ages for colluvial wedge Cg2), the minimum age for colluvial wedge Cg1 suggests that it postdates earthquake NC2. To help limit the minimum time of earthquake NC2, we also included three ^{14}C ages from the original North Creek investigation. These ages are from trench NC-3, which identified unambiguous evidence of two earthquakes. Hanson and others (1981) reported ages of ~1.0–1.3 ka (WC-12-80-6, -8, and -9) for soil sediment postdating the penultimate colluvial wedge; Crone and others (2014) used these ages in their North Creek OxCal model, and thus we also use them to limit the minimum time of earthquake NC2.

The youngest surface-faulting earthquake, NC1, occurred at 0.2 ± 0.1 ka. To limit the maximum time of earthquake NC1, we included a 0.3 ± 0.1 ka (NC-R21) age for soil C2A and an age of 0.4 ± 0.1 ka (NC-R31) for soil 2cA, where buried by colluvial wedge Cg2. Charcoal samples of unit 2d2, which was deposited contemporaneously with C1 and thus postdates earthquake NC1, and colluvial wedge unit Cg2 provide minimum-constraining ages of 0.2 ± 0.2 ka (NC-R22) and 0.4 ± 0.1 ka (NC-R31), respectively. A sample of the C1 colluvial wedge yielded a minimum age constraint for NC1 of 0.4 ± 0.1 ka (NC-R20); however, this age is stratigraphically inverted with the 0.2–0.3-ka ages for NC-R21 and NC-R31 (yields poor agreement in the OxCal model), and thus we excluded it. Finally, we include a minimum age for NC1 of 0.3 ± 0.4 ka (sample WC-12-80-4) for charcoal sampled from the base of the historical debris flow (our unit 3) reported in Hanson and others (1981).

Earthquake Recurrence and Fault Slip Rate

We calculated inter-event and mean recurrence intervals between individual North Creek earthquakes NC5 and NC1 using the mean earthquake times (table 6; appendix L). Inter-event recurrence intervals between earthquakes NC5 and NC1 range from ~0.6 kyr for NC5–NC4 to ~1.4 kyr for NC4–NC3 and NC3–NC2 (table 6). However, using the modal time for earthquake NC3 yields inter-event recurrence times of 1.8 kyr for NC4–NC3 and 1.0 kyr for NC3–NC2. These mean inter-event recurrence times yield a COV on recurrence of 0.35 (0.39 kyr standard deviation divided by 1.11 kyr mean recurrence). We also calculated a COV excluding the interval for NC5–NC4 on account of the uncertainty in the earthquake NC5 interpretation. The COV for NC4–NC1 is 0.22 (0.28 kyr divided by 1.27 kyr).

Mean recurrence intervals measured between earthquakes NC5 to NC3 and NC1 (e.g., NC5–NC1 or NC4–NC1) are consistently between 1.1 and 1.3 kyr (table 6). Using the modal time for earthquake NC3 results in a shorter mean recurrence for NC3–NC1 of 1.0 kyr. Similar to the Spring Lake site, the mean recurrence values indicate a more constant rate of earthquakes when averaged over thousands of years. We have the most confidence in the 1.3-kyr mean recurrence value, which includes three intervals between the four best-constrained earthquakes (NC4–NC1).

Because of uncertainty in the displacement per event at North Creek, we only calculate vertical slip rates using the sum of several surface-faulting-earthquake displacements (e.g., NC4–NC1) (table 7; appendix L). Based on our discussion of total displacement (see Wasatch Fault Zone section above), the total displacement of possibly correlative units

Table 7. *Vertical slip rates at the North Creek site.*

Slip Rate Type[1]	Total Displacement[2] (m)	Elapsed Time[3] (kyr)	Slip Rate (mm/yr)
Geologic rate	10.4 (6.0–14.8) (units 1c/2a)	5.3 (5.0–5.4) (soil 1bA)	2.0 (1.1–2.9)
Interval rate	8.3 (3.9–12.7) (NC4–NC1)	4.4 (3.8–5.1) (NC5–NC1)	1.9 (0.8–3.3)

[1] Geologic rate – open-ended geologic slip rate (e.g., total displacement divided by unit or surface age). Interval rate – closed-interval slip rate (e.g., displacement in one or more earthquakes divided by their preceding time intervals).

[2] Total vertical displacement. For the geologic rate, the total displacement of units 1c and 2a is shown. For the interval rate, the total displacement is the displacement of units 1c and 2a minus 2.1 m to account for earthquake NC5 (see text for discussion).

[3] For the geologic rate, the elapsed time is the age of soil 1bA: the mean and lower-bound ages for soil 1bA are based on the 5.3 ka age for sample NC-R9; the upper-bound age is based on the 5.4 ka mean age of Bucknam (1978). For the interval rate, the elapsed time is the mean and central 95% time between earthquakes NC5 and NC1, modeled using OxCal (appendices H and J).

2a and 1c is 10.4 m. This displacement postdates soil 1bA dated to about 5.3 ± 0.1 ka (NC-R9) or 5.2 ± 0.6 ka (Bucknam, 1978). These ages yield a geologic (open-ended) slip rate of 2.0 mm/yr and an approximate 95% range of 1.1–2.9 mm/yr. We also calculated an interval slip rate by dividing the estimated displacement in earthquakes NC4–NC1 by the elapsed time between earthquakes NC5 and NC1. To estimate the NC4–NC1 displacement, we took the mean and lower- and upper-bound total displacement values (10.4 m, 6.0–14.8 m) and subtracted the mean per-event displacement of 2.1 m to account for the NC5 displacement. The resulting displacement for NC4–NC1 is 8.3 m (3.9–12.7-m range). Using the ~4.4 kyr (3.8–5.1 kyr 95% range) closed seismic interval between NC5 and NC1, the slip rate is 1.9 mm/yr (0.8–3.3 mm/yr approximate 95% range).

Comparison with Previous North Creek Data

We compare our North Creek earthquake chronology with the results of the original North Creek investigation, as reinterpreted by Crone and others (2014). The Crone and others (2014) earthquake times are comparable to our results because they reflect similar assumptions regarding calendar calibration of ^{14}C ages (using Reimer and others, 2013) and stratigraphic model development and earthquake-time modeling in OxCal. Our North Creek investigation yielded five earthquakes at ~0.2 ka (NC1), ~1.2 ka (NC2), ~2.6 ka (NC3), ~4.0 ka (NC4), and ~4.7 ka (NC5). Based on the Hanson and others (1981) stratigraphic and numerical data, Crone and others (2014) report stratigraphic evidence for two North Creek earthquakes at ~0.4 ka and ~1.4 ka, and geomorphic evidence (a faulted terrace) for an additional event at ~1.9 ka.

Earthquakes NC1 (0.2 ± 0.1 ka) and NC2 (1.2 ± 0.1 ka) identified in our investigation likely correspond with the most recent and penultimate earthquakes, respectively, reported by Hanson and others (1981). Based on the Crone and others (2014) interpretation of the Hanson and others (1981) data, NC2 occurred at ~1.4 ± 0.3 ka, predating five charcoal and soil ages clustered between 1.0 and 1.5 ka; NC1 occurred at 0.4 ± 0.5 ka, postdating these ages. The broad uncertainty for the most recent earthquake time stems from the lack of a minimum limiting time constraint (Crone and others, 2014). We note similarities in the colluvial packages for these earthquakes in both investigations. Units C2 (this study) and 5a (Hanson and others, 1981) are both somewhat limited colluvial wedges juxtaposed against sheared sediment. Hanson and others (1981) interpreted unit 5a as the basal part of the most-recent-earthquake colluvium at the site (unit 5b), showing the steep eastern boundary of unit 5a as a buried free face. In contrast, we break these units (units 5a and 5b of Hanson and others, 1981; units C2 and C1, this study) into separate colluvial wedges on the basis of unambiguous shearing (rotated clasts) in unit C2. Units C1 (this study) and 5b (Hanson and others, 1981) indicate the youngest, unfaulted colluvial wedges in both studies.

In both our North Creek investigation and that of Hanson and others (1981), there is stratigraphic and geochronologic evidence for an earthquake at about 2 ka. Earthquake NC3 occurred at 2.6 ± 0.9 ka; however, as discussed above, the time distribution is asymmetrically skewed and yields a modal value of 2.2 ka. Comparably, the original North Creek data indicate an earthquake at 1.9 ± 0.5 ka (Crone and others, 2014) based partly on a poorly understood soil sample (WC-12-80-3) from trench NC-1A (Hanson and others, 1981). Despite the uncertainty in this earthquake time, it corresponds well with the 2.2-ka modal time for earthquake NC3. In addition, the colluvial wedge for earthquake NC3 (unit C3) likely corresponds with unit 3 of the original investigation. Although Hanson and others (1981) tentatively interpreted unit 3 as a mudflow deposit, we note that it has a wedge shape (very similar in shape and extent to their unit 5a) and buries a back-rotated soil (their soil 2s).

Our North Creek investigation includes two older earthquakes, at 4.0 ± 0.1 ka (NC4) and 4.7 ± 0.7 ka (NC5), than those identified by Hanson and others (1981) (NC3–NC1). Earthquake NC4 is based on a colluvial wedge (unit C4) that Hanson and others (1981) likely exposed but did not date. Our colluvial wedge C4 may correspond with their unit 2a, described as scarp-derived colluvium or alluvium. Although Hanson and others (1981) reported an age for a soil developed on unit 2a (their soil 2s), the age is anomalously young at ~0.3 ka. Earthquake NC5 is likely the oldest earthquake that postdates the footwall fan gravel and soil. Colluvial wedge unit C5, which provides the basis for this earthquake, was not exposed in the Hanson and others (1981) trenches.

DISCUSSION

Paleoseismology of the Northern Strand

At least five to seven surface-faulting earthquakes have ruptured the Spring Lake site since ~13 ka (table 3). The five-event model assumes that colluvial wedges C3 and C4 were both deposited following earthquake SL4, and C5 and C6 following earthquake SL6; the seven-event model accounts for separate earthquakes for each colluvial wedge exposed at the site. Although we cannot rule out the possibility of multiple distinct colluvial wedges (e.g., C6 and C5) deposited following a single surface-faulting earthquake, we consider the scenario of separate earthquakes for each individual colluvial wedge to be most likely considering the stratigraphic information and numerical data. Although earthquake SL7 remains poorly constrained, we include this earthquake because of the upward fault terminations exposed in the footwall of fault F1. These earthquakes show that the northern strand has been active over the Holocene, generating earthquakes about every 1.2 kyr (using earthquakes SL6 to SL1; table 3).

Our Spring Lake data compare well with previous data for the northern strand (table 8; figure 16). The youngest earthquake, SL1 at ~0.9 ka, is likely a separate, older earthquake than earthquake SQ1 identified at the Santaquin site at ~0.3–0.5 ka (using the mean times from the interpretations of DuRoss and others [2008] and DuRoss and others [2016b]). In either interpretation of SQ1, the upper bound of the 95% confidence range is ~0.5 ka, younger than the lower bound of 0.7 ka for earthquake SL1. In contrast, the two earthquakes identified at the Picayune Canyon site likely correspond with earthquakes interpreted at the Spring Lake site. We constructed an OxCal model for the Picayune Canyon site (appendix H), which yields earthquake times of 2.4 ± 0.4 ka (2σ) (PC1) and 3.3 ± 0.4 ka (PC2). These earthquake times are similar (but ~0.5 kyr younger) than earthquakes SL2 (~2.9 ka) and SL3 (~4.0 ka) at Spring Lake. The differences in these earthquake times may be related to the complexities of soil formation and sampling at the two sites, or the limited geochronologic control (few maximum and no minimum ages) for the Picayune Canyon site. Importantly, correlating earthquakes SL3 and PC2 provides support for two separate earthquakes for SL4 (unit C4) and SL3 (unit C3), because no older colluvial wedges predating earthquake PC2 (which could correspond with the time of earthquake SL4) were present at the Picayune Canyon site. Interestingly, earthquakes SL3/PC2 and SL2/PC1, as well as SL1, were not identified at the Santaquin site; however, this is most reasonably explained considering the young (~0.5–1.5 ka) age of the faulted alluvial-fan surface and the detrital charcoal (having inherited ages) prevalent in the buried soils and fan sediments at the site (DuRoss and others, 2008).

In 2010, Utah Valley University (D. Horns, written communication, 2011, 2015) excavated a trench at the Payson site, about 0.3 km north of the Spring Lake site. The Payson trench exposed colluvial-wedge evidence of two post-Bonneville earthquakes (PA1 and PA2). Charcoal extracted from soils buried by scarp colluvium indicate earthquake times younger than 0.7 ka and between ~2.4 and 2.8 ka. We constructed an OxCal model for the Payson site (appendix H), which indicates earthquakes at 0.5 ± 0.3 ka (PA1) and 2.7 ± 0.2 ka (PA2) (figure 16); modal values and 95% ranges for the earthquakes are 0.6 (0.2–0.7) ka (PA1) and 2.8 (2.4–2.8) ka (PA2). For PA1, the earthquake timing distribution is asymmetrically skewed toward the maximum-limiting age (~0.7 ka) as no ages constrain the minimum time of the event. These earthquake times correspond reasonably well with Spring Lake earthquakes SL1 at ~0.9 ± 0.2 ka and SL2 at 2.9 ± 0.7 ka. However, the time of PA1 also overlaps with Santaquin earthquake SQ1 at ~0.5 ka. Despite the similar ages, only a single maximum ^{14}C age constrains the time of earthquake PA1, and evidence of an earthquake younger than ~0.7 ka was not exposed at either Spring Lake or Picayune Canyon, which are between the Payson and Santaquin sites. Thus, we consider it likely that SL1 and PA1 correspond and are evidence of the same earthquake at ~0.7 ka. However, because of the limited documentation for PA1 and PA2, we do not use the Payson trench data in our interpretation of the Nephi-segment paleoseismology.

These data suggest that at least seven (excluding Spring Lake earthquake SL5) to eight (including SL5) earthquakes have ruptured the northern strand since ~13 ka (table 8). Excluding

Table 8. *Summary of earthquake timing data for the northern and southern strands of the Nephi segment.*

Northern Strand[1]			Southern Strand[1]		
Spring Lake (ka)	Picayune Canyon (ka)	Santaquin (ka)	North Creek (ka)	Willow Creek (ka)	Red Canyon (ka)
no evidence	*no evidence*	~0.3–0.5 (SQ1)	0.2 ± 0.1 (NC1)	0.2 ± 0.1 (WC1)	0.5 ± 0.5 (RC1)
0.9 ± 0.2 (SL1)	*no evidence*	*no evidence*	1.2 ± 0.1 (NC2)	1.2 ± 0.1 (WC2)	1.2 ± 0.3 (RC2)
2.9 ± 0.7 (SL2)	~2.5 (PC1)	*not exposed?*	2.6 ± 0.9 [2.2] (NC3)	1.9 ± 0.6 (WC3)	*no evidence*
4.0 ± 0.5 (SL3)	~3.5 (PC2)	*not exposed*	4.0 ± 0.1 (NC4)	*no evidence*	*no evidence*
4.8 ± 0.8 (SL4)	*not exposed*	-	4.7 ± 0.7 (NC5)	4.7 ± 1.8 (WC4)	4.7 ± 2.7 (RC3)
5.7 ± 0.8 (SL5)	-	-	*not exposed*	*not exposed*	*not exposed*
6.6 ± 0.7 (SL6)	-	-	-	-	-
13.1 ± 4.0 (SL7)	-	-	-	-	-

[1] Color of shading indicates earthquakes that may correspond along the northern strand (lighter color shading) and along the southern strand (darker color shading). See figure 16 for a comparison of earthquake-timing probability density functions. For earthquake NC3, the modal time is shown in parentheses. For SQ1, the range reflects the mean values from the interpretations of DuRoss and others (2008) and DuRoss and others (2016a).

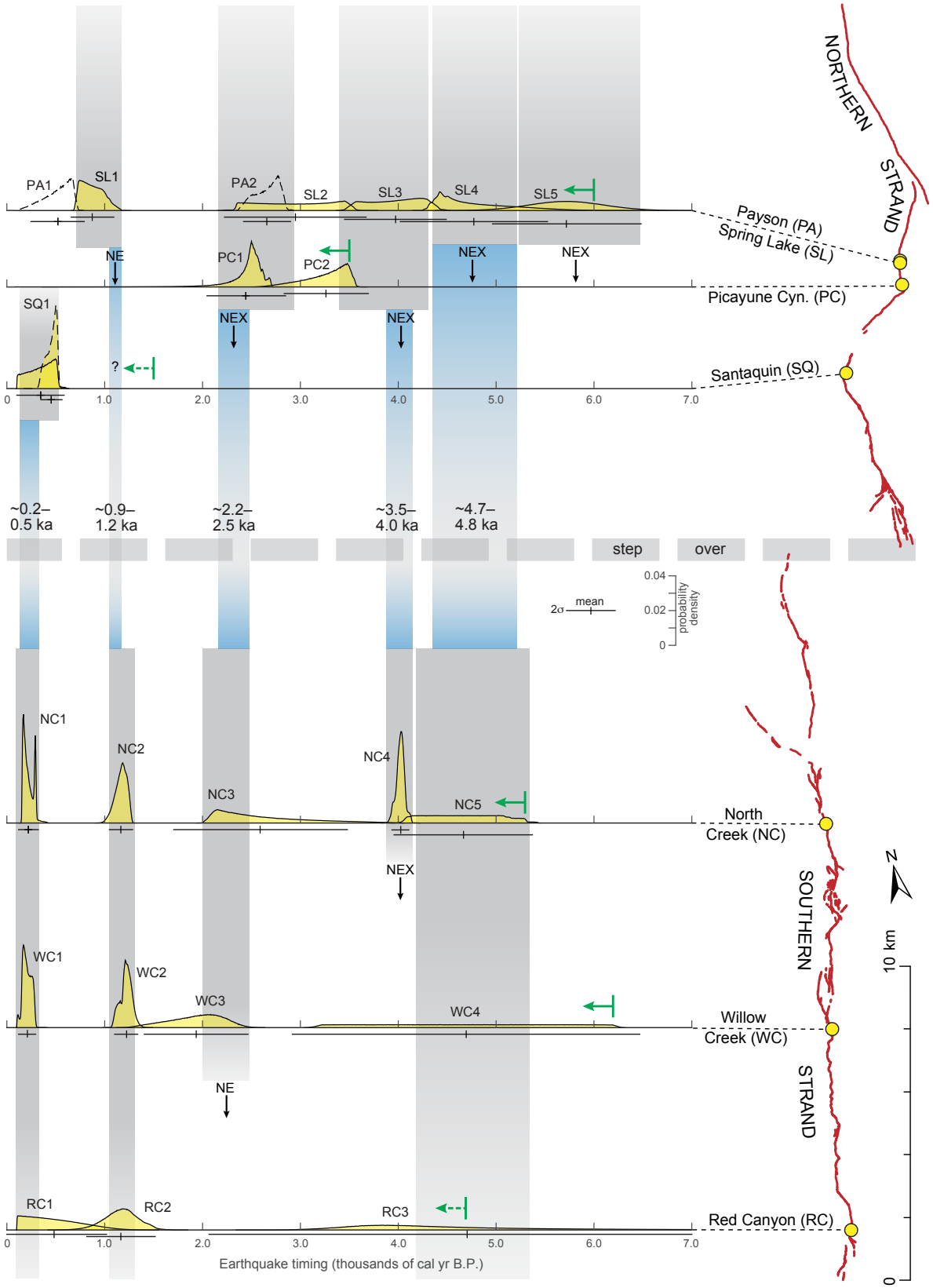

Figure 16. *Comparison of site earthquake ages along the Nephi segment. Earthquake-timing probability density functions (PDFs) are derived from site-specific OxCal models (appendix H); only earthquakes younger than 7.0 ka are shown. Vertical gray bars indicate possible correlation of site PDFs along either the northern or southern strands (e.g., NC1, WC1, and RC1 likely correspond with the youngest earthquake on the southern strand). Blue bars show possible correlation and timing overlap for earthquakes on both strands. Horizontal gray dashed line indicates the step-over zone between the northern and southern strands. NE – no evidence of earthquake at adjacent site; NEX – earthquake not exposed at adjacent site(s). Holocene trace of the Nephi segment (figure 2) shown in red.*

poorly constrained earthquake SL7, the mean recurrence is ~1.0 kyr using six intervals in the ~6.2-kyr elapsed time between earthquakes SL6 and SQ1, or ~1.2 kyr using five intervals in the same time period. Including only mid-Holocene or younger events (SL4–SL1 and SQ1), the mean recurrence is ~1.1 kyr (four intervals in the ~4.4-kyr elapsed time between SL4 and SQ1). These results for the entire northern Nephi strand correspond well with our Spring Lake mean recurrence estimate of 1.2 kyr (SL6–SL1) and the ~1-kyr elapsed time between PC2 and PC1.

Paleoseismology of the Southern Strand

At least five (NC5–NC1) surface-faulting earthquakes have occurred at the North Creek site since about ~4.7 ka (table 6). Although earthquake NC5 remains questionable because of its limited exposure, we include the earthquake considering the structural, textural, stratigraphic, and timing data in support of it. Our North Creek earthquake chronology compares well with the interpretation of southern-strand data by Crone and others (2014) (table 8; figure 16), which is largely based on the Willow Creek investigation, but also includes paleoseismic data from the North Creek (Hanson and others, 1981) and Red Canyon (Jackson, 1991) investigations. In our discussion of these southern-strand earthquake data, we only include our results for the North Creek site; a discussion of how our results compare to those for the Hanson and others (1981) North Creek investigation is presented above (see Comparison with Previous North Creek Data section above). Together, these data show that the southern strand has generated large-displacement (~2 m) earthquakes about every 1.3 kyr since the mid-Holocene (using earthquakes NC4 to NC1).

Four of five earthquakes identified in our North Creek investigation likely correspond with earthquakes previously identified on the southern strand (table 8). North Creek earthquake NC5 (~4.7 ka) could correspond with Willow Creek earthquake WC4 and/or Red Canyon earthquake RC3, which both have mean times of 4.7 ka. However, uncertainty in this correlation stems from the broadly defined time distributions for WC4 and RC3 (1.8–2.7-kyr 2σ uncertainties; figure 16), and thus, WC4 and RC3 could possibly be earthquakes older than ~5 ka that predate the North Creek stratigraphic record. Earthquake NC4, which occurred at about ~4.0 ka, is the only earthquake that does not have corresponding evidence from the Willow Creek or Red Canyon sites. However, NC4 could have occurred within the ~2.9–6.5 ka time period represented by WC4; because stratigraphic evidence of WC4 was not exposed at the Willow Creek site, more than one earthquake could have occurred during the broad WC4 time. Earthquake NC3 occurred at ~2.6 ka, but the time distribution is asymmetrically skewed, and has a more meaningful modal time of 2.2 ka and 95% range of 2.0–2.5 ka. The NC3 time is similar to that for earthquake WC3 (mean time of 1.9 ka), which is oppositely skewed (figure 16) and has a modal time of 2.1 ka and 95% range of 1.4–2.4 ka. Using the mean ages from the Red Canyon earthquake chronology (Crone and others, 2014), no earthquakes ruptured the site between ~1.2 ka (RC2) and 4.7 ka (RC3); however, considering the ~0.3-kyr uncertainty for RC2 it could possibly correlate with NC3. We consider this scenario unlikely considering the low probability, based on the two-sigma timing uncertainties, that NC3 and WC3 are younger than 1.3–1.7 ka and RC2 is older than 1.5 ka. Finally, earthquakes NC2 (~1.2 ka) and NC1 (~0.2 ka) likely correspond with earthquakes at the Willow Creek and Red Canyon sites (table 8). Earthquakes NC2, WC2, and RC2 all have nearly identical mean times (~1.2 ka) and small (≤0.3 kyr) 2σ uncertainties. Earthquakes NC1, WC1, and RC1 also have similar mean times (~0.2–0.5 ka); however, the times for NC1 and WC1 are most similar, and are well constrained by maximum and minimum limiting ages. Earthquake RC1 is similar in time to NC1, but has a broad uncertainty (± 0.5 ka) that stems from the lack of a minimum time constraint.

These data suggest that at least five earthquakes have ruptured the southern strand since ~4.7 ka (table 8). This includes newly identified earthquake NC4, and the correlation of earthquakes NC5, WC4, and RC3. However, it is possible that WC4 and/or RC3 could correspond with either NC4 or an older earthquake not identified at North Creek (prior to ~5–6 ka). These scenarios do not affect the mean recurrence for the southern strand, which is ~1.1 kyr using the four intervals between earthquakes NC5 (~4.7 ka) and NC1 (~0.2 ka), or ~1.3 kyr using three intervals between NC4 (~4.0 ka) and NC1 (~0.2 ka).

Paleoseismology of the Nephi Segment

Paleoseismic data for the North Creek and Spring Lake sites, as well as our analysis of how these data compare with previous data for the northern and southern Nephi strands, show that the Nephi segment has produced several surface-faulting earthquakes during the Holocene. Since the mid-Holocene (~5 ka), the time period over which the earthquake record for the segment is best constrained, both the northern and southern strands have had at least five surface-faulting earthquakes (table 8). These earthquakes, as well as earthquakes at ~6 and 7 ka on the northern strand, yield similar mean recurrence intervals of ~1.0–1.2 kyr for the northern strand and ~1.1–1.3 kyr for the southern strand.

Rupture Behavior of the Northern and Southern Strands

One of the major goals of our study was to determine whether the northern and southern Nephi strands rupture together or independently. To achieve this, we qualitatively compared earthquake histories for sites on the northern and southern strands, looking for clear discordance or overlap in the earthquake time distributions. We interpret timing overlap as consistent with through-going (synchronous) rupture, although uncertainties in the timing of individual earthquakes allow for asynchronous rupture. To a lesser degree, we also considered the shapes of the earthquake timing distributions, the

number and location (along the fault) of sites having evidence of a particular event, and the per-event vertical displacement observations.

Our evaluation of the rupture behavior of the northern and southern strands is limited by moderate (~0.1–0.6 kyr) to large (≥0.7 kyr) uncertainties in the timing of individual events and sparse paleoseismic data for the northern strand (table 8, figure 16). For example, site earthquakes NC5, WC4, and RC3 identified on the southern strand have identical mean times of ~4.7 ka, but large (0.7–2.7 kyr) timing uncertainties that cloud both the correlation of these events along the southern strand and the interpretation of their relation to the northern strand (e.g., to earthquake SL4 at ~4.8 ka). We identified moderately well-constrained earthquakes (2σ uncertainties of 0.1–0.5 kyr) on both the southern and northern strands at ~4.0 ka (SL3 and NC4); however, these earthquakes have only been identified at one site on each strand. An earthquake at ~3.5 ka at the Picayune Canyon site (PC2) may provide additional evidence of the ~4-ka event.

Minimal overlap in the timing of the youngest, best-constrained events also adds uncertainty to the correlation of northern- and southern-strand earthquakes. For example, the youngest three earthquakes on the strands have mostly moderate 2σ timing uncertainties (<0.7 kyr), but less overlap in their time ranges than between the older northern- and southern-strand earthquakes (table 8, figure 16). This reduced overlap may simply relate to how well individual events are constrained (well-constrained events have fewer opportunities to overlap with each other) rather than the quality of the correlation. In particular, northern- and southern-strand earthquakes at 2–3 ka (SL2, PC1, NC3, and WC3) overlap at 2σ, but have disparate mean times (2.5–2.9 ka on the northern strand and 1.9–2.2 ka on the southern strand). Comparably, earthquake SL1 on the northern strand at ~0.9 ka overlaps with the ~1.2-ka earthquake on the southern strand (NC2, WC2, and RC2) at 2σ, but not 1σ.

Vertical displacement data for the southern and northern strands show important differences (table 9), but do not unequivocally support synchronous or independent rupture. Vertical displacements for sites on the northern strand are moderate (~0.8–1.5 m), with the exception of the 3-m displacement for SQ1. Collectively, data from the northern strand suggest that individual-event displacements increase southward. Southern-strand displacements are consistently larger, increasing northward from Red Canyon (~1.4–1.7 m per event) to Willow Creek and North Creek (2.1–2.4 m per event). In general, these data suggest that per-event displacements peak near the center of the Nephi segment, near the northern-southern strand step-over. However, we caution that these displacements are limited by assumptions regarding how colluvial-wedge thickness and displacement relate and the averaged

Table 9. *Summary of vertical displacement data for the northern and southern strands of the Nephi segment.*

Northern Strand				**Southern Strand**			
Earthquake timing[2]	**Vertical displacement**[1] (m)			**Earthquake timing**[2]	**Vertical displacement**[1] (m)		
	Spring Lake[3]	Picayune Canyon	Santaquin		North Creek	Willow Creek	Red Canyon
~0.3–0.5 ka	*NE*	*NE*	3.0 ± 0.2 (SQ1)	~0.2–0.5 ka	2.1 ± 0.7 (NC1)	2.4 ± 0.1 (WC1)	1.4 ± 0.3 (RC1)
~0.9 ka	1.1 ± 0.3 (SL1)	*NE*	*NE*	~1.2 ka	2.1 ± 1.0 (NC2)	2.4 ± 0.1 (WC2)	1.5 ± 0.2 (RC2)
~2.5–2.9 ka	0.8 ± 0.2 (SL2)	~1.5 m? (PC1)	*NEX?*	~1.9–2.2 ka	2.1 ± 1.2 (NC3)	2.4 ± 0.1 (WC3)	*NE*
~3.5–4.0 ka	1.0 ± 0.3 (SL3)	~1.5 m? (PC2)	*NEX*	~4.0 ka	2.1 ± 0.7 (NC4)	*NE*	*NE*
~4.8 ka	0.9 ± 0.2 (SL4)	*NEX*	-	~4.7 ka	2.1 ± 0.9 (NC5)	unknown (WC4)	1.7 ± 0.3 (RC3)

[1] Vertical displacement observations for sites on the northern and southern strands. Unknown indicates earthquake observed, but displacement unknown. *NE* – no evidence of earthquake, *NEX* – earthquake evidence not exposed.

[2] Mean earthquake time or range in mean times from table 8.

[3] For clarity, displacements for earthquakes SL5 (1.0 ± 0.3 m), SL6 (1.0 ± 0.3 m) and SL7 (unknown) are not shown. Displacement references: Spring Lake and North Creek – this study; Picayune Canyon – Horns and others (2009); Santaquin – DuRoss and others (2008); Willow Creek – Crone and others (2014); and Red Canyon – Jackson (1991).

nature of some of the observations, where total displacement is sometimes divided by the number of earthquakes at the site.

Despite the limitations in the Nephi segment paleoseismic data, we interpret similar late Holocene earthquake histories for the northern and southern strands as evidence of complex patterns of rupture on the Nephi segment. Using possible correlations of individual earthquakes along the segment, we developed three rupture scenarios: (1) simultaneous rupture of both strands (the entire Nephi segment), (2) rupture of one strand plus partial rupture of the other strand, and (3) independent rupture of the strands.

Simultaneous rupture of both strands (i.e., complete rupture of the Nephi segment) is possible for earthquakes at ~4.7–4.8 ka and ~2.2–2.5 ka (figure 16). The ~4.7–4.8-ka earthquake, which has been identified at Spring Lake and North Creek, predates the stratigraphic records at Picayune Canyon and Santaquin. The oldest ruptures at Willow Creek and Red Canyon may be evidence of the ~4.7–4.8-ka event; however, uncertainty of this correlation remains because of their large timing uncertainties. Earthquakes on the northern strand at ~2.2–3.5 ka and southern strand at ~1.3–2.5 ka may also be evidence of a full-segment rupture, but there is minimal overlap (at ~2.2–2.5 ka) in the time ranges for these events. Per-event displacements for these events that increase toward the center of the Nephi segment are consistent with, but do not unequivocally support, synchronous rupture.

Two earthquakes on the Nephi segment may have ruptured one strand and only part of the other strand. The ~4-ka rupture, identified at Spring Lake, Picayune Canyon, and North Creek, is possibly evidence of the full rupture of the northern strand and partial rupture of the southern strand (figure 16). Evidence of the 4-ka earthquake was not identified south of North Creek, although the event could correspond with the broadly constrained WC4 or RC3 earthquakes. Full rupture of the southern strand and partial rupture of the northern strand may also have occurred at ~0.2–0.5 ka based on Santaquin earthquake SQ1 (~0.3–0.5 ka), which may be the northernmost extent of the southern-strand most recent earthquake (MRE) at ~0.2 ka. DuRoss and others (2008) and Crone and others (2014) considered this possibility as well as a scenario where earthquake SQ1 is a separate rupture from the southern-strand MRE and is possibly simultaneous with the ~0.6-ka MRE on the Provo segment. However, considering the similar earthquake times for SQ1 and the southern-strand MRE (NC1, WC1, and RC1), lack of evidence for an earthquake younger than 0.5 ka north of Santaquin (at the Spring Lake and Picayune sites), and the large (~3.0 m) displacement for SQ1 that suggests a rupture length in excess of the northern-strand length (DuRoss and others, 2008), we have more confidence in correlating Santaquin earthquake SQ1 with the southern-strand MRE identified in this study.

The penultimate earthquakes on the northern strand at ~0.9 ka and southern strand at ~1.2 ka can be interpreted as evidence of either independent or simultaneous rupture of the strands. Arguments for independent rupture include (1) the minimal overlap in the 2σ time ranges (at ~1.1 ka), and (2) the absence of an earthquake in this time period (~0.9–1.2 ka) on the southern strand south of the Spring Lake site (at the Picayune and Santaquin sites). Furthermore, the SL1 time is very similar to an earthquake at ~0.9 ka interpreted from preliminary data derived from the Water Canyon trench site on the southernmost Provo segment (Ostenaa, 1990), raising the possibility of spill-over rupture from the southern Provo segment to the Nephi northern strand. However, we cannot rule out rupture of the northern and southern strands together at ~1.1 ka because of the overlapping earthquake time ranges.

Conclusions

Based on these data and interpretations, synchronous rupture of the northern and southern strands, including the rupture of one strand and the simultaneous partial rupture of the other, appears to be the most common mode of rupture on the Nephi segment. That is, both strands may rupture synchronously, but they may not both rupture in entirety. Independent rupture of the northern and southern strands or rupture of the Provo segment and northern strand together appears less likely and may have only occurred at ~0.9–1.2 ka on the southern strand; however, these scenarios cannot be ruled out because of uncertainties in earthquake timing. Additional paleoseismic data for the Nephi and Provo segments (e.g., Bennett and others, 2014) and the analysis of along-strike surface offsets (e.g., from lidar data) may help confirm and refine these rupture scenarios. In particular, new paleoseismic data for the southernmost part of the southern strand are needed to update legacy data (the Red Canyon site), and new data for the southernmost part of the northern strand would serve to expand the paleoseismic record to the mid-Holocene.

The similar northern- and southern-strand earthquake histories and our interpretation of the rupture extent of Nephi-segment earthquakes suggest that the ~4-km step-over between the strands is not a significant barrier to rupture propagation. If the step-over acted as a barrier, such as those between most WFZ segments (Machette and others, 1992), we would expect to see unique late Holocene surface-faulting chronologies on the fault strands (see, for example, those for the Weber and Brigham City segments; DuRoss and others, 2011; Personius and others, 2012). The similar earthquake histories for the Nephi strands, but somewhat variable rupture length may be related to the completeness of the paleoseismic records for the strands (e.g., an incomplete earthquake chronology prior to 0.5 ka for the southern half of the northern strand and broadly constrained events prior to 3.0 ka on the southern half of the southern strand), or possibly to rupture nucleation and direction. For example, the scenario of full rupture of one strand and partial rupture of the other strand could be an indication of earthquake nucleation on one strand and the subsequent loss of rupture energy at the fault step-over between the strands, resulting in the partial rupture of the other strand. Alterna-

tively, a bilateral rupture nucleating near the step-over may have sufficient energy to rupture both strands in their entirety. Rupture of the northern and southern strands across the 4-km fault step-over is consistent with Wesnousky (2008), who concluded that historical, laterally propagating normal-fault surface ruptures have propagated across fault-trace discontinuities (e.g., gaps or step-overs) of up to ~4 km in dimension.

SUMMARY AND CONCLUSIONS

Paleoseismic investigations at Spring Lake and North Creek have helped refine the Holocene surface-faulting earthquake history of the Nephi segment. At least five to seven earthquakes ruptured the Spring Lake site, on the northern strand of the Nephi segment, at ~0.9 ka, ~2.9 ka, ~4.0 ka, ~4.8 ka, ~5.7 ka, ~6.6 ka, and ~13.1 ka, yielding a mean recurrence of ~1.2–1.5 kyr and vertical slip rate of ~0.5–0.8 mm/yr (excluding the poorly constrained ~13-ka earthquake). These data compare well with the results of previous investigations and show that the northern strand has a mean recurrence of ~1.0–1.2 kyr since the mid-Holocene. At least five earthquakes ruptured the North Creek site, on the southern strand, at ~0.2 ka, ~1.2 ka, ~2.2–2.6 ka, ~4.0 ka, and ~4.7 ka, yielding a mean recurrence of 1.1–1.3 kyr and vertical slip rate of ~1.9–2.0 mm/yr. These data compare well with previous paleoseismic data and indicate a mean recurrence of ~1.1–1.3 kyr for the southern strand, which is very similar to that for the northern strand. These Nephi-segment mean recurrence intervals correspond well with mean estimates of 1.1–1.3 kyr for WFZ segments to the north (Provo to Brigham City segments), which stem from the paleoseismic data synthesis of DuRoss and others (2014, 2016a, 2016b).

We compared late Holocene earthquake chronologies for the northern and southern strands to evaluate whether they rupture together or independently. Although uncertainty in the rupture behavior of the strands persists due to their moderate to large individual earthquake timing uncertainties, the strands have similar late Holocene earthquake histories and per-event vertical displacements that peak near the center of the segment. These data suggest complex rupture behavior, including synchronous rupture of both strands and the rupture of one strand and simultaneous rupture of part of the other strand. We have less confidence in a model of independent rupture of only one strand of the Nephi segment; however, this model, as well as the potential for simultaneous rupture of the northern Nephi strand and Provo segment, cannot be ruled out given the available data. Our new paleoseismic data help refine the surface-faulting earthquake history of the Nephi segment and help resolve the complexities of surface rupture and moment release across a major structural complexity in the trace of the WFZ. Ultimately, these data are important to improving our understanding of earthquake rupture propagation along multi-segment normal faults and will contribute to more accurate probabilistic earthquake forecasts for the Wasatch Front region.

ACKNOWLEDGMENTS

This collaborative paleoseismic study of the Nephi segment was funded by the Utah Geological Survey and U.S. Geological Survey, National Earthquake Hazards Reduction Program, award no. G12AP20076. We thank the Mower family (Spring Lake site) and the Utah Division of Wildlife Resources (North Creek site) for their interest in this project and for granting permission to perform our trench investigations. Jay Hill (UGS) digitized the trench logs and prepared the plates. We appreciate peer reviews by Steve Bowman and William Lund (UGS) and Scott Bennett (USGS), which helped strengthen this report. Any use of trade, firm, or product names is for descriptive purposes only and does not imply endorsement by the U.S. Government.

REFERENCES

Aitken, M.J., 1994, Optical dating—a non-specialist review: Quaternary Geochronology (Quaternary Science Reviews), v. 13, p. 503–508.

Bennett, S.E.K., DuRoss, C.B., Gold, R.D., Briggs, R.W., Personius, S.F., and Mahan, S.A., 2014, Preliminary paleoseismic trenching results from the Flat Canyon site, southern Provo segment, Wasatch fault zone—testing Holocene fault-segmentation at the Provo-Nephi segment boundary [abs.]: Seismological Research Letters, v. 85, no. 2, p. 546.

Birkeland, P.W., Machette, M.N., and Haller, K.M., 1991, Soils as a tool for applied Quaternary geology: Utah Geological and Mineral Survey Miscellaneous Publication 91-3, 63 p.

Black, B.D., Hecker, S., Hylland, M.D., Christenson, G.E., and McDonald, G.N., 2003, Quaternary fault and fold database and map of Utah: Utah Geological Survey Map 193DM, scale 1:50,000, CD.

Bowman, S.D., Hiscock, A.I., and Unger, C., 2015, Compilation of 1970s Woodward-Lundgren & Associates Wasatch fault investigation reports and low-sun-angle aerial photography, Wasatch Front and Cache Valley, Utah and Idaho: Utah Geological Survey Open-File Report 632, 8 p., 6 plates, 9 DVDs.

Bowman, S.D., and Lund, W.R., 2013, Compilation of U.S. Geological Survey National Earthquake Hazards Reduction Program final technical reports for Utah—Paleoseismology of Utah, Volume 23: Utah Geological Survey Miscellaneous Publication 13-3, 9 p., 56 reports, DVD.

Bronk Ramsey, C., 1995, Radiocarbon calibration and analysis of stratigraphy—the OxCal program: Radiocarbon, v. 37, no. 2, p. 425–430.

Bronk Ramsey, C., 2001, Development of the radiocarbon program OxCal: Radiocarbon, v. 43, no. 2a, p. 355–363.

Bronk Ramsey, C., 2008, Depositional models for chronological records: Quaternary Science Reviews, v. 27, no. 1-2, p. 42–60.

Bronk Ramsey, C., 2009, Bayesian analysis of radiocarbon dates: Radiocarbon, v. 51, no. 4, p. 337–360.

Bronk Ramsey, C., 2013, OxCal analysis details: Online, http://c14.arch.ox.ac.uk/oxcalhelp/hlp_analysis_detail.html, accessed December 2013.

Bucknam, R.C., 1978, Northwestern Utah seismotectonics studies, *in* Seiders, W., and Thomson, J., compilers, Summaries of technical reports, v. VII: Menlo Park, California, U.S. Geological Survey Office of Earthquake Studies, p. 64.

Cluff, L., Brogan, G., and Glass, C., 1973, Wasatch fault, southern portion, earthquake fault investigation & evaluation, a guide to land use planning: unpublished consultant's report for the Utah Geological and Mineralogical Survey, variously paginated.

Crone, A.J., Personius, S.F., DuRoss, C.B., Machette, M.N., and Mahan, S.A., 2014, History of late Holocene earthquakes at the Willow Creek site and on the Nephi segment, Wasatch fault zone, Utah—Paleoseismology of Utah, Volume 25: Utah Geological Survey Special Study 151, 55 p.

Davis, F.D., 1983, Geologic map of the southern Wasatch Front, Utah: Utah Geological and Mineral Survey Map 55-A, scale 1:100,000.

Duller, G.A.T., 2008, Luminescence dating—guidelines on using luminescence dating in archaeology: Swindon, United Kingdom, English Heritage Publishing, 45 p.: Online, http://users.aber.ac.uk/ggd/duller_english_heritage_luminescence_dating.pdf, accessed November 2016.

DuRoss, C.B., 2004, Spatial and temporal trends of surface rupturing on the Nephi segment of the Wasatch fault, Utah—implications for fault segmentation and the recurrence of paleoearthquakes: Salt Lake City, University of Utah, M.S. thesis, 120 p.

DuRoss, C.B., 2008, Holocene vertical displacement on the central segments of the Wasatch fault zone, Utah: Bulletin of the Seismological Society of America, v. 98, no. 6, p. 2918–2933.

DuRoss, C.B., and Bruhn, R.L., 2005, Active tectonics of the Nephi segment, Wasatch fault zone, Utah, *in* Lund, W.R., editor, Western States Seismic Policy Council Proceedings Volume of the Basin and Range Province Seismic Hazards Summit II: Utah Geological Survey Miscellaneous Publication 05-2, 25 p., CD.

DuRoss, C.B., Hylland, M.D., McDonald, G.N., Crone, A.J., Personius, S.F., Gold, R.D., and Mahan, S.A., 2014, Holocene and latest Pleistocene paleoseismology of the Salt Lake City segment of the Wasatch fault zone, Utah, at the Penrose Drive trench site, *in* DuRoss, C.B. and Hylland, M.D., Evaluating surface faulting chronologies of graben-bounding faults in Salt Lake Valley, Utah—new paleoseismic data from the Salt Lake City segment of the Wasatch fault zone and the West Valley fault zone—Paleoseismology of Utah, Volume 24: Utah Geological Survey Special Study 149, p. 1–39, 6 appendices, 1 plate, CD.

DuRoss, C.B., McDonald, G.N., and Lund, W.R., 2008, Paleoseismic investigation of the northern strand of the Nephi segment of the Wasatch fault zone at Santaquin, Utah—Paleoseismology of Utah, Volume 17: Utah Geological Survey Special Study 124, 33 p., 1 plate, CD.

DuRoss, C.B., Personius, S.F., Crone, A.J., Olig, S.S., Hylland, M.D., Lund, W.R., and Schwartz, D.P., 2016a, Fault segmentation—new concepts from the Wasatch fault zone, Utah, USA: Journal of Geophysical Research—Solid Earth, 121, 27 pp. doi: 10.1002/2015JB012519.

DuRoss, C.B., Personius, S.F., Crone, A.J., Olig, S.S., Hylland, M.D., Lund, W.R., and Schwartz, D.P., 2016b, Holocene paleoseismology of the central segments of the Wasatch fault zone, Utah—Appendix B, *in* Working Group on Utah Earthquake Probabilities (WGUEP), Earthquake probabilities for the Wasatch Front region in Utah, Idaho, and Wyoming: Utah Geological Survey Miscellaneous Publication 16-3, p. B1–B70.

DuRoss, C.B., Personius, S.F., Crone, A.J., Olig, S.S., and Lund, W.R., 2011, Integration of paleoseismic data from multiple sites to develop an objective earthquake chronology—application to the Weber segment of the Wasatch fault zone: Bulletin of the Seismological Society of America, v. 101, no. 6, p. 2765–2781.

Felger, T.J., Machette, M.N., and Sorensen, M.L., 2004, Provisional geologic map of the Mona quadrangle, Juab and Utah Counties, Utah: Utah Geological Survey Open-File Report 428, 2 plates, scale 1:24,000.

Godsey, H.S., Currey, D.R., and Chan, M.A., 2005, New evidence for an extended occupation of the Provo shoreline and implications for regional climate change, Pleistocene Lake Bonneville, Utah, USA: Quaternary Research, v. 63, no. 2, p. 212–223, doi:10.1016/j.yqres.2005.01.002.

Godsey, H.S., Oviatt, C.G., Miller, D.M., and Chan, M.A., 2011, Stratigraphy and chronology of offshore to nearshore deposits associated with the Provo shoreline, Pleistocene Lake Bonneville, Utah: Palaeogeography, Palaeoclimatology, Palaeoecology, v. 310, no. 3–4, p. 442–450, doi: 10.1016/j.palaeo.2011.08.005.

Gray, H.J., Mahan, S.A., Rittenour, T., and Nelson, M.S., 2015, Invited paper—Guide to luminescence dating techniques and their application for paleoseismic research, *in* Lund, W.R., editor, Proceedings volume, Basin and Range Province Seismic Hazards Summit III: Utah Geological Survey Miscellaneous Publication 15-5, variously paginated, DVD.

Hanson, K.L., Swan, F.H., and Schwartz, D.P., 1981, Study of earthquake recurrence intervals on the Wasatch fault, Utah: San Francisco, California, Woodward-Clyde Consultants, sixth annual technical report prepared for U.S. Geological Survey under contract no. 14-08-0001-19115, 22 p.

Hanson, K.L., Swan, F.H., and Schwartz, D.P., 1982, Study of earthquake recurrence intervals on the Wasatch fault, Utah: San Francisco, California, Woodward-Clyde Consultants,

seventh annual technical report prepared for U.S. Geological Survey under contract no. 14-08-0001-19842, 10 p.

Harty, K.M., Mulvey, W.E., and Machette, M.N., 1997, Surficial geologic map of the Nephi segment of the Wasatch fault zone, eastern Juab County, Utah: Utah Geological Survey Map 170, 14 p., 1 plate, scale 1:50,000.

Hintze, L.F., 1973, Geologic road log of western Utah and eastern Nevada, part 1: Brigham Young University Geology Studies, v. 20, pt. 2, p. 10.

Hiscock, A.I., and Hylland, M.D., 2015, Surface fault rupture hazard maps of the Levan and Fayette segments of the Wasatch fault zone, Juab and Sanpete Counties, Utah: Utah Geological Survey Open-File Report 640, 7 plates, scale 1:24,000.

Horns, D.M., Rey, K.A., Barnes, C.S., Mcshinsky, R.D., and Palmer, M., 2009, New constraints on the timing of prehistoric earthquakes on the northernmost part of the Nephi segment of the Wasatch fault zone, Utah [abs.]: Geological Society of America Abstracts with Programs, v. 41, no. 6, p. 42.

Huntley, D.J., Godfrey-Smith, D.I., and Thewalt, M.L.W., 1985, Optical dating of sediments: Nature, v. 313, p. 105–107.

Hylland, M.D., 2007a, Surficial-geologic reconnaissance and scarp profiling on the Collinston and Clarkston Mountain segments of the Wasatch fault zone, Box Elder County, Utah—paleoseismic inferences, implications for adjacent segments, and issues for diffusion-equation scarp-age modeling—Paleoseismology of Utah, Volume 15: Utah Geological Survey Special Study 121, 18 p., CD.

Hylland, M.D., 2007b, Spatial and temporal patterns of surface faulting on the Levan and Fayette segments of the Wasatch fault zone, central Utah, from surficial geologic mapping and scarp profile data, *in* Willis, G.C., Hylland, M.D., Clark, D.L., and Chidsey, T.C., Jr., editors, Central Utah—diverse geology of a dynamic landscape: Utah Geological Association Publication 36, p. 255–271.

Hylland, M.D., and Machette, M.N., 2008, Surficial geologic map of the Levan and Fayette segments of the Wasatch fault zone, Juab and Sanpete Counties, Utah: Utah Geological Survey Map 229, 37 p., 1 plate, scale 1:50,000.

Jackson, M., 1991, Number and timing of Holocene paleoseismic events on the Nephi and Levan segments, Wasatch fault zone, Utah—Paleoseismology of Utah, Volume 3: Utah Geological Survey Special Study 78, 23 p.

Lienkaemper, J.J., and Bronk Ramsey, C., 2009, OxCal—versatile tool for developing paleoearthquake chronologies—a primer: Seismological Research Letters, v. 80, no. 3, p. 431–434.

Lund, W.R., 2005, Consensus preferred recurrence-interval and vertical slip-rate estimates—review of Utah paleoseismic-trenching data by the Utah Quaternary Fault Parameters Working Group: Utah Geological Survey Bulletin 134, 109 p., CD.

Lund, W.R., 2010, Summary—Third Meeting—Working Group on Utah Earthquake Probabilities: minutes of the Working Group on Utah Earthquake Probabilities, 16 p., online, http://geology.utah.gov/docs/pdf/WGUEP-2010C_Summary.pdf, accessed November 2016.

Lund, W.R., 2013, Working Group on Utah Earthquake Probabilities preliminary fault characterization parameters for faults common to the Working Group study area and the U.S. National Seismic Hazard Maps—data provided to the U.S. Geological Survey for use in the 2014 update of the National Seismic Hazard Maps in Utah: Utah Geological Survey Open-File Report 611, 6 p.

Machette, M.N., 1992, Surficial geologic map of the Wasatch fault zone, eastern part of Utah Valley, Utah County and parts of Salt Lake and Juab Counties, Utah: U.S. Geological Survey Miscellaneous Investigations Series Map I-2095, scale 1:50,000, 30 p. pamphlet.

Machette, M.N., Crone, A.J., Personius, S.F., Mahan, S.A., Dart, R.L., Lidke, D.J., and Olig, S.S., 2007, Paleoseismology of the Nephi segment of the Wasatch fault zone, Juab County, Utah—preliminary results from two large exploratory trenches at Willow Creek: U.S. Geological Survey Scientific Investigations Map SI-2966, 2 plates.

Machette, M.N., Personius, S.F., and Nelson, A.R., 1992, Paleoseismology of the Wasatch fault zone—a summary of recent investigations, interpretations, and conclusions, *in* Gori, P.L., and Hays, W.W., editors, Assessment of regional earthquake hazards and risk along the Wasatch Front, Utah: U.S. Geological Survey Professional Paper 1500-A, p. A1–A71.

Nelson, A.R., Lowe, M., Personius, S., Bradley, L.A., Forman, S.L., Klauk, R., and Garr, J., 2006, Holocene earthquake history of the northern Weber segment of the Wasatch fault zone, Utah—Paleoseismology of Utah, Volume 13: Utah Geological Survey Miscellaneous Publication 05-8, 39 p., 2 plates.

Open Topography, 2016, Open Topography: Online, http://www.opentopography.org, accessed November, 2016.

Ostenaa, D., 1990, Late Holocene displacement history, Water Canyon site, Wasatch fault zone [abs.]: Geological Society of America Abstracts with Programs, v. 22, no. 6, p. 42.

Oviatt, C.G., 1997, Lake Bonneville fluctuations and global climate change: Geology, v. 25, p. 155–158.

Oviatt, C.G., 2015, Chronology of Lake Bonneville, 30,000 to 10,000 yr B.P.: Quaternary Science Reviews, v. 110, p. 166–171.

Oviatt, C.G., Currey, D.R., and Sack, D., 1992, Radiocarbon chronology of Lake Bonneville, eastern Great Basin, USA: Palaeogeography, Palaeoclimatology, Palaeoecology, v. 99, p. 225–241.

Personius, S.F., DuRoss, C.B., and Crone, A.J., 2012, Holocene behavior of the Brigham City segment—implications for forecasting the next large-magnitude earthquake on the

Wasatch fault zone, Utah: Bulletin of the Seismological Society of America, v. 102, no. 6, p. 2265–2281.

Prescott, J.R., and Hutton, J.T., 1994, Environmental dose rates and radioactive disequilibrium from some Australian luminescence dating sites: Quaternary Science Reviews, v. 14, no. 4, p. 439–448.

Puseman, K., and Cummings, L.S., 2005, Separation and identification of charcoal and organics from bulk sediment samples for improved radiocarbon dating and stratigraphic correlations, *in* Lund, W.R., editor, Western States Seismic Policy Council, Proceedings Volume of the Basin and Range Province Seismic Hazards Summit II: Utah Geological Survey Miscellaneous Publication 05-2, 10 p., CD.

Reheis, R.C., Adams, K.D., Oviatt, C.G., and Bacon, S.N., 2014, Pluvial lakes in the Great Basin of the western United States—a view from the outcrop: Quaternary Science Reviews, no. 97, p. 33–57.

Reimer, P.J., Bard, E., Bayliss, A., Beck, J.W., Blackwell, P.G., Bronk Ramsey, C., Grootes, P.M., Guilderson, T.P., Haflidason, H., Hajdas, I., Hattz, C., Heaton, T.J., Hoffmann, D.L., Hogg, A.G., Hughen, K.A., Kaiser, K.F., Kromer, B., Manning, S.W., Niu, M., Reimer, R.W., Richards, D.A., Scott, E.M., Southon, J.R., Staff, R.A., Turney, C.S.M., and van der Plicht, J., 2013, IntCal13 and Marine13 radiocarbon age calibration curves 0–50,000 years cal BP: Radiocarbon, v. 55, no. 4, p. 1869–1887.

Rhodes, E.J., 2011, Optically stimulated luminescence dating of sediments over the past 200,000 years: Annual Review of Earth and Planetary Sciences, v. 39, p. 461–488, doi: 10.1146/annurev-earth-040610-133425.

Solomon, B.J., Clark, D.L., and Machette, M.N., 2007, Geologic map of the Spanish Fork quadrangle, Utah County, Utah: Utah Geological Survey Map 227, 3 plates.

U.S. Department of Agriculture, 2017, Aerial Photography Field Office, National Agriculture Imagery Program: Online, https://www.fsa.usda.gov/programs-and-services/aerial-photography/imagery-programs/naip-imagery/index, accessed January 2017.

Utah Automated Geographic Reference Center, 2017, GIS map data: Online, https://gis.utah.gov/#data, accessed January 2017.

Wesnousky, S.G., 2008, Displacement and geometrical characteristics of earthquake surface ruptures—issues and implications for seismic-hazard analysis and the process of earthquake rupture: Bulletin of the Seismological Society of America, v. 98, no. 4, p. 1609–1632, doi: 10.1785/0120070111.

Witkind, I.J., and Weiss, M.P., 1985, Geologic map of the Nephi 30' x 60' quadrangle, Carbon, Emery, Juab, Sanpete, Utah, and Wasatch Counties, Utah: U.S. Geological Survey Miscellaneous Investigations Series Map I-1937, scale 1:100,000.

APPENDICES

APPENDIX A
DESCRIPTION OF STRATIGRAPHIC UNITS AT THE SPRING LAKE SITE

APPENDIX A

DESCRIPTION OF STRATIGRAPHIC UNITS IN TRENCHES AT THE SPRING LAKE TRENCH SITE

Unit, genesis[1]	Station no. (trench)[2]	Textural name[3]	Texture (%)[4]				Clasts		Plast-icity[3]	Density/ consistency[3]	Cementation	HCL reaction	Clast angularity	Bedding	Structure	Sorting	Lower bound.[5]	Color[6] dry (moist)	Notes
			F	S	G	C/B	Largest (cm)	Average (cm)											
N1a, L	24h, 6-7v	sandy gravel with cobbles	5	40	45	10	21	2-6	none	very loose-loose	none-very weak	moderate-strong	rounded-subrounded	well bedded	some imbri-cation	moderate well	not exposed	10YR 5/2 (10YR 3/3)	Lacustrine (Bonneville transgressive) gravel with boulder lag at top; oldest unit exposed.
N1b, L	19h, 9-10v	silty sand	19	80	1	-	2	0.01-0.03	non-plastic	loose	weak	strong	subangular	well bedded	low-angle trough cross bedding	well	clear	10YR 6/3 (10YR 3/3)	Lacustrine (Bonneville transgressive near-shore) sand, with cm-scale, alternating sand-clay/silt layers.
N1c, L?	21h, 10-11v	massive silty sand with occasional gravel	10	85	5	-	9	3-4	non-plastic	loose	none-very weak	moderate strong	subrounded-subangular	no bedding; massive	none	poorly sorted	gradual	10YR 6/2 (10YR 3/3)	Possibly Bonneville sand reworked by eolian or slope-wash processes; massive.
N1d, A?	16h, 12-13v	boulder/cobble flow with sandy matrix	10	40	10	40	80	20	non-plastic	medium-dense to loose	non-very weak	strong	subrounded-subangular	no bedding	none	poorly sorted	clear	10YR 6/3 (10YR 4/3)	Likely post-Bonneville flood, sediment derived from Bonneville shoreline; unit includes subunits N1d1 and N1d2.
N2, S-DF	15h, 11-13v	silty gravel with sand and cobbles	20	35	40	5	30	5-10	slight plastic	medium-dense to medium stiff	weak	strong	subrounded-angular	weakly bedded	variable	variable	clear	10YR 6/4 (10YR 5/4)	Post Bonneville channel/debris flow deposits; mostly laterally discontinuous.
N3aA, DF, A	33-39h, 1-2v	A horizon soil in silty sandy gravel with cobbles	10	30	50	10	15	0.5-3	low	med-high	weak	-	angular-subangular	poor	none	poor	not exp.	-	Soil A horizon developed in debris flow; poor to no soil structure present.
N3b, DF	36-42h, 0-1v	matrix supported gravel with cobbles	10	30	50	10	20	-	very low	med-high	weak-moderate	-	angular-subangular	poor	none	poor-moderate	gradual to clear	-	Includes two matrix-rich debris flows.
N3c, S-DF	31-43h, 1-5v	clast and matrix supported gravel with cobbles	5	25	50	20	40	-	low	mod-high	weak-moderate	-	angular-subrounded	poor-moderate	channel complex.	poor-moderate	clear to gradual	-	Includes series of channel complexes with clear cobble/gravel thalwegs.
N3d, S-DF	31-37h, 2-3v	clast and matrix supported gravel with cobbles	10	30	50	10	22	-	low	low-high	weak-moderate	-	angular-rounded	poor-moderate	channel complex.	poor-moderate	clear to gradual	-	Includes channel complexes with low angle margins.
N3f, S-DF	31-44h, 1-6v	clast and matrix supported silty, sandy gravel	10	20	60	10	15	-	low	low-high	moderate	-	angular-subrounded	poor-moderate	none	moderate-well	gradual	-	Includes clast supported gravel with well sorted horizontal beds/lenses of open-work gravel; locally cemented.
N3g, DF	31-44h, 1-6v	matrix supported sandy gravel with cobbles	10	20	35	35	40	-	low	medium-high	weak-moderate	-	angular-subrounded	poor	none	very poor	clear to gradual	-	Massive silt/sand supported gravel with cobbles.
S3a-f, DF	31-41h, 0-3v	matrix (sand) supported gravel with cobbles	10	30	40	20	30	-	very low	medium-high	weak-moderate	-	angular-subangular	poor	none	very poor	gradual to clear	-	Poorly sorted sand-supported gravel with cobbles; includes a poorly sorted pebble-rich debris flow.
S3g, S-DF	31-42h, 3-4v	sand/pebble supported gravel with cobbles	5	25	50	20	45	-	low	low-high	moderate	-	subangular-rounded	poor-moderate	channel complex.	poor-moderate	clear to gradual	-	Series of stacked channels consisting of poor to well-sorted pebble gravel.
S3h, DF	31-45h, 3-5v	matrix supported gravel with cobbles	10	20	35	35	40	-	low	medium-high	weak	-	angular-subrounded	poor	none	poor	clear to gradual	-	Matrix supported massive gravel.
S3i, DF	31-45h, 3-6v	matrix supported gravel with cobbles	15	15	50	20	20	-	low	medium-high	weak	-	subangular-subrounded	poor	none	moderate-poor	clear to gradual	-	Matrix supported massive gravel.
S3j, DF	31-43h, 4-6v	matrix supported gravel with some cobbles	20	10	60	10	15	-	low	medium-high	weak	-	subangular-subrounded	poor	none	moderate	clear to gradual	-	Matrix supported massive gravel.

C1, C	26-27h, 7v	gravely silt with some fine sand and cobbles	50	15	30	5	10	2-5	moderate	medium stiff	weak	strong	angular to subangular	weak slope fabric	slope fabric	poorly sorted	gradual	10YR 6/2 (10YR 3/2)	Colluvial wedge C1.
C2, C	27h, 6v	gravelly sandy silt with cobbles	40	20	25	15	25	5-10	slight	medium stiff	weak	strong	angular to subangular	slope fabric	slope fabric	poorly sorted	gradual	10YR 5/2 (10YR 3/3)	Colluvial wedge C2
C3, C	27h, 6v	gravelly sandy silt with cobbles	35	25	25	15	30	5-10	slight	stiff to loose	weak	very strong	angular to subangular	weak slope fabric	slope fabric	poorly sorted	gradual	10YR 7/3 (10YR 5/4)	Colluvial wedge C3
C4, C	27h, 5v	sandy gravel with silt and small cobbles	30	35	30	5	15	2-5	none to slight	loose to medium dense	weak	very strong	angular to subangular	very weak slope fabric	slope fabric	moderate sorted	gradual	10YR 7/3 (10YR 5/3)	Colluvial wedge C4
C5, C	27h, 4v	sandy gravel with cobbles	15	40	30	15	40	5-10	non-plastic	loose	weak to none	strong	angular to subrounded	weak slope fabric	slope fabric	poorly sorted	gradual	10YR 6/3 (10YR 4/4)	Colluvial wedge C5
C6, C	28h, 3v	sand (massive)	10	84	5	1	10	0-5	non-plastic	loose to medium dense	none	strong	subangular to subrounded	massive to weak slope fabric	none	moderate to well sorted	gradual	10YR 6/2 (10YR 4/2)	Colluvial wedge C6
CF3	11.4h, 14.2v	cobble gravel with clayey sand	5	25	40	30	25	3-8	high	medium	none	moderate strong	subrounded to angular	none	none	poorly sorted	clear	10YR 4/2 (10YR 3/2)	Footwall colluvial wedge; moderately organic rich; stage 1 carbonate development
CF1	21.3h, 10.2v	gravel with sand	30	25	40	5	15	3-9	low	loose	none	strong	subangular to angular	none	none	poorly sorted	clear	10YR 6/2 (10YR 5/3)	Footwall colluvial wedge; moderately organic rich; stage 1 carbonate development

[1] Units correspond with plates 1 and 2. Genesis: S - stream, DF - debris flow, L - lacustrine, C - colluvium, F - fill. A indicates A horizon soil.

[2] Horizontal and vertical meters correspond to the north wall (plate 1).

[3] Texture name approximated using the Unified Soil Classification System (density/consistency after Birkeland and others [1991]). Textural information may not be representative of entire unit due to vertical and horizontal heterogeneity in units.

[4] Percentages of clast-size fractions (based on area) are field estimates. F – fines (silt and clay), S – sand, G – gravel, C/B – cobbles and boulders. We used a U.S. Standard #10 (2 mm) sieve to separate matrix (clay, silt, and sand) from gravel.

[5] Lower boundary modified from Birkeland and others (1991). Distinctness: abrupt (1 mm-2.5 cm), clear (2.5-6 cm), gradual (6-12.5 cm). Not exp. - base of unit not exposed.

[6] Munsell color (year 2000, revised version) of matrix.

APPENDIX B
DESCRIPTION OF STRATIGRAPHIC UNITS AT THE NORTH CREEK SITE

APPENDIX B

DESCRIPTION OF STRATIGRAPHIC UNITS IN TRENCHES AT THE NORTH CREEK TRENCH SITE

Unit, genesis[1]	Station no. (trench)[2]	Textural name[3]	Texture (%)[4]				Clasts		Plast-icity[3]	Density/ consistency[3]	Cementation	HCL reaction	Clast angularity	Bedding	Structure	Sorting	Lower bound.[5]	Color[6] dry (moist)	Notes
			F	S	G	C/B	Largest (cm)	Average (cm)											
1a, S-DF	23h, 3v	gravely sand with some large boulders	10	25	50	15	50	25	non-plastic	nonsticky	weak	strong	subrounded	well bedded	none	poorly sorted	clear	10YR 7/3 (10YR 6/3)	Interbedded stream and debris-flow deposits in fault footwall.
1b, S	31h, 10v	silty gravel with some cobbles	25	10	40	25	40	10	slight. plastic	sticky	moderate	strong	subangular	well bedded	none	moderate sorted	diffuse	10YR 6/3 (10YR 5/3)	Interbedded stream deposits; locally contains open-work gravel.
1c, S-DF	37h, 12-13v	silty sand with some cobbles	35	30	25	10	20	5-10	slight. plastic	sticky	strong	very strong	subangular	poor	none	poorly sorted	clear	10YR 6/3 (10YR 4/2)	Alluvial-fan deposits; locally contains channels.
2a, S	8h, 1v	silt with occasional cobbles	79	10	1	10	30	<1	plastic	very sticky	strong	strong	angular	none	none	poorly sorted	not exp.	10YR 6/3 (10YR 4/2)	Silt horizon at base of hanging-wall exposure.
2b, S	8h, 2v	sandy gravel with occasional cobbles	10	20	50	20	20	5	non-plastic	nonsticky	weak	moderate strong	subrounded	moderate bedded	none	moderate sorted	clear	10YR 6/3 (10YR 5/3)	Fluvial gravel package
2c, S	7h, 3v	sandy gravel with occasional cobbles	5	20	55	20	10	5	non-plastic	nonsticky	weak	moderate strong	subrounded	moderate bedded	none	moderate sorted	clear	10YR 6/2 (10YR 5/3)	Fluvial gravel package
2d1, S	17h, 3v	silt	88	5	5	2	5	<2	very plastic	very stick	strong	very strong	subangular	none	none	well sorted	clear	10YR 4/3 (10YR 3/3)	Thin silt bed
2d2, S	17h, 3v	silty sand with gravel	30	40	25	5	30	5	slight. plastic	slightly sticky	moderate	strong	subangular to angular	poor	none	poorly sorted	abrupt	10YR 4/4 (10YR 3/3)	Fluvial sand
3, DF	15h, 3v	silty gravel	25	15	30	30	25	10	slight. plastic	slightly sticky	moderate	strong	subangular to angular	none	none	poorly sorted	clear	10YR 5/2 (10YR 4/2)	Debris flow
Cg2, C	12h, 2v	silty gravel	25	15	40	20	6	2-5	plastic	sticky	moderate	strong	subrounded	some slope fabric	none	poorly sorted	clear	10YR 4/3 (10YR 3/2)	Colluvial wedge in the hanging-wall graben.
C1, C	22h, 5v	sandy gravel with cobbles	5	20	55	20	20	10	non-plastic	nonsticky	moderate	strong	subrounded to subangular	well-defined slope fabric	slope fabric	moderate sorted	gradual	10YR 5/4 (10YR 4/3)	Youngest colluvial wedge (C1).
C2, C	21h, 4v	sandy gravel with cobbles	15	30	35	20	15	5	slight. plastic	slightly sticky	weak	strong	subrounded	weak slope fabric	slope fabric	poorly sorted	clear	10YR 6/3 (10YR 5/2)	Colluvial wedge C2
C3, C	20h, 3v	silty gravel with cobbles	35	15	30	20	14	5	plastic	sticky	moderate	strong	subrounded to subangular	none	none	poorly sorted	gradual	10YR5/2 (10YR 3/3)	Colluvial wedge C3
C4, C	21h, 1v	silty gravel with cobbles	25	15	35	25	14	10	plastic	sticky	strong	strong	subrounded to subangular	weak-moderate slope fabric	slope fabric	poorly sorted	gradual	10YR 5/4 (10YR 4/3)	Colluvial wedge C4
C5?, C	21h, 1v	silty gravel	30	20	35	15	17	2-4	slight. plastic	slightly sticky	weak-moderate	-	subangular	none	none	poorly sorted	not exp.	10YR 6/4 (10YR 4/4)	Basal colluvial wedge exposed along main fault (F1).

[1] Units correspond with plates 3 and 4. Genesis: S - stream, DF - debris flow, L - lacustrine, C - colluvium, F - fill. A indicates A horizon soil.

[2] Horizontal and vertical meters correspond to the north wall (plate 2).

[3] Texture name approximated using the Unified Soil Classification System (density/consistency after Birkeland and others [1991]). Textural information may not be representative of entire unit due to vertical and horizontal heterogeneity in units.

[4] Percentages of clast-size fractions (based on area) are field estimates. F – fines (silt and clay), S – sand, G – gravel, C/B – cobbles and boulders. We used a U.S. Standard #10 (2 mm) sieve to separate matrix (clay, silt, and sand) from gravel.

[5] Lower boundary modified from Birkeland and others (1991). Distinctness: abrupt (1 mm-2.5 cm), clear (2.5-6 cm), gradual (6-12.5 cm). Not exp. - base of unit not exposed.

[6] Munsell color (year 2000, revised version) of matrix.

APPENDIX C
EXAMINATION OF BULK SOIL FOR RADIOCARBON DATEABLE MATERIAL

APPENDIX C

EXAMINATION OF CHARCOAL AND BULK SOIL SAMPLES FOR RADIOCARBON DATABLE MATERIAL FROM THE SPRING LAKE NORTH AND NORTH CREEK TRENCH SITES ON THE NEPHI SEGMENT OF THE WASATCH FAULT ZONE, UTAH

By

Kathryn Puseman

With assistance from
Peter Kováčik,
R. A. Varney,
and
Linda Scott Cummings

PaleoResearch Institute
Golden, Colorado

PaleoResearch Institute Technical Report 12-129

Prepared for

Utah Geological Survey, Salt Lake City, Utah
and
U.S. Geological Survey, Denver, Colorado

February 2013

APPENDIX C

INTRODUCTION

Bulk soil samples and detrital charcoal samples from trenches at the Spring Lake North (SPL) site and the North Creek (NC) site were examined to recover organic fragments suitable for radiocarbon analysis. Trenches were excavated to investigate the timing of Holocene surface-faulting earthquakes on the northern and southern parts of the Nephi segment of the Wasatch Fault, central Utah. Samples were recovered from scarp-derived colluvium and alluvial fan sediments. Botanic components and detrital charcoal were identified, and potentially radiocarbon datable material was separated. Charred material will be submitted to Woods Hole Oceanographic Institution for dating.

METHODS

Flotation and Identification

The bulk samples were floated using a modification of the procedures outlined by Matthews (1979). Each sample was added to approximately 3 gallons of water. The sample was stirred until a strong vortex formed, which was allowed to slow before pouring the light fraction through a 150-micron-mesh sieve. All material that passed through the screen was retained for possible microcharcoal or particulate soil organics extraction. Additional water was added and the process repeated until all visible macrofloral material was removed from the sample (a minimum of five times). The material that remained in the bottom (the heavy fraction) was poured through a 0.5-mm-mesh screen. The floated portions were allowed to dry.

The light fractions were weighed, then passed through a series of graduated screens (US Standard Sieves with 4-mm, 2-mm, 1-mm, 0.5-mm, and 0.25-mm openings) to separate the charcoal debris and to initially sort the remains. The contents of each screen then were examined. Charcoal fragments were broken to expose fresh cross, radial, and tangential sections, then examined under a binocular microscope at a magnification of 70x and under a Nikon Optiphot 66 microscope at magnifications of 320–800x. The remaining light fraction in the 4-mm, 2-mm, 1-mm, 0.5-mm, and 0.25-mm sieves was scanned under a binocular stereo microscope at a magnification of 10x, with some identifications requiring magnifications of up to 70x. The material that passed through the 0.25-mm screen was not examined. The coarse or heavy fractions also were screened and examined for the presence of botanic remains. Remains from both the light and heavy fractions were recorded as charred and/or uncharred, whole and/or fragments. The term "seed" is used to represent seeds, achenes, caryopses, and other disseminules.

Detrital charcoal samples were water-screened through a 250-micron mesh and allowed to dry. Samples initially were examined under a binocular microscope at a magnification of 10x. Charcoal fragments were separated from the water-screened sample matrix and broken to expose fresh cross, radial, and tangential sections. Charcoal fragments were examined under a binocular microscope at a magnification of 70x and under a Nikon Optiphot 66 microscope at magnifications of 320-800x.

Macrofloral remains, including charcoal, were identified using manuals (Carlquist 2001; Core et al. 1976; Hoadley 1990; Martin and Barkley 1961; Panshin and de Zeeuw 1980;

Petrides and Petrides 1992) and by comparison with modern and archaeological references. Because charcoal and possibly other botanic remains were to be submitted for radiocarbon dating, clean laboratory conditions were used during flotation and identification to avoid contamination. All instruments were washed between samples, and samples were protected from contact with modern charcoal.

Microcharcoal Recovery

It is now possible to recover microscopic charcoal and particulate soil organics from sediments for the purpose of obtaining an AMS radiocarbon age. A chemical extraction technique based on that used for pollen, and relying upon heavy liquid extraction, has been modified to recover microscopic charcoal and particulate soil organics for the purpose of obtaining an AMS radiocarbon age. Hydrochloric (HCl) acid (10%) was added to the material retained from flotation that had passed through the 250 micron mesh sieve to remove calcium carbonates. The sample then was rinsed until neutral, and a small quantity of sodium hexametaphosphate was added to begin clay removal. Sample beakers then were filled with reverse osmosis deionized (RODI) water and allowed to settle according to Stoke's Law. After two hours, the supernatant, containing clay, was poured off and the sample was rinsed with RODI water three more times, being allowed to settle according to Stoke's Law to remove more clays.

Once the clays had been removed, the samples were freeze-dried. Sodium polytungstate (SPT) with a density of 1.8 was used for the flotation process. The dry sample was mixed with SPT and centrifuged at 1500 rpm for 10 minutes to separate organic from inorganic remains. The supernatant containing pollen, organic remains, and microscopic charcoal was decanted. Sodium polytungstate again was added to the inorganic fraction to repeat the separation process until the organic material had been recovered (usually three repetitions). The microscopic charcoal fragments were recovered from the SPT by diluting this mixture with RODI and centrifuging, after which they were rinsed thoroughly with RODI water.

This resulting mixture of charcoal and particulate soil organics was then subjected to the standard acid-base-acid chemical pre-treatment required prior to radiocarbon dating. Following completion of this, the sample was subjected to a nitric acid treatment in which a small quantity of concentrated hot nitric acid was added to each sample tube, which was then allowed to sit for approximately 15 minutes. Following this treatment the sample was rinsed copiously with RODI water, vacuum dried, then examined again using a binocular microscope at a magnification of up to 30x to check for the presence of charcoal and particulate organics. If uncharred particulate organics remain and the quantity of the sample is large enough the nitric acid treatment was repeated. The freeze-dried microscopic charcoal fragments were then weighed and placed in a glass tube for shipment.

DISCUSSION

The Spring Lake North and North Creek sites are located on west-facing alluvial-fan surfaces along the western base of the Wasatch Range in central Utah. The alluvial-fan surfaces are noted to be approximately middle to early Holocene in age and have been

vertically offset by the Wasatch fault. Local vegetation in these areas consists primarily of grasses and mountain brush, mostly oak (*Quercus*).

Spring Lake North Site

The Spring Lake North site is situated south of Payson, Utah, at an elevation of 1480–1490 meters. This elevation is below the highest shoreline of Lake Bonneville. The trench exposed Lake Bonneville lacustrine sediments, stream and debris flow (alluvial-fan) deposits, and fault scarp-derived colluvium. The drainage basin that is the source of the alluvial fan deposits ranges in elevation from 1510–1780 meters. A wildfire in 2001 burned both the trench site and the drainage basin. A total of 8 detrital charcoal samples and 15 bulk soil samples were examined from this site.

Unit C1A

Bulk samples SLN-R15 and SLN-R16 were recovered from an A horizon developed on or within (organic stringer) scarp colluvium in Unit C1A (Table 1). Sample SLN-R15 contained several fragments of charcoal too small for identification that weighed a total of 0.0011 g (Tables 2 and 3). Since the minimum weight of charred material needed for dating reported by Woods Hole Oceanographic Institution is 0.5 mg (0.0005 g), the 0.0011 g of charcoal recovered in sample SLN-R15 should be sufficient for AMS radiocarbon dating. The sample also contained an uncharred *Lactuca* seed, an uncharred Poaceae A floret, a few root fragments, and numerous rootlets from modern plants in the area. A few insect chitin fragments, two insect puparia, and several snail shells also were noted.

Several fragments of charcoal too small for identification and weighing 0.0019 g were present in sample SLN-R16, which should be a sufficient weight for dating. Two uncharred Poaceae stem fragments note modern grasses. In addition, the sample yielded a few root fragments, numerous rootlets, numerous snails with a depressed shape, and a few snails with an oblong shape.

Unit C1

Samples SLN-R13 and SLN-R21 were collected from scarp colluvium in Unit C1. Sample SLN-R13 yielded two fragments of Asteraceae charcoal weighing 0.0016 g, reflecting a woody member of the sunflower family that burned. Several fragments of charred monocot/herbaceous dicot stem fragments weighing 0.0026 g might reflect local grasses and other herbaceous plants that burned. A single insect puparium, a moderate amount of snail shells with a depressed shape, and seven snails with an oblong shape also were noted.

Detrital charcoal sample SLN-R21 was examined first. This sample consisted of several pieces of unidentified hardwood charcoal weighing 0.0006 g. A few rootlets and sclerotia were present. Because this charcoal is close to the minimum weight of 0.0005 g for dating, bulk sample SLN-R21 was floated to recover additional material. An additional 0.0003 g of unidentifiable charcoal fragments were recovered from the bulk sample, for a total charcoal weight of 0.0009 g. The sample also yielded root and rootlet fragments, a few insect chitin fragments, and a few depressed snail shells.

APPENDIX C

Unit C2

Bulk samples SLN-R23, SLN-R17, and SLN-R18 were taken from an A horizon developed on or within scarp colluvium in Unit C2A. The 15 fragments of charcoal in sample SLN-R23 were too small for identification and weighed only 0.0005 g. Extraction of microcharcoal is likely to result in additional charred material to supplement the charcoal for radiocarbon dating.

Several fragments of *Artemisia* charcoal in sample SLN-R17 yielded a total weight of 0.0074 g, which is sufficient for dating. Numerous snails with a depressed shape were noted in this sample, as well as fewer snails with an oblong shape. A few insect chitin fragments note insect activity in the area, while root fragments and rootlets represent modern plants.

Sample SLN-R18 yielded several pieces of charcoal too small for identification, although the total weight of 0.0014 g should be adequate for radiocarbon dating. Sub-surface disturbance indicators include a few insect chitin fragments, an insect puparium, a few depressed snails, several oblong snails, and a moderate amount of worm castings. The sample also yielded a few sclerotia. Sclerotia are commonly called "carbon balls." They are small, black, solid or hollow spheres that can be smooth or lightly sculpted. These forms range from 0.5 to 4 mm in size. Sclerotia are the resting structures of mycorrhizae fungi, such as *Cenococcum graniforme*, that have a mutualistic relationship with tree roots. Many trees are noted to depend heavily on mycorrhizae and might not be successful without them. "The mycelial strands of these fungi grow into the roots and take some of the sugary compounds produced by the tree during photosynthesis. However, mycorrhizal fungi benefit the tree because they take in minerals from the soil, which are then used by the tree" (Kricher and Morrison 1988:285). Sclerotia appear to be ubiquitous and are found with coniferous and deciduous trees including *Abies* (fir), *Juniperus communis* (common juniper), *Larix* (larch), *Picea* (spruce), *Pinus* (pine), *Pseudotsuga* (Douglas fir), *Alnus* (alder), *Betula* (birch), *Populus* (poplar, cottonwood, aspen), *Quercus* (oak), and *Salix* (willow). These forms originally were identified by Dr. Kristiina Vogt, Professor of Ecology in the School of Forestry and Environmental Studies at Yale University (McWeeney 1989:229-230; Trappe 1962).

Sample SLN-R22 was recovered in the north wall of Unit C2 from scarp-derived colluvial wedge. Charcoal in this sample includes a single vitrified piece of twig charcoal weighing 0.0008 g and several fragments of charcoal too small and vitrified for identification weighing 0.0002 g. The single piece of vitrified twig charcoal, either alone or combined with the unidentified charcoal fragments, can be submitted for radiocarbon dating. In addition, the sample contained a few uncharred rootlet fragments and numerous uncharred root fragments from modern plants, as well as a few depressed snail shells and a single oblong-shaped snail shell.

Unit C3A

Bulk sample SLN-R19 reflects an A horizon developed on or within scarp colluvium in Unit C3A. The sample contained four fragments of charred parenchymous tissue weighing 0.0008 g that can be submitted for dating, although it is possible that these fragments represent roots. Parenchyma is the botanical term for relatively undifferentiated tissue composed of many similar cells with thin primary walls. Parenchyma occurs in many different plant tissues in varying amounts, especially large fleshy organs such as roots and stems, but also in fruits,

seeds, cones, periderm (bark), leaves, needles, etc. (Hather 2000:1; Mauseth 1988). A sufficient amount (0.0010 g) of very small, unidentifiable charcoal fragments also were present. We recommend keeping these charcoal fragments separate from the charred parenchyma fragments, since the latter might represent roots. Non-floral remains include a few uncharred bone fragments and a moderate amount of snail shells.

Unit N3g

Bulk sample SLN-R27 represents alluvial fan sediments in Unit N3g. This sample yielded several fragments of charcoal too small for identification and weighing a total of 0.0010 g, which should be sufficient for radiocarbon dating. Numerous uncharred rootlets from modern plants and a few snail shells were the only other remains to be recovered.

Unit C4

Bulk sample SLN-R20 was recovered from scarp colluvium in Unit C4. This sample also contained several fragments of charcoal too small for identification that weighed 0.0008 g. This weight should be adequate for radiocarbon dating. Root and rootlet fragments, a moderate amount of depressed snail shells, and a few oblong snail shells also were noted.

Units S3g/h/N3e

Detrital charcoal samples SLN-R05 and SLN-R06 were taken from alluvial-fan sediments in Unit S3g/h/N3e. Two tiny pieces of unidentifiable charred tissue weighing less than 0.0001 g were noted in sample SLN-R06, while the six fragments of charcoal in sample SLN-R05 also were too small for identification and too small for dating, weighing less than 0.0001 g. An additional bulk sample SLN-R11 from Unit S3h1 was recovered adjacent to samples SLN-R05 and SLN-R06. This sample also yielded several fragments of charcoal too small for identification; however, a total weight of 0.0022 g for these charcoal fragments should be adequate for radiocarbon dating. A few uncharred roots and rootlets from modern plants also were present.

Unit S3bA

Sample SLN-R02 consists of charcoal from the A horizon developed on or within alluvial-fan sediments in Unit S3bA. The several fragments of charcoal present in this sample were too small and vitrified for identification; however, the fragments weighed a total of 0.0012 g, which should be sufficient for radiocarbon dating. Vitrified charcoal has a shiny, glassy appearance that can range from still recognizable in structure “to a dense mass, completely ‘molten’ and non-determinable” (Marguerie and Hunot 2007; McParland et al. 2010). Although vitrification of charcoal has been attributed to burning at high temperature and/or burning green wood, it currently is not clear what conditions produce vitrified charcoal. It likely is a combination of factors (McParland, et al. 2010). We have noted that vitrified charcoal often loses more mass during chemical pre-treatment than charcoal that is not vitrified.

Unit S3d

Detrital charcoal samples SLN-R01, SLN-R03, and SLN-R04 were collected from alluvial-fan sediments in Unit S3d. Sample SLN-R01 yielded a single piece of charred

parenchymous tissue weighing 0.0018 g that can be submitted for radiocarbon dating. A single piece of unidentified hardwood twig charcoal in sample SLN-R03 weighs 0.0012 g and also can be submitted for dating. The small pieces of unidentified hardwood charcoal in sample SLN-R04 yielded a weight of 0.0009 g. Single pieces of charcoal, when compared to multiple pieces with the same weight, usually loose less mass during chemical pre-treatment.

Unit C6

Samples SLN-R09 and SLN-R10 were recovered from scarp colluvium in Unit C6. Detrital charcoal sample SLN-R09 contained only a few small rocks; therefore, bulk sample SLN-R09 was processed. The bulk sample yielded five fragments of charcoal too small for identification and weighing less than 0.0001 g. The probability of obtaining sufficient microscopic charcoal from this bulk sample is small because the visible charcoal recovered from this bulk sample weighed so little.

Bulk sample SLN-R10 yielded five fragments of charred parenchymous tissue weighing less than 0.0001 g and five pieces of charred, vitrified tissue weighing 0.0007 g. This amount of charred material should be sufficient for radiocarbon dating.

Unit CF3

Bulk sample SLN-R25, collected from scarp colluvium in Unit CF3, yielded only three pieces of charcoal too small for identification and weighing less than 0.0001 g. Numerous uncharred rootlets and a few rocks were the only other remains to be recovered. A very minute quantity of visible charcoal was noted in this sample; however, it was selected for microcharcoal extraction. This sample yielded 0.0345 g of microscopic charcoal that can be submitted for dating.

Unit S2bA

Bulk sample SLN-R26 was taken from an A horizon developed on or within alluvial-fan sediments in Unit S2bA. Five fragments of charred, vitrified tissue were noted in this sample, weighing total of 0.0005 g. No other charred remains were recovered. The sample did contain root fragments and rootlets from modern plants, as well as a few oblong snail shells. It is likely that microscopic charcoal can be extracted from this bulk sample to boost the weight for dating.

Unit S2cA

The nine pieces of charcoal in sample SLN-R24, collected from an A horizon developed on or within alluvial-fan sediments in Unit S2cA, were too small and vitrified for identification. These charcoal fragments yielded a total weight of 0.0012 g, which should be sufficient for AMS radiocarbon dating. Numerous uncharred rootlets, an insect puparium fragment, and a few depressed and oblong snail shells also were noted.

North Creek Trench Site

The North Creek Trench site is located northeast of Mona, Utah, at an elevation of 1730–1740 meters. This elevation is above the highest shoreline of Lake Bonneville. Stream

and debris flow (alluvial-fan) deposits and fault scarp-derived colluvium were exposed in the trench. The drainage basin that is the source of the alluvial fan deposits ranges in elevation from 1170–3300 meters. In addition to mountain brush, conifers are noted in the drainage basin. A total of 11 detrital charcoal samples and 13 bulk soil samples were examined from this site.

Unit C1A

Charcoal and bulk sample NC-R14 was taken from an A horizon developed on or within (organic stringer) scarp colluvium in Unit C1A (Table 4). The charcoal sample contained nine fragments of charcoal too small for identification and weighing 0.0006 g (Tables 5 and 3). Because this weight is so close to the minimum weight of 0.0005 g needed for radiocarbon dating, bulk sample NC-R14 was floated. An additional 0.0020 g of unidentifiable charcoal fragments were recovered, for a total charcoal weight of 0.0026 g. This amount should be sufficient for dating. The sample also yielded a moderate amount of root fragments and rootlets, a few sclerotia, a moderate amount of insect puparia, and two snail shell fragments with a depressed shape.

Unit C1

Charcoal sample NC-R28 and bulk sample NC-R20 were recovered from an A horizon developed on or within scarp colluvium in Unit C1. Charcoal sample NC-R28 contained a piece of Asteraceae charcoal weighing 0.0007 g, a piece of *Juniperus* charcoal weighing 0.0024 g, a *Pseudotsuga menziesii* charcoal fragment weighing 0.0016 g, and three pieces of unidentified hardwood charcoal too small for identification and weighing 0.0004 g. Because western juniper and Douglas-fir can be relatively long-lived trees, the Asteraceae charcoal should be combined with the unidentified hardwood charcoal to obtain a total weight of 0.0011 g and submitted for dating.

Bulk sample NC-R20 contained a single charred monocot/herbaceous dicot stem fragment weighing 0.0010 g that can be submitted for dating. Twelve fragments of conifer charcoal weighing 0.0009 g and thirteen pieces of charcoal too small for identification and weighing 0.0005 g also were noted. The single charred stem fragment would be preferential for dating, although the unidentified charcoal can be combined with it for a total weight of 0.0014 g and also sent for dating. The sample yielded a moderate amount of root fragments, numerous rootlets, a moderate amount of insect eggs and insect puparia, a few depressed snail shells, and a single oblong snail shell.

Unit 2d1

Sample NC-R22c consists of detrital charcoal from alluvial fan sediments in Unit 2d1. This sample contained seven pieces of *Juniperus* charcoal, reflecting juniper that burned. These charcoal fragments yielded a total weight of 0.0046 g, which is sufficient for radiocarbon dating.

Unit C2A

Bulk samples NC-R21 and NC-R15 were recovered from an A horizon developed on or within scarp colluvium in Unit C2A. Pieces of *Juniperus* charcoal weighing 0.0069 g also were

present in sample NC-R21 that can be submitted for radiocarbon dating. A single piece of *Quercus - Leucobalanus* group charcoal weighing 0.0007 g and three charred dry fruit fragments weighing 0.0008 g also were noted. Because of the potential for long-lived junipers, the *Quercus* charcoal and/or charred unidentified fruit fragments would be the preferred material for dating. Modern plants at the site are reflected by an uncharred Poaceae A floret, an uncharred unidentified dry fruit fragment, numerous root fragments, a few rootlets, and a moderate amount of sclerotia.

The charcoal fragments in sample NC-R15 were too small for identification; however, these charcoal fragments yielded a total weight of 0.0020 g that should be sufficient for radiocarbon dating. The sample also contained a moderate amount of root fragments and rootlets, a few sclerotia, and a few depressed and oblong snail shells.

Unit 2c2A

Bulk sample NC-R16 was taken from an A horizon developed on or within alluvial-fan sediments in Unit 2c2A. Several types of charcoal were noted in this sample, including eight pieces of conifer weighing 0.0027 g, six fragments of *Pseudotsuga menziesii* weighing 0.0016 g, seven fragments of *Quercus* weighing 0.0010 g, two pieces of unidentified hardwood twig charcoal weighing 0.0033 g, fragments of unidentified hardwood charcoal too small for identification weighing 0.0013 g, one piece of vitrified hardwood charcoal weighing 0.0027 g, and two pieces of charcoal too small for identification weighing 0.0008 g. Many of these charcoal types are of a sufficient weight for radiocarbon dating, although the unidentified hardwood twig charcoal is the preferred material for dating. This sample also presents the option of dating some of the charcoal representing longer-lived trees, budget permitting. The advantage in doing this is to have some comparison between dates on the presumably shorter-lived woody plants represented by the unidentified hardwood twig charcoal and the longer-lived *Pseudotsuga* and *Quercus* charcoal fragments to better understand the age offsets that might be typical at this location and represented in other samples.

Charcoal sample NC-R01, charcoal sample NC-R03, and bulk sample NC-R31 were taken from an A horizon developed on or within alluvial-fan sediments in Unit 2c2A. Charcoal sample NC-R01 contained four fragments of unidentified hardwood charcoal weighing 0.0032 g that can be submitted for dating. The three pieces of charred parenchymous tissue in sample NC-R03 weighed a total of 0.0009 g, which should be sufficient for dating.

Several types of charcoal were present in bulk sample NC-R31, including two pieces of Asteraceae weighing 0.0008 g, a single fragment of conifer charcoal weighing less than 0.0001 g, a piece of *Juniperus* charcoal weighing 0.0037 g, two fragments of *Quercus - Leucobalanus* group charcoal weighing 0.0028 g, a small piece of *Quercus* charcoal weighing 0.0001 g, and two pieces of Salicaceae charcoal with a diffuse porous distribution of vessels that weighed 0.0017 g. The Salicaceae charcoal is the preferred material for dating. The Asteraceae charcoal could be combined with the Salicaceae charcoal to provide additional material. In addition, the sample contained a moderate amount of root fragments and rootlets, a moderate amount of sclerotia, a few uncharred bone fragments, numerous insect eggs, a few depressed snail shells, and a moderate amount of worm castings.

APPENDIX C

Unit CHA

Charcoal sample NC-R02 and bulk sample NC-R32 were collected from an A horizon developed on or within scarp colluvium in Unit CHA. Charcoal in sample NC-R02 consists of three pieces of conifer weighing 0.0005 g, two fragments of *Pseudotsuga menziesii* weighing 0.0002 g, a piece of unidentified hardwood charcoal weighing 0.0006 g, and three fragments of charcoal too small for identification weighing 0.0002 g. These charcoal types can be combined to produce a total weight of 0.0015 g that can be sent for radiocarbon dating.

Charred remains noted in bulk sample NC-R32 include three pieces of parenchymous tissue weighing 0.0029 g, six fragments of conifer charcoal weighing 0.0066 g, a piece of *Juniperus* charcoal weighing 0.0020 g, four pieces of *Pseudotsuga menziesii* charcoal weighing 0.0057 g, ten fragments of *Quercus* charcoal weighing 0.0083 g, a single Rosaceae twig charcoal fragment weighing 0.0016 g, and four fragments of unidentified hardwood charcoal weighing 0.0038 g. Although all of these charcoal types are present in sufficient quantities for dating, the single piece of Rosaceae twig charcoal is the preferred charcoal type for dating. Most woody members of the rose family have short to moderate lifespans and single pieces of charcoal are preferable for dating, when they exist. The sample also contained a moderate amount of root fragments and rootlets, a few sclerotia, three snail shells with a depressed shape, and a moderate amount of worm castings.

Unit C3A

Bulk samples NC-R23 and NC-R18 were taken from an A horizon developed on or within scarp colluvium in Unit C3A. Sample NC-R23 yielded several types of charcoal, including ten fragments of conifer weighing 0.0017 g, four fragments of *Juniperus* weighing 0.0035 g, four pieces of *Pseudotsuga menziesii* weighing 0.0010 g, eight fragments of *Quercus* weighing 0.0016 g, a piece of *Quercus* - *Leucobalanus* group charcoal weighing less than 0.0001 g, a piece of Salicaceae weighing 0.0001 g, several fragments of unidentified hardwood charcoal weighing 0.0026 g, and eight pieces of charcoal too small for identification weighing 0.0011 g. Recovery of five uncharred *Artemisia* wood fragments notes modern sagebrush in the area, while several uncharred fragments of conifer wood reflect modern conifers. To be consistent with recommendations for other samples, the unidentified hardwood charcoal is the preferred charcoal type for AMS radiocarbon dating. If desired, the small quantities of *Quercus* and Salicaceae charcoal may be added to this charcoal to increase the sample weight. A single charred Poaceae B caryopsis fragment weighing 0.0001 g reflects grasses that burned. The sample also yielded a moderate amount of uncharred root fragments, a few rootlets, a moderate amount of sclerotia, a few insect chitin fragments, and a few depressed-shaped snail shells.

The four pieces of conifer charcoal weighing 0.0008 g, the two fragments of unidentified hardwood charcoal weighing 0.0004 g, and the two fragments of charcoal too small for identification weighing 0.0003 g in sample NC-R18 could be added together to obtain 0.0015 g of charcoal for radiocarbon dating. Other items noted in this sample include a moderate amount of root fragments and rootlets, numerous sclerotia, a few depressed snail shells, and several oblong snail shells.

APPENDIX C

Unit C4A

Bulk sample NC-R29 was recovered from an A horizon developed on or within scarp colluvium in Unit C4A. Small fragments of conifer charcoal weighing 0.0013 g, two pieces of *Juniperus* charcoal weighing 0.0101 g, a fragment of *Pseudotsuga menziesii* charcoal weighing 0.0001 g, nine *Quercus* charcoal fragments weighing 0.0012 g, and two pieces of hardwood charcoal too small for further identification weighing 0.0007 g were noted in this sample and reflect juniper, Douglas-fir, possibly another type of conifer, oak, and possibly another type of hardwood that burned. The *Quercus* charcoal is the preferred charcoal for dating. The unidentified hardwood charcoal could be added to the *Quercus* charcoal to provide additional material for dating. Uncharred conifer wood fragments again note modern conifers. In addition, the sample contained root fragments, rootlets, sclerotia, a few insect chitin fragments, and a single oblong-shaped snail shell.

Unit C4

Sample NC-R13 consists of charcoal from an A horizon developed on or within scarp colluvium in Unit C4. Nine fragments of vitrified unidentified hardwood charcoal weighing 0.0021 g can be submitted for radiocarbon dating. A few uncharred periderm fragments and two sclerotia also were noted.

Unit 2bA

Bulk sample NC-R19 was collected from an A horizon developed on or within alluvial-fan sediments in Unit 2bA. Several charred fragments of a dry fruit (0.0090 g) and 14 pieces of unidentified hardwood charcoal (0.0057 g) are present in sufficient quantities for radiocarbon dating. The charred dry fruit fragments represent an annual that can be dated, while dating the unidentified hardwood charcoal would be more consistent with wood charcoal selected for dating from other samples. In addition, the sample contained two pieces of conifer charcoal weighing 0.0009 g, three fragments of charcoal too small for identification weighing 0.0006 g, a moderate amount of root fragments and rootlets, numerous sclerotia, a moderate amount of snail shells with a depressed shape, and several snail shells with an oblong shape.

Unit 1bA

Charcoal samples NC-R05, NC-R07, and NC-R09 were taken from an A horizon developed on or within alluvial-fan sediments in Unit 1bA. All three samples yielded sufficient charcoal for AMS radiocarbon dating. Sample NC-R05 contained 20 pieces of unidentified hardwood charcoal weighing 0.0093 g. The nine fragments of *Quercus* charcoal in sample NC-R07 yielded a total weight of 0.0035 g, while the 10 pieces of *Quercus* charcoal in sample NC-R09 weighed a total of 0.0042 g.

Unit 1c4A

Samples NC-R12 and NC-R11 also were collected from an A horizon developed on or within alluvial-fan sediments. Bulk sample NC-R12 contained several fragments of charcoal too small for identification that weighed a total of 0.0008 g. This weight may be sufficient for AMS radiocarbon dating. The sample also yielded root fragments, rootlets, sclerotia, and an oblong snail shell and snail shell fragment.

APPENDIX C

Charcoal sample NC-R11 contained only a few pieces of uncharred periderm and three sclerotia. As a result, bulk sample NC-R11 was floated. The bulk sample contained six pieces of conifer charcoal weighing 0.0021 g, as well as seven fragments of charcoal too small for identification weighing 0.0004 g. The conifer charcoal is present in sufficient quantity for radiocarbon dating. Other remains noted in the sample include root fragments, rootlets, numerous sclerotia, a few insect chitin fragments, and a few depressed and oblong snail shells.

SUMMARY AND CONCLUSIONS

Examination of detrital charcoal samples and flotation of bulk samples from trenches at the Spring Lake North (SPL) site and the North Creek (NC) site on the northern and southern parts of the Nephi segment of the Wasatch Fault, Utah, resulted in recovery of charcoal and other charred botanic remains that can be sent for radiocarbon dating to investigate the timing of Holocene surface-faulting earthquakes in the area. A total of 17 samples yielded macroscopic charcoal in sufficient quantities for AMS radiocarbon dating. The charcoal types represent woody vegetation found in either the trench sites or the drainage basins identified as the sources of the alluvial-fan deposits. Fewer fragments of charcoal and fewer charcoal types were noted in the Spring Lake North samples. The majority of the charcoal fragments in the SLN samples were too small for identification. Identifiable pieces of *Artemisia* and Asteraceae charcoal reflect sagebrush and another woody member of the sunflower family. A few fragments of charcoal could at least be identified as a type of hardwood. In order to obtain sufficient charred material for radiocarbon dating, sample SLN-R25 was processed to extract microscopic charcoal. A total of 0.0345 g of microcharcoal was recovered, which can be submitted for dating.

By comparison, samples from the North Creek site yielded a variety of charcoal, including conifers from the drainage basin. Ten of the NC samples contained charcoal identified only as conifer, while identifiable juniper charcoal was present in 7 samples and identifiable Douglas-fir charcoal was noted in six samples. Oak charcoal was found in seven of the NC samples, and three samples yielded oak charcoal identifiable as part of the white oak group. Charcoal from a woody member of the sunflower family and charcoal from a woody member of the willow family were noted in two samples each. A single sample contained a twig fragment from a woody member of the rose family. Twelve samples contained pieces of hardwood charcoal, while charcoal in eleven of the samples was too small for identification. All of the samples from the North Creek site contained charcoal or other charred botanic material in sufficient quantities for dating.

APPENDIX C

TABLE 1
PROVENIENCE DATA FOR SAMPLES FROM THE SPRING LAKE NORTH TRENCH SITE
ON THE NEPHI SEGMENT OF THE WASATCH FAULT ZONE, UTAH

Sample No.	Wall	Unit	Relation to Earthquake	Description/ Provenience	Analysis
SLN-R15	South	C1A	Min P1	A horizon developed on or within (organic stringer) scarp colluvium	Float
SLN-R16				A horizon developed on or within (organic stringer) scarp colluvium	Float
SLN-R13		C1		Scarp colluvium	Float
SLN-R21	North			Charcoal and scarp colluvium	Charcoal ID/Float
SLN-R23		C2A	Min P2, Max P1	A horizon developed on or within scarp colluvium	Float
SLN-R17	South			A horizon developed on or within scarp colluvium	Float
SLN-R18				A horizon developed on or within scarp colluvium	Float
SLN-R22	North	C2		Scarp-derived colluvial wedge	Float
SLN-R19	South	C3A	Min P3, Max P2	A horizon developed on or within scarp colluvium	Float
SLN-R27	North	N3g		Alluvial fan sediments	Float
SLN-R20	South	C4	Min P4, Max P3	Scarp colluvium	Float
SLN-R05		S3g/h / N3e	Min P5, Max P4	Detrital charcoal from alluvial-fan sediments	Charcoal ID
SLN-R06				Detrital charcoal from alluvial-fan sediments	Charcoal ID
SLN-R11		S3h1		Detrital charcoal from alluvial-fan sediments	Float
SLN-R02		S3bA	Min P6, Max P5	Detrital charcoal from A horizon developed on or within alluvial-fan sediments	Charcoal ID
SLN-R01		S3d		Detrital charcoal from alluvial-fan sediments	Charcoal ID
SLN-R03				Detrital charcoal from alluvial-fan sediments	Charcoal ID

APPENDIX C

TABLE 1 (Continued)

Sample No.	Wall	Unit	Relation to Earthquake	Description/ Provenience	Analysis
SLN-R04	South	S3d	Min P6, Max P5	Detrital charcoal from alluvial-fan sediments	Charcoal ID
SLN-R09	North	C6	Min P6, Max P5	Charcoal and scarp colluvium	Charcoal ID/Float
SLN-R10				Scarp colluvium	Float
SLN-R25	South		Min CF3	Scarp colluvium	Float Microcharcoal
SLN-R26		S2bA	Max CF3	A horizon developed on or within alluvial-fan sediments	Float
SLN-R24		S2cA		A horizon developed on or within alluvial-fan sediments	Float

CF = Earthquake related to footwall colluvial wedge deposits (correlation to P1-P6 not known)

APPENDIX C

TABLE 2
MACROFLORAL REMAINS FROM THE SPRING LAKE NORTH TRENCH SITE
ON THE NEPHI SEGMENT OF THE WASATCH FAULT ZONE, UTAH

Sample No.	Identification	Part	Charred		Uncharred		Weights/ Comments
			W	F	W	F	
SLN-R15	Liters Floated						1.50 L
Unit C1A	Light Fraction Weight						0.934 g
Min P1	FLORAL REMAINS:						
	Lactuca	Seed			1		
	Poaceae A	Floret			1		
	Roots					X	Few
	Rootlets					X	Numerous
	CHARCOAL/WOOD:						
	Total charcoal ≥ 0.25 mm						0.0011 g
	Unidentifiable -small	Charcoal		X			0.0011 g
	NON-FLORAL REMAINS:						
	Insect	Chitin				X	Few
	Insect	Puparia			2		
	Rock					X	Moderate
	Snail shell - depressed ≥ 1 mm				32	9	
	Snail shell - depressed < 1 mm				X	X	Few
	Snail shell - oblong ≥ 0.5 mm				5	2	
SLN-R16	Liters Floated						1.30 L
Unit C1A	Light Fraction Weight						0.452 g
Min P1	FLORAL REMAINS:						
	Poaceae	Stem				2	0.0051 g
	Roots					X	Few
	Rootlets					X	Numerous
	CHARCOAL/WOOD:						
	Total charcoal ≥ 0.25 mm						0.0019 g
	Unidentifiable - small	Charcoal		X			0.0019 g
	NON-FLORAL REMAINS:						
	Rock					X	Numerous
	Snail shell - depressed ≥ 1 mm				26	11	
	Snail shell - depressed < 1 mm				X	X	Numerous
	Snail shell - oblong ≥ 0.5 mm				4		
	Snail shell - oblong < 0.5 mm					X	Few

APPENDIX C

TABLE 2 (Continued)

Sample No.	Identification	Part	Charred W	Charred F	Uncharred W	Uncharred F	Weights/ Comments
SLN-R13	Liters Floated						1.90 L
Unit C1	Light Fraction Weight						1.587 g
Min P1	FLORAL REMAINS:						
	Monocot/Herbaceous dicot	Stem		23			0.0026 g
	Unidentified	Seed		1			< 0.0001 g
	Roots					X	Moderate
	Rootlets					X	Numerous
	CHARCOAL/WOOD:						
	Total charcoal ≥ 0.5 mm						0.0016 g
	Asteraceae	Charcoal		2			0.0016 g
	NON-FLORAL REMAINS:						
	Insect	Puparia			1		
	Rock					X	Moderate
	Snail shell - depressed ≥ 1 mm				36	28	
	Snail shell - depressed < 1 mm				X	X	Moderate
	Snail shell - oblong ≥ 0.5 mm				7		
SLN-R21	Bulk Sample Liters Floated						1.10 L
Unit C1	Bulk Sample Light Fraction Weight						0.775 g
Min P1	Charcoal Sample Weight						0.002 g
	FLORAL REMAINS:						
	Roots					X	Moderate
	Rootlets					X	Numerous
	Sclerotia				X	X	Few
	CHARCOAL/WOOD:						
	Total charcoal ≥ 0.25 mm						0.0009 g
	Unidentified hardwood twig	Charcoal		X			0.0009 g
	NON-FLORAL REMAINS:						
	Rock					X	Few
SLN-R23	Liters Floated						1.00 L
Unit C2A	Light Fraction Weight						0.869 g
Min P2,	FLORAL REMAINS:						
Max P1	Roots					X	Few
	Rootlets					X	Moderate

APPENDIX C

TABLE 2 (Continued)

Sample No.	Identification	Part	Charred W	Charred F	Uncharred W	Uncharred F	Weights/ Comments
SLN-R23	CHARCOAL/WOOD:						
Unit C2A	Total charcoal ≥ 0.25 mm						0.0005 g
Min P2,	Unidentifiable - small	Charcoal		15			0.0005 g
Max P1	NON-FLORAL REMAINS:						
	Insect	Chitin				X	Few
	Insect	Puparia			2		
	Rock					X	Moderate
	Snail shell - depressed ≥ 0.5 mm					2	
	Snail shell - depressed < 0.5 mm					X	Few
SLN-R17	Liters Floated						1.80 L
Unit C2A	Light Fraction Weight						0.769 g
Min P2,	FLORAL REMAINS:						
Max P1	Roots					X	Few
	Rootlets					X	Numerous
	CHARCOAL/WOOD:						
	Total charcoal ≥ 0.5 mm						0.0074 g
	Artemisia	Charcoal		36			0.0074 g
	NON-FLORAL REMAINS:						
	Insect	Chitin				X	Few
	Rock					X	Numerous
	Snail shell - depressed ≥ 1 mm				23		
	Snail shell - depressed < 1 mm				X	X	Numerous
	Snail shell - oblong ≥ 0.5 mm				13	15	
	Snail shell - oblong < 0.5 mm					X	Few
SLN-R18	Liters Floated						1.40 L
Unit C2A	Light Fraction Weight						1.828 g
Min P2,	FLORAL REMAINS:						
Max P1	Roots					X	Few
	Rootlets					X	Numerous
	Sclerotia				X	X	Few
	CHARCOAL/WOOD:						
	Total charcoal ≥ 0.25 mm						0.0014 g
	Unidentifiable - small	Charcoal		X			0.0014 g

APPENDIX C

TABLE 2 (Continued)

Sample No.	Identification	Part	Charred W	Charred F	Uncharred W	Uncharred F	Weights/ Comments
SLN-R18	NON-FLORAL REMAINS:						
Unit C2A	Insect	Chitin				X	Few
Min P2,	Insect	Puparia			1		
Max P1	Rock					X	Moderate
	Snail shell - depressed ≥ 1 mm				2		
	Snail shell - depressed < 1 mm				2	X	Few
	Snail shell - oblong ≥ 0.5 mm				27	26	
	Worm castings				X	X	Moderate
SLN-R22	Liters Floated						0.80 L
Unit C2	Light Fraction Weight						0.950 g
Min P2,	FLORAL REMAINS:						
Max P1	Roots					X	Few
	Rootlets					X	Numerous
	CHARCOAL/WOOD:						
	Total charcoal ≥ 0.25 mm						0.0010 g
	Unidentifiable - small, vitrified	Charcoal		10			0.0002 g
	Unidentifiable twig - vitrified	Charcoal		1			0.0008 g
	NON-FLORAL REMAINS:						
	Rock/Gravel					X	Moderate
	Snail shell - depressed				X	X	Few
	Snail shell - oblong				1		
SLN-R19	Liters Floated						1.50 L
Unit C3A	Light Fraction Weight						0.950 g
Min P3,	FLORAL REMAINS:						
Max P2	Parenchymous tissue ≥ 0.25 mm			4			0.0008 g
	Roots					X	Few
	Rootlets					X	Numerous
	CHARCOAL/WOOD:						
	Total charcoal ≥ 0.25 mm						0.0010 g
	Unidentifiable - small	Charcoal		X			0.0010 g

APPENDIX C

TABLE 2 (Continued)

Sample No.	Identification	Part	Charred W	Charred F	Uncharred W	Uncharred F	Weights/ Comments
SLN-R19	NON-FLORAL REMAINS:						
Unit C3A	Bone ≥ 1 mm					1	0.0003 g
Min P3,	Bone < 1 mm					2	
Max P2	Rock					X	Moderate
	Snail shell - depressed ≥ 1 mm				15	3	
	Snail shell - depressed < 1 mm				X	X	Moderate
	Snail shell - oblong ≥ 0.5 mm				3	2	
SLN-R27	Liters Floated						1.10 L
Unit N3g	Light Fraction Weight						0.707 g
Min P3,	FLORAL REMAINS:						
Max P2	Rootlets					X	Numerous
	CHARCOAL/WOOD:						
	Total charcoal ≥ 0.25 mm						0.0010 g
	Unidentifiable - small	Charcoal		X			0.0010 g
	NON-FLORAL REMAINS:						
	Rock					X	Moderate
	Snail shell - depressed ≥ 0.25 mm				1		
	Snail shell - oblong ≥ 0.5 mm				6	1	
SLN-R20	Liters Floated						1.30 L
Unit C4	Light Fraction Weight						0.869 g
Min P4,	FLORAL REMAINS:						
Max P3	Roots					X	Moderate
	Rootlets					X	Numerous
	CHARCOAL/WOOD:						
	Total charcoal ≥ 0.25 mm						0.0008 g
	Unidentifiable - small	Charcoal		X			0.0008 g
	NON-FLORAL REMAINS:						
	Rock					X	Moderate
	Snail shell - depressed ≥ 1 mm				1		
	Snail shell - depressed < 1 mm					X	Few
	Snail shell - oblong ≥ 0.5 mm				1		

APPENDIX C

TABLE 2 (Continued)

Sample No.	Identification	Part	Charred		Uncharred		Weights/ Comments
			W	F	W	F	
SLN-R05	Sample Weight						0.019 g
Unit S3g/h / N3e	CHARCOAL/WOOD:						
	Unidentifiable - small	Charcoal		6			< 0.0001 g
	NON-FLORAL REMAINS:						
	Sediment					X	Few
SLN-R06	Sample Weight						0.035 g
Unit S3g/h / N3e	FLORAL REMAINS:						
	Unidentifiable - small	Tissue		2			< 0.0001 g
	NON-FLORAL REMAINS:						
	Sediment					X	Few
SLN-R11	Liters Floated						1.20 L
Unit S3h1 Min P5 Max P4	Light Fraction Weight						0.187 g
	FLORAL REMAINS:						
	Roots					X	Few
	Rootlets					X	Moderate
	CHARCOAL/WOOD:						
	Total charcoal ≥ 0.25 mm						0.0022 g
	Unidentifiable - small, vitrified	Charcoal		X			0.0022 g
	NON-FLORAL REMAINS:						
	Rock					X	Moderate
SLN-R02	Sample Weight						0.991 g
Unit S3bA Min P6, Max P5	CHARCOAL/WOOD:						
	Total charcoal ≥ 0.25 mm						0.0012 g
	Unidentifiable - vitrified	Charcoal		31			0.0012 g
	NON-FLORAL REMAINS:						
	Rock/Sand					X	Few
SLN-R01	Sample Weight						0.176 g
Unit S3d Min P6, Max P5	FLORAL REMAINS:						
	Parenchymous tissue			1			0.0018 g
	NON-FLORAL REMAINS:						
	Sand					X	Few
SLN-R03	Sample Weight						0.001 g
Unit S3d	CHARCOAL/WOOD:						
	Unidentified hardwood twig	Charcoal		1			0.0012 g

APPENDIX C

TABLE 2 (Continued)

Sample No.	Identification	Part	Charred W	Charred F	Uncharred W	Uncharred F	Weights/ Comments
SLN-R04	Sample Weight						0.026 g
Unit S3d	CHARCOAL/WOOD:						
Min P6,	Total charcoal ≥ 0.25 mm						0.0009 g
Max P5	Unidentified hardwood - small	Charcoal		X			0.0009 g
SLN-R09	Bulk Sample Liters Floated						1.50 L
Unit C6	Bulk Sample Light Fraction Weight						2.575 g
Min P6,	Charcoal Sample Weight						0.007 g
Max P5	FLORAL REMAINS:						
	Roots					X	Few
	Rootlets					X	Moderate
	CHARCOAL/WOOD:						
	Total charcoal ≥ 0.25 mm						< 0.0001 g
	Unidentifiable - small	Charcoal		5			< 0.0001 g
	NON-FLORAL REMAINS:						
	Rock/Sand					X	Moderate
SLN-R10	Liters Floated						1.50 L
Unit C6	Light Fraction Weight						1.681 g
Min P6,	FLORAL REMAINS:						
Max P5	Parenchymous tissue ≥ 0.5 mm			5			< 0.0001 g
	Vitrified tissue ≥ 0.5 mm			5			0.0007 g
	Roots					X	Moderate
	Rootlets					X	Numerous
	NON-FLORAL REMAINS:						
	Gravel/Sand					X	Moderate
	Snail shell - depressed ≥ 1 mm				1		
SLN-R25	Liters Floated						0.90 L
Min CF3	Light Fraction Weight						0.533 g
	FLORAL REMAINS:						
	Rootlets					X	Numerous
	CHARCOAL/WOOD:						
	Total charcoal ≥ 0.25 mm						< 0.0001 g
	Unidentifiable - small	Charcoal		3			< 0.0001 g
SLN-R25	NON-FLORAL REMAINS:						
	Rock					X	Moderate

APPENDIX C

TABLE 2 (Continued)

Sample No.	Identification	Part	Charred W	Charred F	Uncharred W	Uncharred F	Weights/ Comments
SLN-R26	Liters Floated						0.70 L
Unit	Light Fraction Weight						0.173 g
S2bA	FLORAL REMAINS:						
Min CF3	Vitrified tissue ≥ 0.25 mm			5			0.0005 g
	Roots					X	Few
	Rootlets					X	Moderate
	NON-FLORAL REMAINS:						
	Rock/Gravel					X	Moderate
	Snail shell - oblong ≥ 0.5 mm				2	3	
SLN-R24	Liters Floated						1.00 L
Unit	Light Fraction Weight						0.485 g
S2cA	FLORAL REMAINS:						
Min CF3	Rootlets					X	Numerous
	CHARCOAL/WOOD:						
	Total charcoal ≥ 0.25 mm						0.0012 g
	Unidentifiable - small, vitrified	Charcoal		9			0.0012 g
	NON-FLORAL REMAINS:						
	Insect	Puparia				1	
	Rock					X	Moderate
	Snail shell - depressed ≥ 1 mm				3		
	Snail shell - depressed < 1 mm					X	Few
	Snail shell - oblong ≥ 0.5 mm				2	3	

W = Whole
F = Fragment
g = grams
L = liters
mm = millimeters
X = Presence noted in sample

APPENDIX C

TABLE 3
INDEX OF MACROFLORAL REMAINS RECOVERED FROM
THE SPRING LAKE NORTH TRENCH SITE AND THE NORTH CREEK TRENCH SITE
ON THE NEPHI SEGMENT OF THE WASATCH FAULT ZONE, UTAH

Scientific Name	Common Name
FLORAL REMAINS:	
Lactuca	Lettuce
Monocot/Herbaceous dicot	A member of the Monocotyledonae class of Angiosperms, which include grasses, sedges, members of the agave family, lilies, and palms/ A non-woody member of the Dicotyledonae class of Angiosperms
Periderm	Technical term for bark; Consists of the cork (phellum) which is produced by the cork cambium, as well as any epidermis, cortex, and primary or secondary phloem exterior to the cork cambium
Poaceae	Grass family
Poaceae A	Members of the grass family with larger-sized caryopses, such as *Agropyron* (wheatgrass), *Elymus* (ryegrass), *Bromus* (brome grass), etc.
Poaceae B	Members of the grass family with medium-sized caryopses, such as *Festuca* (fescue), *Hordeum* (wild barley), *Stipa* (needlegrass), etc.
Parenchymous tissue	Relatively undifferentiated tissue composed of many similar cells with thin primary walls–occurs in different plant organs in varying amounts, especially large fleshy organs such as roots and stems, but also fruits, seeds, cones, periderm (bark), leaves, needles, etc.
Vitrified tissue	Charred material with a shiny, glassy appearance due to fusion by heat
Sclerotia	Resting structures of mycorrhizae fungi
CHARCOAL/WOOD:	
Asteraceae	Sunflower family
Artemisia	Sagebrush
Conifer	Cone-bearing, gymnospermous trees and shrubs, mostly evergreens, including the pine, spruce, fir, juniper, cedar, yew, hemlock, redwood, and cypress
Juniperus	Juniper
Pseudotsuga menziesii	Douglas-fir

APPENDIX C

TABLE 3 (Continued)

Scientific Name	Common Name
Quercus	Oak
Quercus - *Leucobalanus* group	White oak group - Species in the white oak group exhibit earlywood vessels occluded with tyloses, thin-walled and angular latewood vessels, and longer rays than species in the red oak group
Salicaceae	Willow family
Unidentified hardwood	Wood from a broad-leaved flowering tree or shrub
Unidentified hardwood - small	Wood from a broad-leaved flowering tree or shrub, fragments too small for further identification
Unidentified hardwood - vitrified	Wood from a broad-leaved flowering tree or shrub, exhibiting a shiny, glassy appearance due to fusion by heat
Unidentifiable - small	Charcoal fragments too small for further identification
Unidentifiable - vitrified	Charcoal exhibiting a shiny, glassy appearance due to fusion by heat
NON-FLORAL REMAINS:	
Chitin	A natural polymer found in insect and crustacean exoskeleton
Insect puparium	A rigid outer shell made from tough material that includes chitin (a natural polymer found in insect exoskeleton and crab shells) and hardens from a larva's skin to protect the pupa as it develops into an adult insect
Snail shell - depressed	Snail shell with a depressed (flat) shape where the width is much bigger than the height
Snail shell - oblong	Snail shell with an oblong shape where the height is much bigger than the width

APPENDIX C

TABLE 4
PROVENIENCE DATA FOR SAMPLES FROM THE NORTH CREEK TRENCH SITE
ON THE NEPHI SEGMENT OF THE WASATCH FAULT ZONE, UTAH

Sample No.	Wall	Unit	Relation to Earthquake	Description/ Provenience	Analysis
NC-R14	South	C1A	Min P1	Charcoal and A horizon developed on or within (organic stringer) scarp colluvium	Charcoal ID/Float
NC-R28		C1		Charcoal and A horizon developed on or within scarp colluvium	Charcoal ID
NC-R20	North			A horizon developed on or within scarp colluvium	Float
NC-R22c		2d1		Detrital charcoal from alluvial fan sediments	Charcoal ID
NC-R21		C2A	Min P2, Max P1	A horizon developed on or within scarp colluvium	Float
NC-R15	South			A horizon developed on or within scarp colluvium	Float
NC-R16		2c2A	Max P2	A horizon developed on or within alluvial-fan sediments	Float
NC-R03			Max CH	Detrital charcoal from A horizon developed on or within alluvial-fan sediments	Charcoal ID
NC-R31	North			A horizon developed on or within alluvial-fan sediments	Float
NC-R01	South	CHA	Min CH	Detrital charcoal from A horizon developed on or within alluvial-fan sediments	Charcoal ID
NC-R02			Min CH	Detrital charcoal from A horizon developed on or within scarp colluvium	Charcoal ID
NC-R32	North			A horizon developed on or within scarp colluvium	Float
NC-R23		C3A	Min P3, Max P2	A horizon developed on or within scarp colluvium	Float
NC-R18	South		Min P3	A horizon developed on or within scarp colluvium	Float

APPENDIX C

TABLE 4 (Continued)

Sample No.	Wall	Unit	Relation to Earthquake	Description/ Provenience	Analysis
NC-R29	North	C4A	Min P4, Max P3	A horizon developed on or within scarp colluvium	Float
NC-R13	South	C4	Min P4	Charcoal and A horizon developed on or within scarp colluvium	Charcoal ID
NC-R19		2bA		A horizon developed on or within alluvial-fan sediments	Float
NC-R05		1bA	Max P4	Detrital charcoal from A horizon developed on or within alluvial-fan sediments	Charcoal ID
NC-R07				Detrital charcoal from A horizon developed on or within alluvial-fan sediments	Charcoal ID
NC-R09				Detrital charcoal from A horizon developed on or within alluvial-fan sediments	Charcoal ID
NC-R12		1c4A?		A horizon developed on or within alluvial-fan sediments	Float
NC-R11	North			Charcoal and A horizon developed on or within alluvial-fan sediments	Charcoal ID/Float

CH = Earthquake related to hanging-wall colluvial wedge deposits (likely corresponds to P1 or P2)

APPENDIX C

TABLE 5
MACROFLORAL REMAINS FROM THE NORTH CREEK TRENCH SITE
ON THE NEPHI SEGMENT OF THE WASATCH FAULT ZONE, UTAH

Sample No.	Identification	Part	Charred W	Charred F	Uncharred W	Uncharred F	Weights/ Comments
NC-R14	Bulk Sample Liters Floated						2.60 L
Unit C1A	Bulk Sample Light Fraction Weight						1.037 g
Min P1	Charcoal Sample Weight						0.010 g
	FLORAL REMAINS:						
	Roots					X	Moderate
	Rootlets					X	Moderate
	Sclerotia				X	X	Few
	CHARCOAL/WOOD:						
	Total charcoal ≥ 2 mm						0.0026 g
	Unidentifiable - small	Charcoal		X			0.0026 g
	NON-FLORAL REMAINS:						
	Insect						
	Rock/Gravel						
	Snail shell - depressed ≥ 0.5 mm					2	
NC-R28	Sample Weight						0.005 g
Unit C1	CHARCOAL/WOOD:						
Min P1	Total charcoal ≥ 0.25 mm						0.0051 g
	Asteraceae	Charcoal		1			0.0007 g
	Juniperus	Charcoal		1			0.0024 g
	Pseudotsuga menziesii	Charcoal		1			0.0016 g
	Unidentified hardwood - small	Charcoal		3			0.0004 g
NC-R20	Liters Floated						1.80 L
Unit C1	Light Fraction Weight						1.513 g
Min P1	FLORAL REMAINS:						
	Monocot/Herbaceous dicot	Stem		1			0.0010 g
	Roots					X	Moderate
	Rootlets					X	Numerous
	CHARCOAL/WOOD:						
	Total charcoal ≥ 0.25 mm						0.0014 g
	Conifer	Charcoal		12			0.0009 g
	Unidentifiable - small	Charcoal		13			0.0005 g

APPENDIX C

TABLE 5 (Continued)

Sample No.	Identification	Part	Charred W	Charred F	Uncharred W	Uncharred F	Weights/ Comments
NC-R20	NON-FLORAL REMAINS:						
Unit C1A	Insect	Egg			X		Moderate
Min P1	Insect	Puparia			X	X	Moderate
	Rock					X	Numerous
	Snail shell - depressed ≥ 1 mm				3		
	Snail shell - depressed < 1 mm					X	Few
	Snail shell - oblong ≥ 0.5 mm				1		
NC-R22-c	Sample Weight						0.962 g
Unit 2d1	CHARCOAL/WOOD:						
Min P1	Total charcoal ≥ 1 mm						0.0046 g
	Juniperus	Charcoal		7			0.0046 g
	NON-FLORAL REMAINS:						
	Rock/Sand					X	Few
NC-R21	Liters Floated						2.30 L
Unit C2a	Light Fraction Weight						2.251 g
Min P2,	FLORAL REMAINS:						
Max P1	Unidentified B	Fruit		3			0.0008 g
	Poaceae A	Floret			1		0.0021 g
	Unidentified	Fruit			1		0.0012 g
	Roots					X	Numerous
	Rootlets					X	Few
	Sclerotia				X	X	Moderate
	CHARCOAL/WOOD:						
	Total charcoal ≥ 1 mm						0.0076 g
	Juniperus	Charcoal		13			0.0069 g
	Quercus - Leucobalanus group	Charcoal		1			0.0007 g
	NON-FLORAL REMAINS:						
	Rock					X	Numerous
NC-R15	Liters Floated						2.20 L
Unit C2a	Light Fraction Weight						1.515 g
Min P2,	FLORAL REMAINS:						
Max P1	Roots					X	Moderate
	Rootlets					X	Moderate
	Sclerotia				X	X	Few

APPENDIX C

TABLE 5 (Continued)

Sample No.	Identification	Part	Charred W	Charred F	Uncharred W	Uncharred F	Weights/ Comments
NC-R15	CHARCOAL/WOOD:						
Unit C2a	Total charcoal ≥ 0.25 mm						0.0020 g
Min P2,	Unidentifiable - small	Charcoal		X			0.0020 g
Max P1	NON-FLORAL REMAINS:						
	Rock/Gravel					X	Numerous
	Snail shell - depressed ≥ 1 mm				1		
	Snail shell - depressed < 1 mm				X	X	Few
	Snail shell - oblong ≥ 0.5 mm				2	8	
NC-R16	Liters Floated						2.10 L
Unit 2c2A	Light Fraction Weight						3.046 g
Max P2	FLORAL REMAINS:						
	Roots					X	Numerous
	Rootlets					X	Few
	Sclerotia				X	X	Numerous
	CHARCOAL/WOOD:						
	Total charcoal ≥ 0.5 mm						0.0134 g
	Conifer	Charcoal		8			0.0027 g
	Pseudotsuga menziesii	Charcoal		6			0.0016 g
	Quercus	Charcoal		7			0.0010 g
	Unidentified hardwood twig	Charcoal		2			0.0033 g
	Unidentified hardwood - small	Charcoal		6			0.0013 g
	Unidentified hardwood - vitrified	Charcoal		1			0.0027 g
	Unidentifiable - small	Charcoal		2			0.0008 g
	NON-FLORAL REMAINS:						
	Rock					X	Numerous
	Snail shell - depressed ≥ 1 mm					1	
NC-R02	Sample Weight						0.008 g
Unit CHA	CHARCOAL/WOOD:						
Min CH	Total charcoal ≥ 0.25 mm						0.0015 g
	Conifer	Charcoal		3			0.0005 g
	Pseudotsuga menziesii	Charcoal		2			0.0002 g
	Unidentified hardwood - small	Charcoal		1			0.0006 g
	Unidentifiable - small	Charcoal		3			0.0002 g

APPENDIX C

TABLE 5 (Continued)

Sample No.	Identification	Part	Charred W	Charred F	Uncharred W	Uncharred F	Weights/ Comments
NC-R32	Liters Floated						1.00 L
Unit CHA	Light Fraction Weight						1.090 g
Min CH	FLORAL REMAINS:						
	Parenchymous tissue ≥ 1 mm			3			0.0029 g
	Roots					X	Moderate
	Rootlets					X	Moderate
	Sclerotia				X	X	Few
	CHARCOAL/WOOD:						
	Total charcoal ≥ 1 mm						0.0280 g
	Conifer	Charcoal		6			0.0066 g
	Juniperus	Charcoal		1			0.0020 g
	Pseudotsuga menziesii	Charcoal		4			0.0057 g
	Quercus	Charcoal		10			0.0083 g
	Rosaceae - twig	Charcoal		1			0.0016 g
	Unidentified hardwood - small	Charcoal		4			0.0038 g
	NON-FLORAL REMAINS:						
	Rock/Gravel					X	Moderate
	Snail shell - depressed ≥ 1 mm				2		
	Snail shell - depressed < 1 mm				1		
	Worm castings					X	Moderate
NC-R01	Sample Weight						0.007 g
Unit 2c2A	CHARCOAL/WOOD:						
Min CH	Unidentified hardwood	Charcoal		4			0.0032 g
NC-R03	Sample Weight						0.003 g
Unit 2c2A	FLORAL REMAINS:						
Max CH	Parenchymous tissue			3			0.0009 g
	NON-FLORAL REMAINS:						
	Rock/Sand					X	Few
NC-R31	Liters Floated						1.00 L
Unit 2c2A	Light Fraction Weight						1.008 g
Max CH	FLORAL REMAINS:						
	Roots					X	Moderate
	Rootlets					X	Moderate
	Sclerotia				X	X	Moderate

APPENDIX C

TABLE 5 (Continued)

Sample No.	Identification	Part	Charred W	Charred F	Uncharred W	Uncharred F	Weights/ Comments
NC-R31	CHARCOAL/WOOD:						
Unit 2c2A	Total charcoal ≥ 1 mm						0.0091 g
Max CH	Asteraceae	Charcoal		2			0.0008 g
	Conifer	Charcoal		1			< 0.0001 g
	Juniperus	Charcoal		1			0.0037 g
	Quercus	Charcoal		1			0.0001 g
	Quercus - Leucobalanus group	Charcoal		2			0.0028 g
	Salicaceae	Charcoal		2			0.0017 g
	NON-FLORAL REMAINS:						
	Bone ≥ 1 mm					3	
	Bone < 1 mm					X	Few
	Insect	Egg			X	X	Numerous
	Rock/Gravel					X	Moderate
	Snail shell - depressed ≥ 1 mm					3	
	Snail shell - depressed < 1 mm					X	Few
	Worm castings				X	X	Moderate
NC-R23	Liters Floated						1.90 L
Unit C3A	Light Fraction Weight						2.434 g
Min P3,	FLORAL REMAINS:						
Max P2	Poaceae B	Caryopsis		1			0.0001 g
	Roots					X	Moderate
	Rootlets					X	Few
	Sclerotia				X	X	Moderate
	CHARCOAL/WOOD:						
	Total charcoal ≥ 0.5 mm						0.0116 g
	Conifer	Charcoal		10			0.0017 g
	Juniperus	Charcoal		4			0.0035 g
	Pseudotsuga menziesii	Charcoal		4			0.0010 g
	Quercus	Charcoal		8			0.0016 g
	Quercus - Leucobalanus group	Charcoal		1			< 0.0001 g
	Salicaceae	Charcoal		1			0.0001 g
	Unidentified hardwood - small	Charcoal		13			0.0026 g
	Unidentifiable - small	Charcoal		8			0.0011 g

APPENDIX C

TABLE 5 (Continued)

Sample No.	Identification	Part	Charred W	Charred F	Uncharred W	Uncharred F	Weights/ Comments
NC-R23	Total wood ≥ 2 mm						0.1091 g
Unit C3A	*Artemisia*	Wood				5	0.0131 g
Min P3,	Conifer	Wood				25	0.0960 g
Max P2	NON-FLORAL REMAINS:						
	Insect	Chitin				X	Few
	Rock					X	Numerous
	Snail shell - depressed ≥ 1 mm				2		
	Snail shell - depressed < 1 mm				X	X	Few
NC-R18	Liters Floated						2.00 L
Unit C3A	Light Fraction Weight						2.392 g
Min P3	FLORAL REMAINS:						
	Roots					X	Moderate
	Rootlets					X	Moderate
	Sclerotia				X	X	Numerous
	CHARCOAL/WOOD:						
	Total charcoal ≥ 0.5 mm						0.0015 g
	Conifer	Charcoal		4			0.0008 g
	Unidentified hardwood - small	Charcoal		2			0.0004 g
	Unidentifiable - small	Charcoal		2			0.0003 g
	NON-FLORAL REMAINS:						
	Rock/Gravel					X	Numerous
	Snail shell - depressed ≥ 0.5 mm				2	4	
	Snail shell -oblong ≥ 0.5 mm				10	22	
NC-R29	Liters Floated						1.50 L
Unit C4A	Light Fraction Weight						2.723 g
Min P4,	FLORAL REMAINS:						
Max P3	Roots					X	Moderate
	Rootlets					X	Few
	Sclerotia				X	X	Moderate

APPENDIX C

TABLE 5 (Continued)

Sample No.	Identification	Part	Charred W	Charred F	Uncharred W	Uncharred F	Weights/ Comments
NC-R29	CHARCOAL/WOOD:						
Unit C4A	Total charcoal ≥ 0.5 mm						0.0134 g
Min P4,	Conifer	Charcoal		16			0.0013 g
Max P3	*Juniperus*	Charcoal		2			0.0101 g
	Pseudotsuga menziesii	Charcoal		1			0.0001 g
	Quercus	Charcoal		9			0.0012 g
	Unidentified hardwood - small	Charcoal		2			0.0007 g
	Total wood ≥ 4 mm						0.2235 g
	Conifer	Wood				6	0.2235 g
	NON-FLORAL REMAINS:						
	Insect	Chitin				X	Few
	Rock					X	Numerous
	Snail shell - oblong ≥ 0.5 mm				1		
NC-R13	Sample Weight						0.008 g
Unit C4	FLORAL REMAINS:						
Min P4	Periderm					X	Few
	Sclerotia				2		
	CHARCOAL/WOOD:						
	Unidentified hardwood - vitrified	Charcoal		9			0.0021 g
	NON-FLORAL REMAINS:						
	Sand					X	Few
NC-R19	Liters Floated						1.50 L
Unit 2bA	Light Fraction Weight						4.420 g
Min P4	FLORAL REMAINS:						
	Unidentified	Fruit		16			0.0090 g
	Roots					X	Moderate
	Rootlets					X	Moderate
	Sclerotia				X	X	Numerous
	CHARCOAL/WOOD:						
	Total charcoal ≥ 1 mm						0.0072 g
	Conifer	Charcoal		2			0.0009 g
	Unidentified hardwood - small	Charcoal		14			0.0057 g
	Unidentifiable - small	Charcoal		3			0.0006 g

APPENDIX C

TABLE 5 (Continued)

Sample No.	Identification	Part	Charred W	Charred F	Uncharred W	Uncharred F	Weights/ Comments
NC-R19	NON-FLORAL REMAINS:						
Unit 2bA	Rock/Gravel					X	Numerous
Min P4	Snail shell - depressed ≥ 1 mm				59	32	
	Snail shell - depressed < 1 mm				X	X	Moderate
	Snail shell - oblong ≥ 0.5 mm				44	15	
NC-R05	Sample Weight						0.042 g
Unit 1bA	CHARCOAL/WOOD:						
Max P4	Total charcoal ≥ 0.5 mm						0.0093 g
	Unidentified hardwood - small	Charcoal		20			0.0093 g
	NON-FLORAL REMAINS:						
	Sediment					X	Few
NC-R07	Sample Weight						0.011 g
Unit 1bA	CHARCOAL/WOOD:						
Max P4	*Quercus*	Charcoal		9			0.0035 g
NC-R09	Sample Weight						0.016 g
Unit 1bA	CHARCOAL/WOOD:						
Max P4	*Quercus*	Charcoal		10			0.0042 g
NC-R12	Liters Floated						2.00 L
Unit	Light Fraction Weight						0.701 g
1c4A?	FLORAL REMAINS:						
Max P4	Roots					X	Moderate
	Rootlets					X	Few
	Sclerotia				X	X	Numerous
	CHARCOAL/WOOD:						
	Total charcoal ≥ 0.25 mm						0.0008 g
	Unidentifiable - small	Charcoal		X			0.0008 g
	NON-FLORAL REMAINS:						
	Rock					X	Numerous
	Snail shell - oblong ≥ 0.5 mm				1	1	

APPENDIX C

TABLE 5 (Continued)

Sample No.	Identification	Part	Charred W	Charred F	Uncharred W	Uncharred F	Weights/ Comments
NC-R11	Bulk Sample Liters Floated						3.00 L
Unit	Bulk Sample Light Fraction Weight						2.764 g
1c4A?	Charcoal Sample Weight						0.003 g
Max P4	FLORAL REMAINS:						
	Periderm ≥ 0.25 mm					6	0.0017 g
	Roots					X	Few
	Rootlets					X	Numerous
	Sclerotia				X	X	Numerous
	CHARCOAL/WOOD:						
	Total charcoal ≥ 0.5 mm						0.0025 g
	Conifer	Charcoal		6			0.0021 g
	Unidentifiable - small	Charcoal		7			0.0004 g
	NON-FLORAL REMAINS:						
	Insect	Chitin				X	Few
	Rock/Gravel					X	Numerous
	Snail shell - depressed ≥ 1 mm				1	1	
	Snail shell - oblong ≥ 0.5 mm				1	1	

W = Whole
F = Fragment
g = grams
L = liters
X = Presence noted in sample
mm = millimeters

APPENDIX C

REFERENCES CITED

Carlquist, Sherwin
2001 *Comparative Wood Anatomy: Systematic, Ecological, and Evolutionary Aspects of Dicotyledon Wood*. Springer Series in Wood Science. Springer, Berlin.

Core, H. A., W. A. Cote, and A. C. Day
1976 *Wood Structure and Identification*. Syracuse University Press, Syracuse, New York.

Hather, Jon G.
2000 *Archaeological Parenchyma*. Archetype Publications Ltd., London.

Hoadley, Bruce
1990 *Identifying Wood: Accurate Results with Simple Tools*. The Taunton Press, Inc., Newtown, Connecticut.

Kricher, John C., and Gordon Morrison
1988 *A Field Guide to Ecology of Eastern Forests*. Houghton Mifflin Company, Boston and New York.

Marguerie, D., and J. Y. Hunot
2007 Charcoal Analysis and Dendrology: Data from Archaeological Sites in Northwestern France. *Journal of Archaeological Science* 34:1417-1433.

Martin, Alexander C., and William D. Barkley
1961 *Seed Identification Manual*. University of California, Berkeley.

Matthews, Meredith H.
1979 Soil Sample Analysis of 5MT2148: Dominguez Ruin, Dolores, Colorado. Appendix B. In *The Dominguez Ruin: A McElmo Phase Pueblo in Southwestern Colorado*, edited by Alan D. Reed. Bureau of Land Management Cultural Resource Series. vol. 7. Bureau of Land Management, Denver, Colorado.

Mauseth, James D.
1988 Parenchyma. Chapter 3. In *Plant Anatomy*, pp. 43-51. The Benjamin/Cummings Publishing Company, Inc., Menlo Park, California.

Mcparland, Laura C., Margaret E. Collinson, Andrew C. Scott, Gill Campbell, and Robyn Veal
2010 Is Vitrification in Charcoal a Result of High Temperature Burning of Wood? *Journal of Archaeological Science* 37:2679-2687.

Mcweeney, Lucinda
1989 What Lies Lurking Below the Soil: Beyond the Archaeobotanical View of Flotation Samples. *North American Archaeologist* 10(3):227-230.

Panshin, A. J., and Carl De Zeeuw
1980 *Textbook of Wood Technology*. McGraw-Hill Book, Co., New York.

APPENDIX C

Petrides, George A., and Olivia Petrides
1992 *A Field Guide to Western Trees*. The Peterson Field Guide Series. Houghton Mifflin Co., Boston.

Trappe, James M.
1962 Fungus Associates of Ectotrophic Mycorrhizae. In *The Botanical Review*. U.S. Department of Agriculture, Washington D.C.

APPENDIX D
RADIOCARBON AGES FOR THE SPRING LAKE SITE

APPENDIX D

SUMMARY OF ^{14}C DATED CHARCOAL FOR THE SPRING LAKE SITE

Sample Name	NOSAMS[1] Accession No.	Trench Wall			Sample	Unit Sampled	Notes	Macrofloral remains (total weight in mg)[2]	Pre-treatment[3]	Laboratory age (^{14}C yr)[4]			Calibrated age (cal yr B.P.)[5]		Calibrated age (rounded) (ka)	
		Horiz. (m)	Vert. (m)	Wall						Age	Age error	$D^{13}C$	Mean	1σ	Mean	2σ
SLN-R01	OS-105419	38.32	1.21	south	charcoal	S3d	Charcoal in massive silt/loess	1-PT (1.8)	ABA	6620	110	-25.18	7507	90	7.5	0.2
SLN-R02	OS-104798	32.47	2.43	south	charcoal	S3bA	Charcoal from A horizon in alluvial-fan sediments	31-UVC (1.2)	A	6680	40	-24.55	7547	36	7.6	0.1
SLN-R03	OS-105243	36.03	1.94	south	charcoal	S3d	Charcoal in massive silt/loess	1-UHT (1.2)	A	6260	80	-23.41	7164	105	7.2	0.2
SLN-R04	OS-105241	38.07	1.71	south	charcoal	S3g4	Charcoal in alluvial-fan sediments	UC (0.9)	A	6110	40	-26.18	7006	79	7.0	0.2
SLN-R05	-	33.71	3.81	south	charcoal	S3h1	Charcoal in alluvial-fan sediments	6-UC (<0.1)	-	-	-	-	-	-	-	-
SLN-R06	-	33.73	3.87	south	charcoal	S3h1	Charcoal in alluvial-fan sediments	2-UT (<0.1)	-	-	-	-	-	-	-	-
SLN-R07	-	38.14	1.29	south	bulk	S3d	Massive silt/loess	-	-	-	-	-	-	-	-	-
SLN-R08	-	33.20	2.23	south	bulk	S3bA	A horizon within alluvial-fan sediments	-	-	-	-	-	-	-	-	-
SLN-R09	-	27.92	3.43	north	bulk + char.	C6	Top of C6	5-UC (<0.1)	-	-	-	-	-	-	-	-
SLN-R10	OS-104444	28.86	3.14	north	bulk	C6	Top of C6	**5-VT(0.7)**, 5-PT(<0.1)	NP	13800	130	25	16920	144	16.9	0.3
SLN-R11	OS-104738	33.67	3.92	south	bulk	S3h1	Alluvial-fan sediments (charcoal fragments)	UC(2.2)	ABA	6170	35	-24.66	7074	57	7.1	0.1
SLN-R12	-	25.23	7.82	south	bulk	S3j	Slopewash above C1	-	-	-	-	-	-	-	-	-
SLN-R13	-	26.15	7.28	south	bulk	S3j	Slopewash above C1	**2-A(1.6)**, 23-MHD(2.6)	ABA	-	-	-	-	-	-	-
SLN-R14	-	25.44	7.51	south	bulk	C1	Soil organics in uppermost C1	-	-	-	-	-	-	-	-	-
SLN-R15	OS-104825	26.55	6.94	south	bulk	C1	Soil organics in uppermost C1	UC (1.1)	A	790	25	-25.28	708	18	0.7	0.04
SLN-R16	OS-104739	25.86	7.06	south	bulk	C1A	Soil organics in C1	UC (1.9)	ABA	2390	25	-25.57	2420	65	2.4	0.1
SLN-R17	OS-104449	25.49	6.83	south	bulk	C2	Soil organics in uppermost C2	36-S (7.4)	ABA	2320	30	-17.6	2333	41	2.3	0.1
SLN-R18	OS-104824	26.09	6.49	south	bulk	C2	Soil organics in C2	UC(1.4)	A	3740	25	-23.05	4089	55	4.1	0.1
SLN-R19	OS-104829	26.22	6.19	south	bulk	C3	Soil organics in uppermost C3	**UC(1.0)**, 4-PT(0.8)	A	3280	40	-21.3	3509	50	3.5	0.1
SLN-R20	OS-105242	27.28	5.43	south	bulk	C4	C4 colluvial sediment	UC(0.8)	A	3930	35	-21.7	4365	62	4.4	0.1
SLN-R21	OS-104831	26.2	7.34	north	bulk + char.	C1	Base of C1 colluvial wedge	14-UC (0.9) ***	A	770	30	-25.76	700	19	0.7	0.04
SLN-R22	OS-104826	26.55	6.96	north	bulk	C2	Top of C2 colluvial wedge	10-UC(0.2), 1-UVT(0.8)	A	1150	30	-24.68	1060	53	1.1	0.1
SLN-R23	-	27.18	6.69	north	bulk + char.	C2	Top of C2 colluvial wedge	15-UC(0.5)	NP	sample lost during processing				-	-	-
SLN-R24	OS-104823	12.28	13.84	south	bulk	S2cA	A horizon within alluvial-fan sediments	9-UC (1.2)	A	5280	40	-21.11	6067	70	6.1	0.1
SLN-R25	OS-104740	11.34	14.08	south	bulk	CF3	Basal CF3	3-UC (<0.1), **MC(34.5)**	ABA	3380	30	-26.91	3624	43	3.6	0.1
SLN-R26	OS-104445	10.24	13.94	south	bulk	S2bA	A horizon within alluvial-fan sediments	5-VT(0.5)	NP	11850	95	-22.91	13684	120	13.7	0.2
SLN-R27	OS-104832	27.85	6.05	north	bulk	N3g	A horizon in alluvial-fan deposits below C2 wedge	UC(1.0)	A	4960	45	-23.76	5697	65	5.7	0.1
SLN-R28	-	21.1	10.1	south	bulk	CF1	CF1 colluvial sediment	-	-	-	-	-	-	-	-	-

[1] National Ocean Sciences Accelerator Mass Spectrometry Facility, Woods Hole Oceanographic Institution (Woods Hole, Massachusetts).

[2] Number of fragments of charcoal and their weight (in parentheses) following sample sorting by PaleoResearch Institute (Golden, Colorado). Unidentified charcoal: MC - microcharcoal, MHD - monocot/Herbaceous dicot, PT - Parenchymous tissue (charred), UC - unidentified charcoal, UHT - unidentified hardwood twig (charred), UVT - unidentified twig (vitrified), UVC - unidentified charcoal (vitrified), UT - unidentified tissue (charred), VT- vitrified tissue. Identified charcoal: A - *Asteraceae* (sunflower family), S - Sagebrush (*Artemisia*). Bold text indicates subset of charcoal dated.

[3] Pretreatment methods: A - acid wash only, ABA - acid-base-acid washes, NP - no pretreatment.

[4] Delta ^{13}C for SLN-R10 is assumed; all other values were measured.

[5] Calibrated using OxCal version 4.2 (Bronk Ramsey, 1995, 2001) and the terrestrial calibration curve of Reimer and others (2009).

APPENDIX E
RADIOCARBON AGES FOR THE NORTH CREEK SITE

APPENDIX E

SUMMARY OF ^{14}C DATED CHARCOAL FOR THE NORTH CREEK SITE

Sample Name	NOSAMS[1] Accession No.	Trench Wall			Sample	Unit Sampled	Notes	Macrofloral remains (total weight in mg)[2]	Pre-treatment[3]	Laboratory age (^{14}C yr)[4]			Calibrated age (cal yr B.P.)[5]		Calibrated age (rounded) (ka)	
		Horiz. (m)	Vert. (m)	Wall						Age	Age error	D^{13}C	Mean	1σ	Mean	2σ
NC-R01	-	7.7	3.78	south	charcoal	2cA2/CgA	Thin soil A horizon within alluvial-fan unit 2c	4-UH(3.2)	-	-	-	-	-	-	-	-
NC-R02	OS-103474	8.42	3.56	south	charcoal	2cA2/CgA	Thin soil A horizon on Cg1 (graben colluvial wedge)	**3-C(0.5)**, 2-DF(0.2), **UH(0.6)**, **3-UC(0.2)**	A	915	25	-25.61	845	43	0.9	0.1
NC-R03	-	8.92	3.35	south	charcoal	2cA	A horizon on 2c below Cg1	3-PT(0.9)	-	-	-	-	-	-	-	-
NC-R04	-	33.80	10.75	south	charcoal	1bA	A horizon within footwall alluvial-fan sediments	-	-	-	-	-	-	-	-	-
NC-R05	-	33.40	10.70	south	charcoal	1bA	A horizon within footwall alluvial-fan sediments	20-UH(9.3)	-	-	-	-	-	-	-	-
NC-R06	-	30.25	10.75	south	bulk/charcoal	1bA	A horizon within footwall alluvial-fan sediments	-	-	-	-	-	-	-	-	-
NC-R07	OS-104336	36.30	11.15	south	charcoal	1bA	A horizon within footwall alluvial-fan sediments	9-Q(3.5)	ABA	7,090	120	-25.62	7913	123	7.9	0.3
NC-R08	-	33.28	10.70	north	charcoal	1bA	A horizon within footwall alluvial-fan sediments	-	-	-	-	-	-	-	-	-
NC-R09	OS-103168	36.25	11.17	south	charcoal	1bA	A horizon within footwall alluvial-fan sediments	10-Q(4.2)	ABA	4590	30	-24.1	5311	103	5.3	0.2
NC-R10	-	27.60	9.75	north	bulk	1bA	A horizon within footwall alluvial-fan sediments	-	-	-	-	-	-	-	-	-
NC-R11	OS-103263	20.80	0.90	north	bulk/charcoal	C5A	A horizon on hanging wall alluvial-fan sediments	**6-C(2.1)**, 7-UC(0.4)	ABA	2010	40	-23.6	1965	51	2.0	0.1
NC-R12	OS-103475	20.78	1.10	south	bulk	C5A	A horizon on hanging wall alluvial-fan sediments	UC(0.8)	A	3680	30	-24.48	4019	52	4.0	0.1
NC-R13	OS-103166	20.63	1.62	south	bulk/charcoal	C4A	Thin soil lense within C4 colluvium	9-UH(2.1)	ABA	4700	30	-26.5	5424	77	5.4	0.2
NC-R14	-	21.13	5.20	south	bulk/charcoal	C1A	Soil organics and slopewash overlying C1	UC(2.6)	ABA							
NC-R15	OS-103167	20.14	4.10	south	bulk	C2A	Weak A horizon on C2 colluvium	UC(2.0)	ABA	5220	30	-23.55	5974	50	6.0	0.1
NC-R16	OS-103264	20.75	3.68	south	bulk	2cA	Well developed A horizon on C3/2c	8-C(2.7), 6-DF(1.6), 7-Q(1.0), **2-UHT(3.3)**, 7-UHC(4.0), 2-UC(0.8)	ABA	1280	30	-25.44	1223	38	1.2	0.1
NC-R17	-	19.9	3.36	south	bulk	2cA	Well developed A horizon on 2c	-	-	-	-	-	-	-	-	-
NC-R18	OS-103265	19.57	2.76	south	bulk	C3	Weak A horizon on C3 colluvium, below 2c	4-C(0.8), 2-UHC(0.4), 2-UC(0.3)	ABA	2110	30	-23.43	2084	55	2.1	0.1
NC-R19	OS-103266	18.38	1.14	south	bulk	2b2	Organics-rich debris flow inter-fingered with C4	**16-UF(9)**, 2-C(0.9), 14-UHC(5.7), 3-UC(0.6)	ABA	3710	40	-25.96	4052	62	4.1	0.1
NC-R20	OS-103476	22.23	5.32	north	bulk	C1	Silt/organic lense in C1 colluvium	**MH(1.0)**, 12-C(0.9), 13-UC(0.5)	A	315	20	-25.12	382	41	0.4	0.1
NC-R21	OS-103477	22.44	4.72	north	bulk	C2A	Well developed A horizon on C2	**3-UF(0.8)**, 13-J(6.9), Q(0.7)	A	245	20	-24.56	257	74	0.3	0.2
NC-R22	OS-103267	17.96	3.49	north	charcoal	2d2	Silt/organic lense likely in C1 colluvium	7-J (4.6)	ABA	160	25	-23.9	157	85	0.2	0.2
NC-R22-b	-	17.96	3.49	north	bulk	2d2	Silt/organic lense likely in C1 colluvium	-	-	-	-	-	-	-	-	-
NC-R23	OS-103169	21.46	3.22	north	bulk	C3A	A horizon on C3 (massive organic-rich sediments)	10-C(1.7), 4-J(3.5), 4-DF(1.0), **8-Q(1.6)**, W(0.1), 21-UHC/UC(3.7)	ABA	590	20	-24.6	599	31	0.6	0.1
NC-R24	-	12.6	2.37	north	bulk/charcoal	Cg2	Base of Cg2/top of 2cA (relation to contact uncertain)	-	-	-	-	-	-	-	-	-
NC-R25	-	16.82	2.26	north	bulk	2b2	Organic-rich gravel below C3	-	-	-	-	-	-	-	-	-
NC-R26	-	15.32	1.35	north	bulk	2b2	Organic-rich gravel below C3	-	-	-	-	-	-	-	-	-
NC-R27	-	14.58	1.08	north	bulk	2bA	A horizon on alluvial-fan gravel 2b1	-	-	-	-	-	-	-	-	-
NC-R28	OS-103170	20.26	4.58	south	bulk/charcoal	C1A	Thin soil lense within C1 colluvium	**A(0.7)**, J(2.4), DF(1.6), UC(0.4)	NP	5450	30	-25	6250	30	6.3	0.1
NC-R29	OS-103405	21.70	2.63	north	bulk	C4A	A horizon on C4, below C3	16-C(1.3), 2-J(10.1), DF(0.1), **9-Q(1.2)**, 2-UH(0.7)	A	180	25	-24.85	163	89	0.2	0.2
NC-R30	-	8.84	2.66	north	bulk	2cA	A horizon on 2c below Cg1	-	-	-	-	-	-	-	-	-
NC-R31	OS-103478	12.33	2.3	north	bulk	2cA	A horizon on 2c below Cg1	**2-A(0.8)**, J(3.7), Q(2.9), 2-W(1.7)	A	365	20	-25.59	415	57	0.4	0.1
NC-R32	OS-103171	12.25	2.53	north	bulk	Cg	Cg1 colluvium	6-C(6.6), 1-J(2.0), 4-DF(5.7), 10-Q(8.3), **1-RT(1.6)**, 4-UHC(3.8)	ABA	215	20	-24.03	183	97	0.2	0.2

[1] National Ocean Sciences Accelerator Mass Spectrometry Facility, Woods Hole Oceanographic Institution (Woods Hole, Massachusetts).

[2] Number of fragments of charcoal and their weight (in parentheses) following sample sorting by PaleoResearch Institute (Golden, Colorado). Unidentified charcoal: MC - microcharcoal, MHD - monocot/Herbaceous dicot, PT - Parenchymous tissue (charred), UC - unidentified charcoal, UHC - unidentified hardwood charcoal, UHT - unidentified hardwood twig (charred), UT - unidentified tissue (charred), UVC - unidentified charcoal (vitrified), UVT - unidentified twig (vitrified), VT- vitrified tissue. Identified charcoal: A - Asteraceae (sunflower family), C - conifer, DF - Douglas fir (*Pseudotsuga menziesii*), J - *Juniperus*, RT - *Roseacaea* twig, S - Sagebrush (*Artemisia*), Q - *Quercus* (oak), W - Willow family (*Salicaceae*). Bold text indicates subset of charcoal dated.

[3] Pretreatment methods: A - acid wash only, ABA - acid-base-acid washes, NP - no pretreatment.

[4] Delta ^{13}C for NC-R28 is assumed; all other values were measured.

[5] Calibrated using OxCal version 4.2 (Bronk Ramsey, 1995, 2001) and the terrestrial calibration curve of Reimer and others (2009).

APPENDIX F
OPTICALLY STIMULATED LUMINESCENCE AGES FOR THE SPRING LAKE SITE

APPENDIX F

OPTICALLY STIMULATED LUMINESCENCE AGES FOR THE SPRING LAKE SITE

Sample[1]	**% Water content**[2]	**K** (%)[3]	**U** (ppm)[3]	**Th** (ppm)[3]	**Cosmic dose**[4] **additions** (Gy/ka)	**Total Dose Rate** (Gy/ka)	**Equivalent Dose** (Gy)	**n**[5]	**Age (yr)**[6] **mean**	**1σ**	**Age (rounded) (ka)** mean	2σ
SL-L1	6 (13)	1.60 ± 0.03	3.53 ± 0.11	9.40 ± 0.33	0.19 ± 0.01	3.28 ± 0.07	17.2 ± 0.43	21 (34)	5240	170	5.2	0.3
SL-L2	5 (14)	0.88 ± 0.06	1.78 ± 0.19	4.29 ± 0.45	0.18 ± 0.01	1.77 ± 0.11	14.1 ± 0.97	21 (28)	7980	740	8.0	1.5
SL-L3	6 (21)	1.26 ± 0.06	2.35 ± 0.20	3.75 ± 0.47	0.18 ± 0.01	2.19 ± 0.12	17.1 ± 0.52	30 (42)	7810	490	7.8	1.0
SL-L4	7 (27)	2.14 ± 0.06	2.57 ± 0.18	10.4 ± 0.48	0.18 ± 0.01	3.49 ± 0.11	21.3 ± 2.044	21 (32)	6100	610	6.1	1.2
SL-L5	4 (18)	2.24 ± 0.06	2.34 ± 0.16	10.0 ± 0.75	0.17 ± 0.01	3.58 ± 0.16	24.9 ± 0.62	12 (20)	6970	360	7.0	0.7
SL-L6	7 (44)	1.50 ± 0.04	2.88 ± 0.16	6.67 ± 0.57	0.23 ± 0.02	2.64 ± 0.13	15.1 ± 0.73	19 (24)	5720	390	5.7	0.8
SL-L7	3 (25)	2.08 ± 0.06	2.93 ± 0.20	8.77 ± 0.76	0.24 ± 0.02	3.48 ± 0.17	>1	2 (20)	>300	-	>0.3	-
SL-L8	2 (26)	2.33 ± 0.06	3.51 ± 0.19	12.4 ± 0.85	0.23 ± 0.02	3.66 ± 0.17	36.5 ± 1.44	25 (48)	9970	580	10.0	1.2
SL-L9	4 (29)	1.94 ± 0.05	2.33 ± 0.15	10.9 ± 0.75	0.19 ± 0.01	3.04 ± 0.15	52.6 ± 1.95	28 (30)	17,300	970	17.3	1.9
SL-L10	9 (25)	1.83 ± 0.04	3.00 ± 0.15	10.7 ± 0.69	0.22 ± 0.02	3.38 ± 0.14	15.2 ± 0.56	26 (30)	4500	240	4.5	0.5

[1] Analyses by the U.S. Geological Survey Luminescence Dating Laboratory (Denver, Colorado).
[2] Field moisture by weight; figures in parentheses indicate the complete sample saturation percent. Ages calculated using approximately 25% of total saturation value, except SL-8 and -9, at 50%.
[3] Analyses obtained using in-situ gamma spectrometry (NaI detector) and laboratory gamma spectrometry (Ge detector).
[4] Cosmic doses and attenuation with depth were calculated using the methods of Prescott and Hutton (1994).
[5] Number of replicated equivalent dose (De) estimates used to calculate the equivalent dose. Figures in parentheses indicate total number of measurements included in calculating the represented equivalent dose and age using radial plots (weighed mean). Not all samples had adequate sand-sized grains for analyses; dispersion varied between 10 and 40%.
[6] Dose rate and age for fine-grained 125-90 microns or 150-125 microns sized quartz. Exponential + linear fit used on equivalent dose, errors to one sigma.

APPENDIX G
OPTICALLY STIMULATED LUMINESCENCE AGES FOR THE NORTH CREEK SITE

APPENDIX G

OPTICALLY STIMULATED LUMINESCENCE AGES FOR THE NORTH CREEK SITE

Sample[1]	**% Water content**[2]	**K** (%)[3]	**U** (ppm)[3]	**Th** (ppm)[3]	**Cosmic dose**[4] **additions** (Gy/ka)	**Total Dose Rate** (Gy/ka)	**Equivalent Dose** (Gy)	**n**[5]	**Age (yr)**[6] **mean**	**1σ**	**Age (rounded) (ka)** mean	2σ
NC-L1	6 (51)	0.99 ± 0.04	1.79 ± 0.08	3.00 ± 0.26	0.18 ± 0.01	1.63 ± 0.07	9.77 ± 0.50	17 (20)	6000	390	6.0	0.8
NC-L2	1 (55)	0.84 ± 0.06	1.56 ± 0.22	4.04 ± 0.36	0.24 ± 0.02	1.56 ± 0.09	2.26 ± 0.22	24 (30)	1450	170	1.5	0.4

[1] Analyses by the U.S. Geological Survey Luminescence Dating Laboratory (Denver, Colorado).
[2] Field moisture by weight; figures in parentheses indicate the complete sample saturation percent. Ages calculated using approximately 25% of total saturation value.
[3] Analyses obtained using in-situ gamma spectrometry (NaI detector) and laboratory gamma spectrometry (Ge detector).
[4] Cosmic doses and attenuation with depth were calculated using the methods of Prescott and Hutton (1994).
[5] Number of replicated equivalent dose (De) estimates used to calculate the equivalent dose. Figures in parentheses indicate total number of measurements included in calculating the represented equivalent dose and age using radial plots (weighed mean). Not all samples had adequate sand-sized grains for analyses; dispersion varied between 25 and 45%.
[6] Dose rate and age for fine-grained 125-90 microns or 150-125 microns sized quartz. Exponential + linear fit used on equivalent dose, errors to one sigma.

APPENDIX H
OXCAL MODELS FOR SELECTED SITES ON THE NEPHI SEGMENT

APPENDIX H

OXCAL MODELS FOR SELECTED SITES ON THE NEPHI SEGMENT

We include OxCal models for the Spring Lake and North Creek sites (this study), as well as the Payson (D. Horns, written communication, 2011, 2015) and Picayune Canyon (Horns and others, 2009) sites created using OxCal calibration and analysis software (version 4.2; Bronk Ramsey, 1995, 2001; using the IntCal13 calibration curve of Reimer and others, 2013). OxCal models for the Santaquin site are in DuRoss and others (2008), and models for the original North Creek (Hanson and others, 1981, 1982), Willow Creek, and Red Canyon sites are in Crone and others (2014). The models include *C_Date* for luminescence ages, *R_Date* for radiocarbon ages, and *Boundary* for undated events (paleoearthquakes). These components are arranged into ordered sequences based on the relative stratigraphic positions of the samples. The sequences may contain *phases*, or groups where the relative stratigraphic ordering information for the individual radiocarbon ages is unknown. Ages following two forward slashes (//) are not considered during model analysis. The models are presented here in reverse stratigraphic order, following the order in which the ages and events are evaluated in OxCal.

Spring Lake Site

```
Plot()
 {
 Sequence("Spring Lake, 2012; ver. 5_int_ZB")
  {
  Boundary("sequence start");
  C_Date("SLN-L9, 17.3 ± 1.9 ka", -15288, 970);
  Date("SL7");
  C_Date("SLN-L8, 10.0 ± 1.2 ka", -7958, 580);
  Phase("Units S3bA/C7?");
  {
   C_Date("SLN-L2, 8.0 ± 1.5 ka", -5968, 740);
   R_Date("SLN-R02, 7.6 ± 0.1 ka", 6680, 40);
   C_Date("SLN-L3, 7.8 ± 1.0 ka", -5798, 490);
   C_Date("SLN-L5, 7.0 ± 0.7 ka", -4958, 390);
  };
  Boundary("SL6");
  Zero_Boundary("ZB1");
  Phase("Units C6/S3d");
  {
   C_Date("SLN-L4, 6.1 ± 1.2 ka", -4088, 610);
   //R_Date("SLN-R01, 7.5 ± 0.1 ka", 6620, 110); [detrital?]
   //R_Date("SLN-R03, 7.2 ± 0.2 ka", 6260, 80); [detrital?]
   //C_Date("SLN-L1, 5.2 ± 0.3 ka", -3228, 170); [stratigraphically inverted]
  };
  Boundary("SL5");
```

```
 //R_Date("SLN-R04", 6110, 40); [relation to P5 unclear]
 Phase("Unit S3h1");
 {
  //R_Date("SLN-R11, 7.1 ± 0.1 ka", 6170, 35); [detrital?]
  C_Date("SLN-L6, 5.7 ± 0.8 ka", -3708, 390);
 };
 //R_Date("SLN-R24", 5280, 40); [unknown relation]
 Boundary("SL4");
 Phase("unit C4");
 {
  R_Date("SLN-R20", 3930, 35);
  C_Date("SLN-L10", -2488, 240);
 };
 Boundary("SL3");
 R_Date("SLN-R19", 3280, 40);
 //R_Date("SLN-R25", 3380, 30); [unknown relation]
 //R_Date("SLN-R27", 4960, 45); [detrital?]
 Boundary("SL2");
 //R_Date("SNL-R18", 3740, 25);
 Phase("uppermost unit C2");
 {
  //R_Date("SLN-R18", 4089, 55); [likely sourced from C3A]
  R_Date("SLN-R17", 2320, 30);
  R_Date("SLN-R22", 1150, 30);
 };
 Boundary("SL1");
 Phase("unit C1");
 {
  //R_Date("SLN-R16", 2390, 25); [likely sourced from C2A]
  R_Date("SLN-R15", 790, 25);
  R_Date("SLN-R21", 770, 30);
 };
 Boundary("Sequence end historic constraint", 1847);
};
Difference("SL7-SL6","SL6","SL7");
Difference("SL6-SL5","SL5","SL6");
Difference("SL5-SL4","SL4","SL5");
Difference("SL4-SL3","SL3","SL4");
Difference("SL3-SL2","SL2","SL3");
Difference("SL2-SL1","SL1","SL2");
Difference("SL7-SL1","SL1","SL7");
Difference("SL6-SL1","SL1","SL6");
Difference("SL5-SL1","SL1","SL5");
Difference("SL4-SL1","SL1","SL4");
Difference("SL3-SL1","SL1","SL3");
};
```

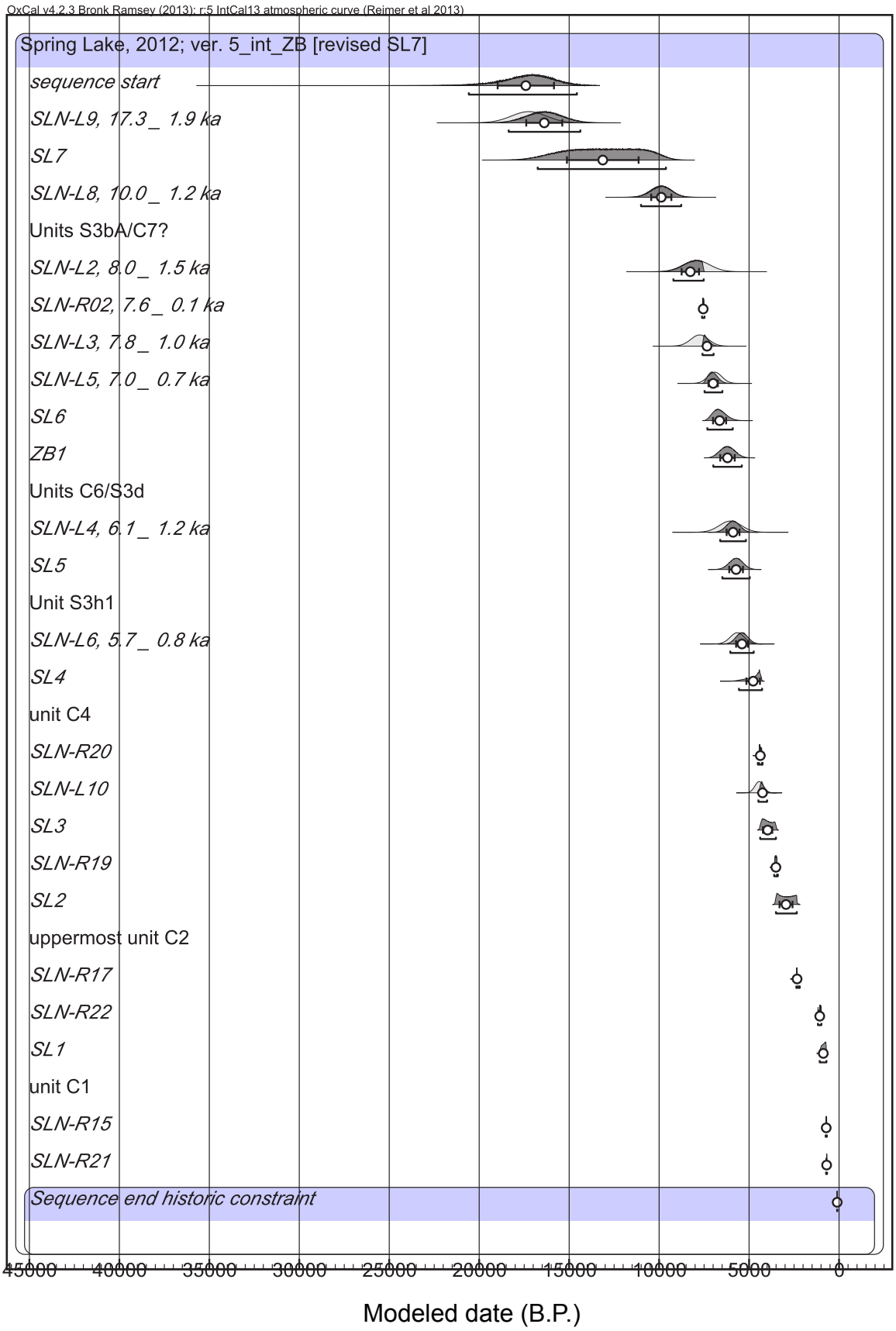
OxCal v4.2.3 Bronk Ramsey (2013); r:5 IntCal13 atmospheric curve (Reimer et al 2013)
Spring Lake, 2012; ver. 5_int_ZB [revised SL7]
sequence start
SLN-L9, 17.3_ 1.9 ka
SL7
SLN-L8, 10.0_ 1.2 ka
Units S3bA/C7?
SLN-L2, 8.0_ 1.5 ka
SLN-R02, 7.6_ 0.1 ka
SLN-L3, 7.8_ 1.0 ka
SLN-L5, 7.0_ 0.7 ka
SL6
ZB1
Units C6/S3d
SLN-L4, 6.1_ 1.2 ka
SL5
Unit S3h1
SLN-L6, 5.7_ 0.8 ka
SL4
unit C4
SLN-R20
SLN-L10
SL3
SLN-R19
SL2
uppermost unit C2
SLN-R17
SLN-R22
SL1
unit C1
SLN-R15
SLN-R21
Sequence end historic constraint
45000
40000
35000
30000
25000
20000
15000
10000
5000
0
Modeled date (B.P.)

	Unmodeled (cal yr B.P.)				Modeled (cal yr B.P.)				
Spring Lake, 2012; ver. 5_int_ZB	central 95%		mean	1 sigma	central 95%		mean	1 sigma	Agreement
sequence start					20577	14569	17410	1565	
SLN-L9, 17.3 ± 1.9 ka	19174	15304	17239	970	18362	14379	16384	1001	81.6
SL7					**16751**	**9623**	**13132**	**1992**	
SLN-L8, 10.0 ± 1.2 ka	11067	8751	9909	580	11007	8771	9880	561	101.4
Units S3bA/C7?									
SLN-L2, 8.0 ± 1.5 ka	9395	6442	7919	740	9207	7522	8266	484	112.1
SLN-R02, 7.6 ± 0.1 ka	7615	7476	7547	36	7617	7479	7551	35	99.5
SLN-L3, 7.8 ± 1.0 ka	8727	6770	7749	490	7592	6971	7337	174	98.7
SLN-L5, 7.0 ± 0.7 ka	7688	6129	6909	390	7476	6485	6995	260	114.6
SL6					**7320**	**5907**	**6640**	**364**	
ZB1					6989	5403	6200	403	
Units C6/S3d									
SLN-L4, 6.1 ± 1.2 ka	7256	4821	6039	610	6605	5177	5890	358	119.2
SL5					**6487**	**4966**	**5722**	**380**	
Unit S3h1									
SLN-L6, 5.7 ± 0.8 ka	6438	4879	5659	390	6044	4743	5396	327	94.7
SL4					**5563**	**4277**	**4773**	**377**	
unit C4									
SLN-R20	4510	4248	4365	61	4515	4252	4377	60	100.2
SLN-L10	4919	3959	4439	240	4483	3998	4254	120	102.2
SL3					**4385**	**3508**	**3971**	**260**	
SLN-R19	3607	3402	3509	47	3606	3402	3510	47	99.8
SL2					**3506**	**2348**	**2948**	**362**	
uppermost unit C2									
SLN-R17	2378	2184	2334	37	2377	2184	2333	38	97.6
SLN-R22	1174	979	1066	57	1175	982	1073	57	97.6
SL1					**1077**	**700**	**876**	**109**	
unit C1									
SLN-R15	739	674	708	18	744	680	713	17	99.8
SLN-R21	734	668	700	19	722	667	690	14	110
Sequence end historic constraint	104	103	104	0	104	103	104	0	100

Intervals:	central 95%		mean	1 sigma
SL7-SL6	2867	10232	6492	2027
SL6-SL5	106	1758	918	438
SL5-SL4	1	1799	950	502
SL4-SL3	-2	1766	802	518
SL3-SL2	82	1860	1023	478
SL2-SL1	1413	2728	2072	380
SL7-SL1	8733	15904	12256	1995
SL6-SL1	4994	6479	5764	380
SL5-SL1	4057	5638	4846	395
SL4-SL1	3290	4731	3897	392
SL3-SL1	2569	3591	3095	281

All values are in calendar years before 1950 (cal yr B.P.)

Indices:

Amodel 106.8

Aoverall 106

North Creek Site

```
Plot()
 {
  Sequence("North Creek, 2012 v3f")
  {
   Boundary("sequence start");
   Phase("footwall burn horizon");
   {
    R_Date("USGSW-4057", 4580, 250);
    R_Date("NC-R9", 4590, 30);
   };
   Date("NC5");
   R_Date("NC-R12", 3680, 30);
   //R_Date("NC-R11", 2010, 40);
   //R_Date("NC-R13", 4700, 30);
   Boundary("NC4");
   R_Date("NC-R19", 3710, 40);
   //R_Date("NC-R29", 180, 25);
   //Delta_R("MRT correction1", 200, 200);
   //R_Date("WC-12-80-3 soil AMRT", 2180, 80);
   Zero_Boundary("ZB");
   Boundary("NC3");
   Delta_R("no MRT correction", 0, 0);
   R_Date("NC-R18", 2110, 30);
   //R_Date("NC-R23", 590, 20);
   R_Date("NC-R16", 1280, 30);
   Boundary("NC2");
   R_Date("WC-12-80-9 AMS char", 1350, 250);
   R_Date("Wc-12-80-8 AMS char", 1200, 300);
   //R_Date("WC-12-80-5 char", 1350, 70); [relation to NC2 is unclear]
   R_Date("WC-12-80-6 char", 1110, 60);
   R_Date("NC-R2", 915, 25);
   Phase("C2A, 2c2A group")
   {
    //R_Date("NC-R15", 5220, 30);
    R_Date("NC-R21", 245, 20);
    R_Date("NC-R31", 365, 20);
   };
   Boundary("NC1");
   //R_Date("NC-R20", 315, 20); [poor agreement with R21]
   //R_Date("NC-R28", 5450, 30);
   R_Date("NC-R32", 215, 20);
   R_Date("NC-R22c", 160, 25);
   R_Date("WC-12-80-4", 250, 300);
   Boundary("Sequence end historic constraint", 1847);
```

```
};
Difference("NC5-NC4","NC4","NC5");
Difference("NC4-NC3","NC3","NC4");
Difference("NC3-NC2","NC2","NC3");
Difference("NC2-NC1","NC1","NC2");
Difference("NC5-NC1","NC1","NC5");
Difference("NC4-NC1","NC1","NC4");
Difference("NC3-NC1","NC1","NC3");
};
```

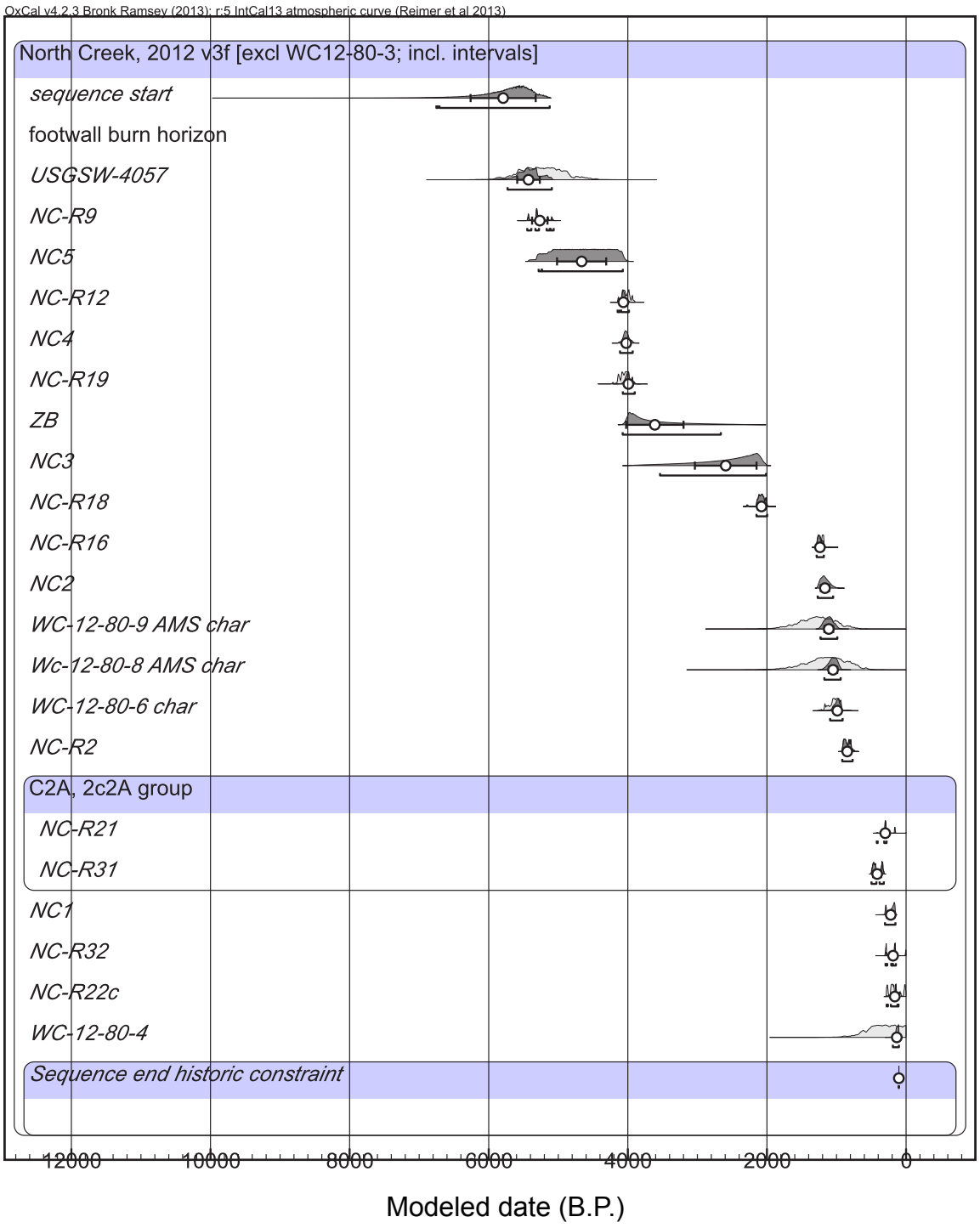
OxCal v4.2.3 Bronk Ramsey (2013); r:5 IntCal13 atmospheric curve (Reimer et al 2013)
North Creek, 2012 v3f [excl WC12-80-3; incl. intervals]
sequence start
footwall burn horizon
USGSW-4057
NC-R9
NC5
NC-R12
NC4
NC-R19
ZB
NC3
NC-R18
NC-R16
NC2
WC-12-80-9 AMS char
Wc-12-80-8 AMS char
WC-12-80-6 char
NC-R2
C2A, 2c2A group
NC-R21
NC-R31
NC1
NC-R32
NC-R22c
WC-12-80-4
Sequence end historic constraint
12000
10000
8000
6000
4000
2000
0
Modeled date (B.P.)

	Unmodeled (cal yr B.P.)				Modeled (cal yr B.P.)				
North Creek, 2012 v3f [excl WC12-80-3; incl. intervals]	95% range		mean	1 sigma	95% range		mean	1 sigma	Agreement
sequence start					6753	5123	5793	468	
footwall burn horizon									
USGSW-4057	5891	4582	5234	312	5730	5093	5428	163	110.2
NC-R9	5448	5075	5312	101	5447	5067	5266	111	88.4
NC5?					**5283**	**4072**	**4665**	**353**	
NC-R12	4139	3914	4019	51	4147	3984	4064	38	101.1
NC4					**4112**	**3930**	**4023**	**43**	
NC-R19	4219	3926	4052	62	4072	3901	3992	43	92.3
ZB					4074	2663	3612	413	
NC3					**3537**	**2014**	**2593**	**443**	
no MRT correction	-0.5	0.5	0	0	-0.5	0.5	0	0	100
NC-R18	2153	1995	2084	54	2151	1996	2079	51	100.1
NC-R16	1288	1176	1226	36	1285	1182	1238	31	100.7
NC2					**1271**	**1048**	**1166**	**60**	
WC-12-80-9 AMS char	1820	783	1282	260	1231	988	1111	63	117.8
Wc-12-80-8 AMS char	1780	562	1152	293	1175	940	1050	61	134.8
WC-12-80-6 char	1176	930	1038	72	1092	912	988	47	107.8
NC-R2	919	767	847	42	918	768	846	42	99.3
C2A, 2c2A group									
NC-R21	312	151	262	67	421	280	299	30	108.6
NC-R31	498	320	415	57	498	320	415	57	99.5
NC1					**303**	**153**	**220**	**50**	
NC-R32	304	...	190	92	295	146	187	46	99
NC-R22c	285	...	157	85	279	109	162	35	98.1
WC-12-80-4	731	...	340	219	190	103	133	26	110.1
Sequence end historic constraint	104	103	104	0	104	103	104	0	100

Intervals:	95% range		mean	1 sigma
NC5?-NC4	36	1245	641	354
NC4-NC3	460	2030	1431	446
NC3-NC2	812	2396	1426	449
NC2-NC1	792	1091	946	79
NC5?-NC1	3842	5080	4445	357
NC4-NC4	3664	3925	3803	66
NC3-NC4	1762	3345	2373	446

All values are in calendar years before 1950 (cal yr B.P.)

Indices:
Amodel 114
Aoverall 115.3

Payson site

```
Plot()
 {
  Sequence("WFZ Payson trench")
  {
   Boundary("Sequence start");
   R_Date("SP-RC-6",2720,30);
   Boundary("P2");
   R_Date("SP-RC-5",2420,20);
   //R_Date("SP_RC-4",4930,35);  excluded - possibly detrital
   R_Date("SP-RC-2",770,25);
   Boundary("P1");
   Zero_Boundary("1");
   Boundary("Begin historical record",1847 AD);
  };
 };
```

Picayune Canyon site

```
Plot()
 {
  Sequence("Picayune Cyn v1")
  {
   Boundary("start");
   R_Date("C5, 4.1 ka", 3730, 20);
   R_Date("C4, 3.6 ka", 3305, 20);
   Boundary("P2");
   Zero_Boundary("ZB1");
   Phase("Soil on units 4 and 8")
   {
    R_Date("C3, 2.6 ka", 2510, 20);
    R_Date("C1, 2.6 ka", 2475, 15);
   };
   Boundary("P1");
   Zero_Boundary("ZB2");
   C_Date("Historical constraint", 1850 AD, 0);
   Boundary("end");
  };
 };
```

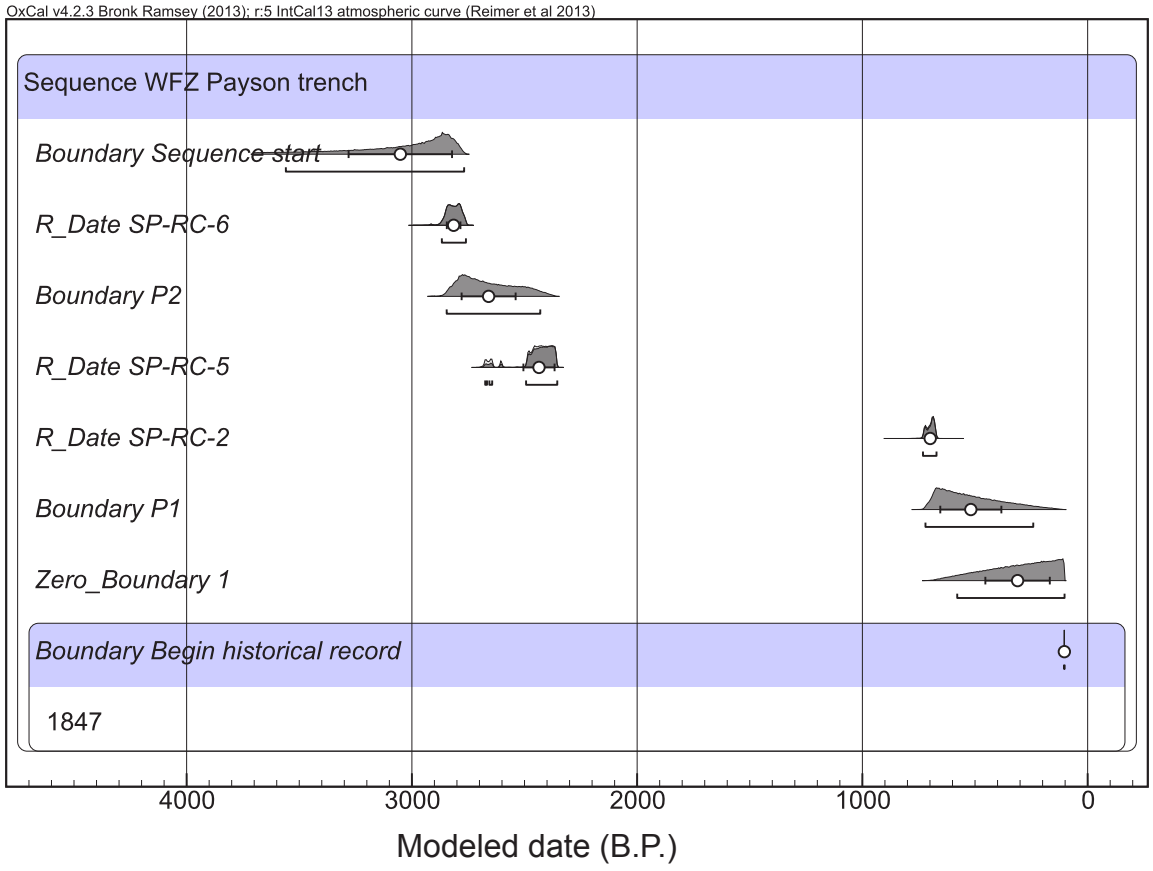
OxCal v4.2.3 Bronk Ramsey (2013); r:5 IntCal13 atmospheric curve (Reimer et al 2013)
Sequence WFZ Payson trench
Boundary Sequence start
R_Date SP-RC-6
Boundary P2
R_Date SP-RC-5
R_Date SP-RC-2
Boundary P1
Zero_Boundary 1
Boundary Begin historical record
1847
4000
3000
2000
1000
0
Modeled date (B.P.)

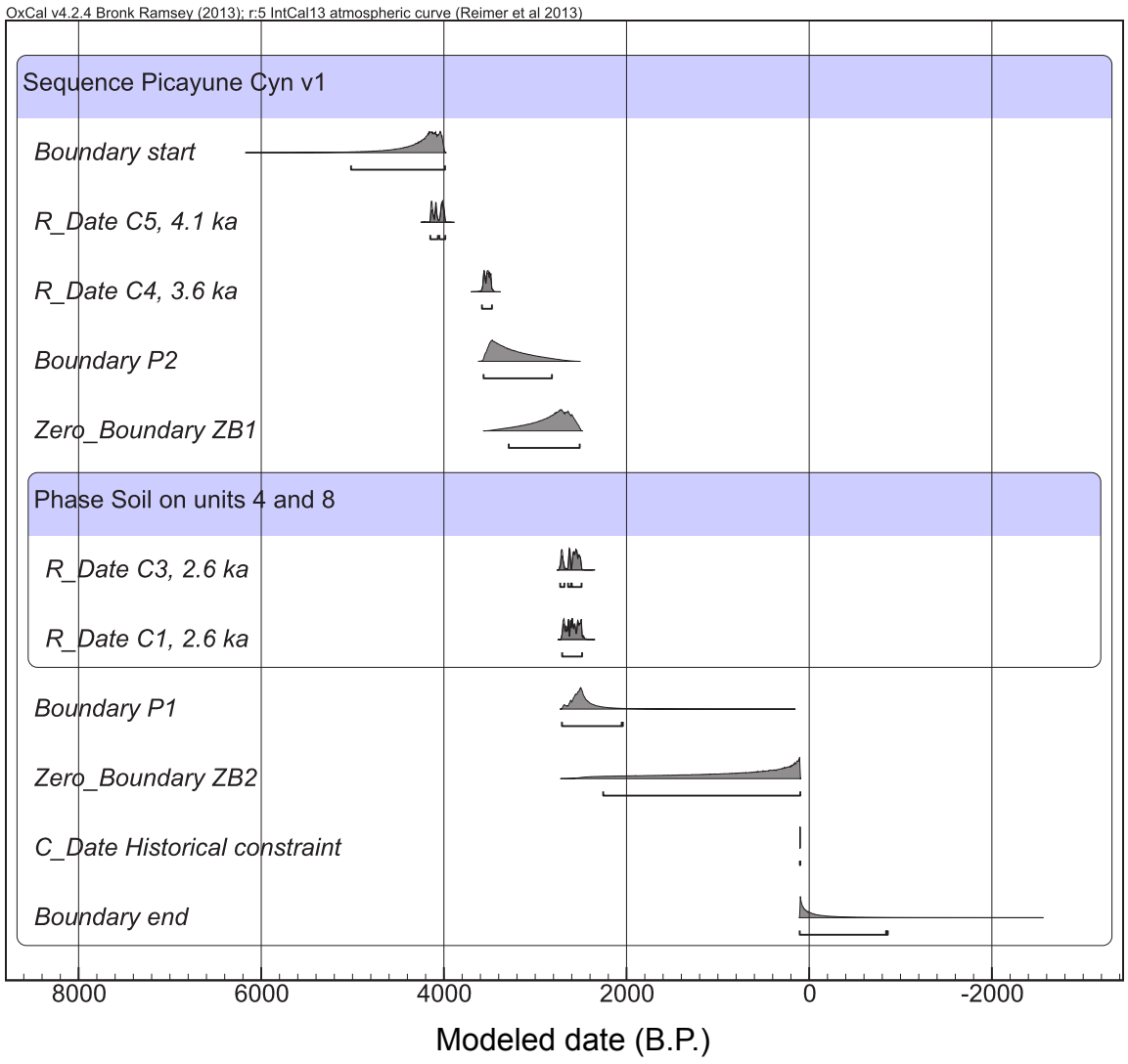
OxCal v4.2.4 Bronk Ramsey (2013); r:5 IntCal13 atmospheric curve (Reimer et al 2013)
Sequence Picayune Cyn v1
Boundary start
R_Date C5, 4.1 ka
R_Date C4, 3.6 ka
Boundary P2
Zero_Boundary ZB1
Phase Soil on units 4 and 8
R_Date C3, 2.6 ka
R_Date C1, 2.6 ka
Boundary P1
Zero_Boundary ZB2
C_Date Historical constraint
Boundary end
8000
6000
4000
2000
0
-2000
Modeled date (B.P.)

Payson site	**Unmodeled (cal yr B.P.)**				**Modeled (cal yr B.P.)**				
	Central 95%		mean	1 sigma	central 95%		mean	1 sigma	Agreement
Sequence WFZ Payson trench									
Boundary Sequence start					3560	2768	3051	230	
R_Date SP-RC-6	2867	2760	2815	30	2867	2760	2815	30	99.8
Boundary P2					2846	2430	2659	120	
R_Date SP-RC-5	2679	2356	2450	84	2675	2355	2436	69	104.3
R_Date SP-RC-2	730	671	698	17	731	671	699	17	97.2
Boundary P1					720	242	519	136	
Zero_Boundary 1					579	103	311	143	
Boundary Begin historical record	104	103	104	0	104	103	104	0	100

Indices:
Amodel 100.6
Aoverall 100.6

Picayune Canyon site	**Unmodeled (cal yr B.P.)**				**Modeled (cal yr B.P.)**				
	Central 95%		mean	1 sigma	central 95%		mean	1 sigma	Agreement
Sequence Picayune Cyn v1									
Boundary start					5017	3988	4307	323	
R_Date C5, 4.1 ka	4150	3988	4072	52	4149	3985	4057	50	97.1
R_Date C4, 3.6 ka	3580	3470	3525	30	3583	3474	3529	31	98.7
Boundary P2					3566	2817	3264	215	
Zero_Boundary ZB1					3290	2513	2840	213	
Phase Soil on units 4 and 8									
R_Date C3, 2.6 ka	2733	2493	2601	71	2727	2493	2591	65	99.1
R_Date C1, 2.6 ka	2711	2486	2592	70	2705	2487	2588	65	99.1
Boundary P1					2708	2041	2446	207	
Zero_Boundary ZB2					2256	98	923	676	
C_Date Historical constraint	101	100	101	0	101	100	101	0	100
Boundary end					104	-860	-134	352	

Indices:
Amodel 97.1
Aoverall 97.3

APPENDIX I
VERTICAL DISPLACEMENT AT THE SPRING LAKE SITE

APPENDIX I

VERTICAL DISPLACEMENT AT THE SPRING LAKE SITE

Total vertical displacement estimates for the Spring Lake trench site. Heavy dashed blue lines show alternate projections of the tops of footwall soils N2cA and S2cA and hanging-wall soils N3aA and S3bA into fault zone F1. For each exposure, the total vertical displacement (heavy vertical bar) is the vertical offset of these soil projections, measured at the horizontal midpoint of the F1 projection (heavy dashed red line). See text for discussion of displacement measurements and plates 1 and 2 for unit and contact descriptions.

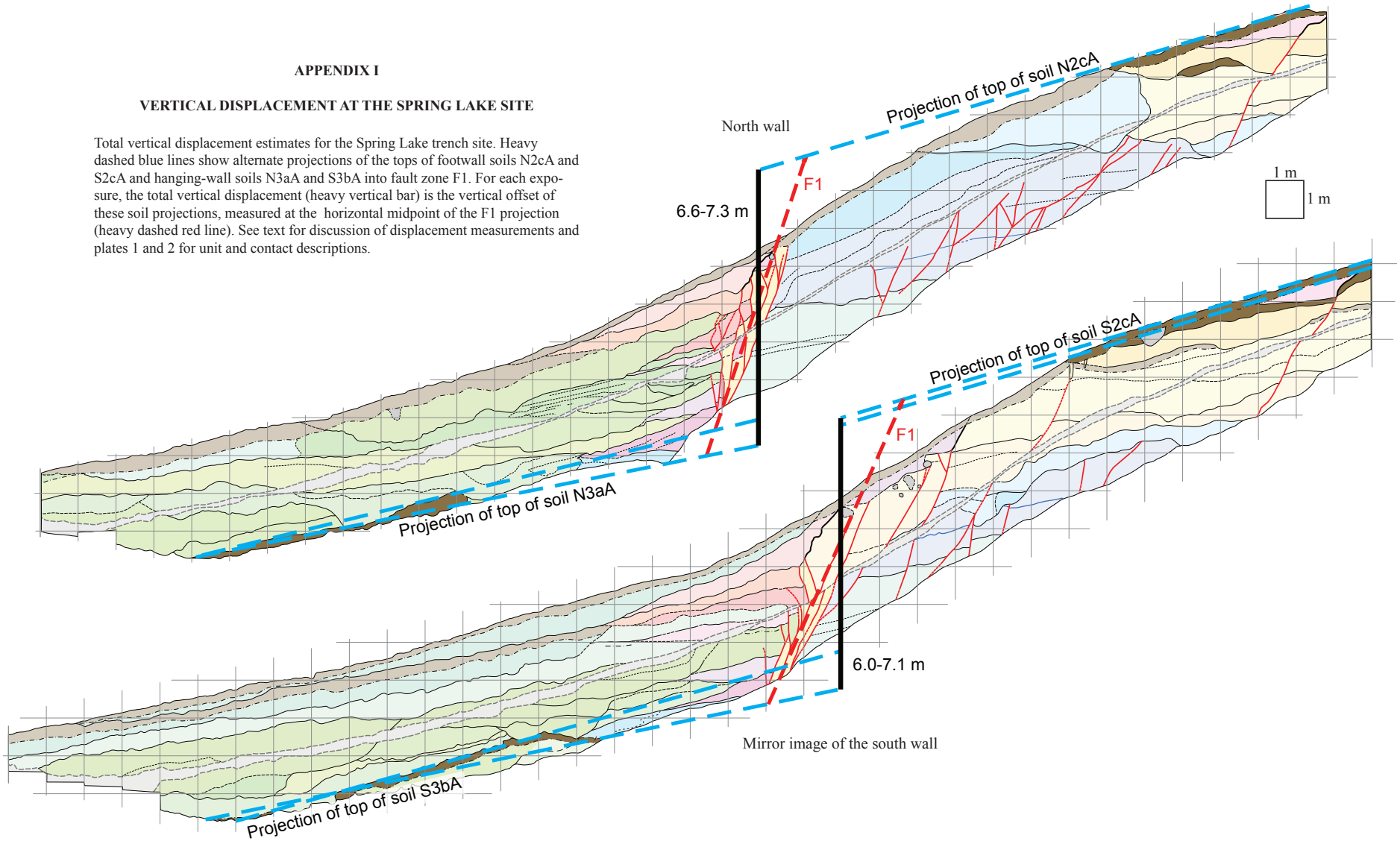

APPENDIX J
VERTICAL DISPLACEMENT AT THE NORTH CREEK SITE

APPENDIX J

VERTICAL DISPLACEMENT AT THE NORTH CREEK SITE

Main fault (F1) and graben (F2-F7) displacements for the North Creek trench site. Heavy dashed blue lines show projections of the top of footwall soil 1cA and hanging-wall unit 2a into fault zone F1. The unit 2a projection accounts for 0.1 m of antithetic displacement along fault F7 (green dotted line). The total vertical site displacement (heavy vertical bar) is the vertical offset of these projections, measured at the horizontal midpoint of the F1 projection (heavy dashed red line). Projections of soils 2bA (purple) and 2cA (pink) across the graben provide evidence of at least two surface-faulting earthquakes. See text for discussion of displacement measurements and plates 3 and 4 for unit and contact descriptions.

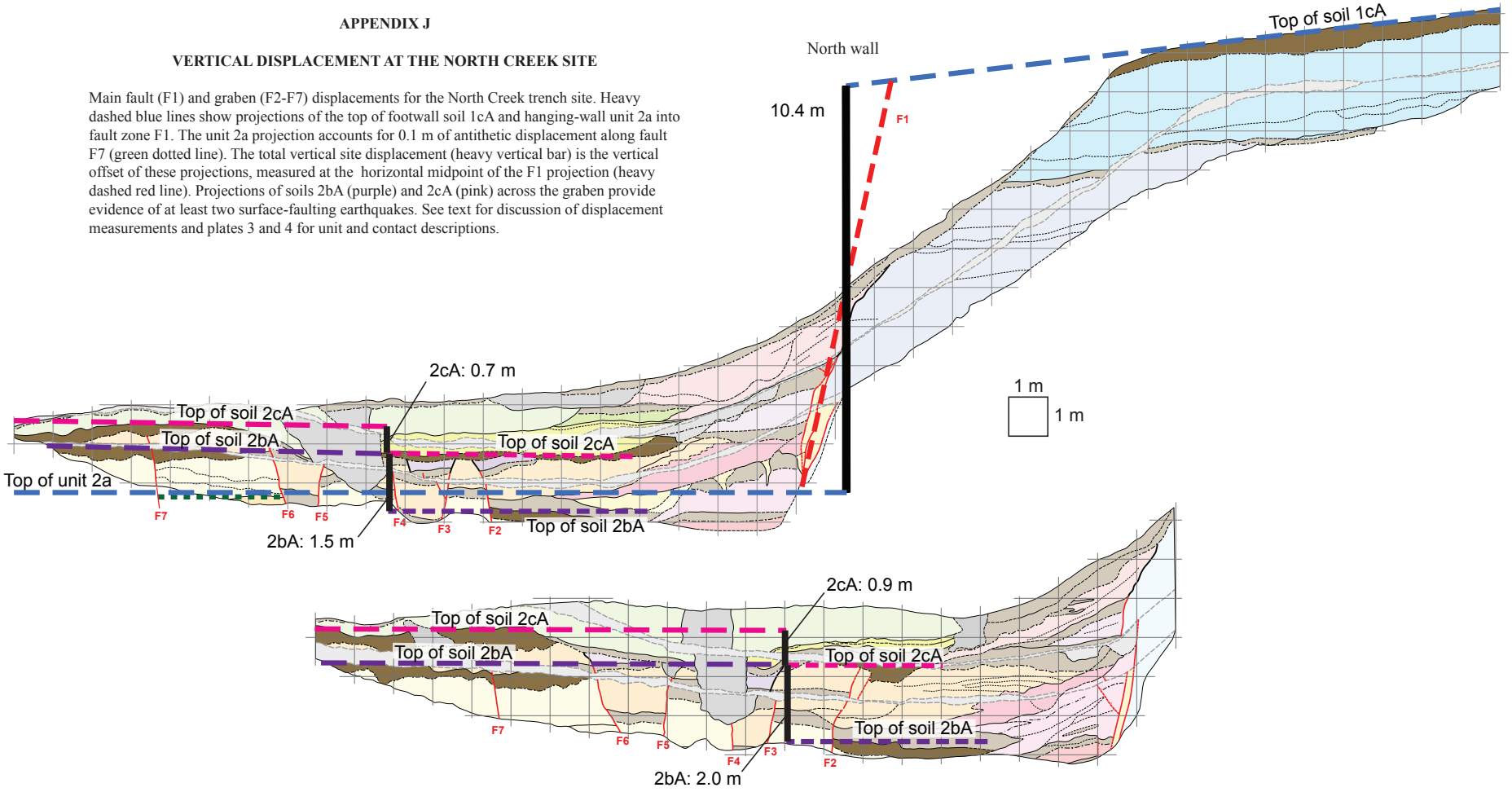

Mirror image of the south wall

APPENDIX K
SUMMARY OF PALEOSEISMIC DATA FOR THE SPRING LAKE SITE

APPENDIX K

SUMMARY OF EARTHQUAKE-TIMING, RECURRENCE, AND FAULT-SLIP-RATE ESTIMATES FOR THE SPRING LAKE SITE

Earthquake timing *(cal yr B.P.)*

Event	mean	1σ	2σ	central 95%	
SL7	13,132	1992	3984	9623	16,751
SL6	6643	364	728	5911	7321
SL5	5722	380	760	4966	6488
SL4	4779	387	774	4279	5562
SL3	3971	260	520	3509	4386
SL2	2948	362	724	2348	3506
SL1	876	109	218	700	1077

OxCal model: Spring_Lake_N/SpringLake_ver_5_int_ZB.

Central 95% range is based on the OxCal time distribution with the highest probability density.

Inter-event recurrence

Events	Mean	1σ	2σ	central 95%	
SL7-SL6	6492	2027	4054	2867	10232
SL6-SL5	920	438	876	109	1759
SL5-SL4	950	502	1004	1	1799
SL4-SL3	802	517	1034	0	1766
SL3-SL2	1023	478	956	82	1859
SL2-SL1	2072	380	760	1414	2728

Coefficient of variation (COV)

events	mean	stdev	COV
SL7-SL1	2043	2228	1.09
SL6-SL1	1153	520	0.45

COV is the standard deviation (stdev) of inter-event recurrence times divided by their mean.

Inter-event intervals (e.g., between SL7 and SL6) calculated using the "Difference" command in OxCal.

Mean recurrence

Events	Total time interval					Intervals	Mean recurrence				
	mean	1σ	2σ	central 95%			mean	1σ	2σ	central 95%	
SL7-SL1	12,256	1995	3990	8733	15,904	6	2043	333	665	1456	2651
SL6-SL1	5766	380	760	4995	6480	5	1153	76	152	999	1296
SL5-SL1	4846	396	792	4058	5639	4	1212	99	198	1015	1410
SL4-SL1	3897	392	784	3293	4734	3	1299	131	261	1098	1578
SL3-SL1	3095	281	562	2569	3592	2	1548	141	281	1285	1796

Total time intervals between events (eg., SL7 and SL1) calculated using the "Difference" command in OxCal.

Mean recurrence is elapsed time divided by the number of intervals.

Slip rate

Event	Mean time	Ind. displacement			Total displacement				Total time interval				Slip rate		
		midpt	min	max	events	midpt	min	max	events	mean	95th range		mean	min	max
SL7	13,132	-	-	-	-	-	-	-	-	-	-	-	-	-	-
SL6	6643	1.1	0.8	1.4	SL6-SL1	5.9	4.4	7.4	SL7-SL1	12,256	8733	15904	0.48	0.28	0.85
SL5	5722	0.95	0.7	1.2	SL5-SL1	4.8	3.6	6.0	SL6-SL1	5766	4995	6480	0.83	0.56	1.20
SL4	4779	0.9	0.7	1.1	SL4-SL1	3.85	2.9	4.8	SL5-SL1	4846	4058	5639	0.79	0.51	1.18
SL3	3971	1.05	0.8	1.3	SL3-SL1	2.95	2.2	3.7	SL4-SL1	3897	3293	4734	0.76	0.46	1.12
SL2	2948	0.8	0.6	1.0	SL2-SL1	1.9	1.4	2.4	SL3-SL1	3095	2569	3592	0.61	0.39	0.93
SL1	876	1.1	0.8	1.4	SL1	1.1	0.8	1.4	SL2-SL1	2072	1414	2728	0.53	0.29	0.99

Slip rate is total displacement (e.g., for earthquakes SL6 to SL1) divided by the total time interval (e.g., SL7 to SL1).

APPENDIX L
SUMMARY OF PALEOSEISMIC DATA FOR THE NORTH CREEK SITE

APPENDIX L

SUMMARY OF EARTHQUAKE-TIMING, RECURRENCE, AND FAULT-SLIP-RATE ESTIMATES FOR THE NORTH CREEK SITE

Earthquake timing *(cal yr B.P.)*

Event	mean	1σ	2σ	central 95%	
NC5	4665	353	706	4072	5283
NC4	4023	43	86	3930	4112
NC3	2593	443	886	2014	3537
NC2	1166	60	120	1048	1271
NC1	220	50	100	153	303

(mode: 2150)

OxCal model: North Creek, 2012 v3f [excl WC12-80-3; incl. intervals] (appendix E).
Central 95% range is based on the OxCal time distribution with the highest probability density.

Inter-event recurrence

Events	Mean	1σ	2σ	central 95%		
NC5-NC4	641	354	708	36	1245	
NC4-NC3	1431	446	892	460	2030	*(mode: 1845)*
NC3-NC2	1426	449	898	812	2396	*(mode: 1015)*
NC2-NC1	946	79	158	792	1091	

Inter-event intervals (e.g., between NC4 and NC1) calculated using the "Difference" command in OxCal.

Coefficient of variation (COV)

Events	mean	stdev	COV
NC5-NC1	1111	387	0.35
NC4-NC1	1268	279	0.22

COV is the standard deviation (stdev) of inter-event recurrence times divided by their mean.

Mean recurrence

Events	Total time interval					Intervals	Mean recurrence				
	mean	1σ	2σ	central 95%			mean	1σ	2σ	central 95%	
NC5-NC1	4445	357	714	3842	5080	4	1110	90	180	960	1270
NC4-NC1	3803	66	132	3664	3925	3	1270	20	40	1220	1310
NC3-NC1	2373	446	892	1762	3345	2	1190	220	450	880	1670

Total time intervals between events (eg., NC4 and NC1) calculated using the "Difference" command in OxCal.
Mean recurrence is elapsed time divided by the number of intervals.

Slip rate

Total displacement				Total time interval				Slip rate		
events	midpt	min	max		mean	central 95%		mean	min	max
Units 1c/2a	10.4	6.0	14.8	soil 1bA	5268	5048	5433	2.0	1.1	2.9
NC4-NC1	8.3	3.9	12.7	NC5-NC1	4445	3842	5080	1.9	0.8	3.3

The slip rate for NC5 is the total displacement for earthquakes NC5-NC1 divided by the mean time of footwall soil 1bA.
For NC4, the slip rate is the displacement in NC4-NC1 divided by the elapsed time between NC5 and NC1.